Analysis and Optimization of Communication Technologies for Smart Grid Applications

by

Fariba Aalamifar

B.Sc., Isfahan University of Technology, 2009
M.A.Sc., Queen's University, 2012

A THESIS SUBMITTED IN PARTIAL FULFILLMENT OF
THE REQUIREMENTS FOR THE DEGREE OF

DOCTOR OF PHILOSOPHY

in

The Faculty of Graduate and Postdoctoral Studies

(Electrical and Computer Engineering)

THE UNIVERSITY OF BRITISH COLUMBIA
(Vancouver)

June 2018

The following individuals certify that they have read, and recommend to the Faculty of Graduate and Postdoctoral Studies for acceptance, the dissertation entitled:

Analysis and Optimization of Communication Technologies for Smart Grid Applications

submitted by Fariba Aalamifar in partial fulfillment of the requirements for the degree of Doctor of Philosophy in Electrical and Computer Engineering

Examining Committee:

Prof. Lutz Lampe, Electrical and Computer Engineering
Supervisor

Prof. Vincent Wong, Electrical and Computer Engineering
Supervisory Committee Member

Prof. Juri Jatskevich, Electrical and Computer Engineering
Supervisory Committee Member

Prof. Sathish Gopalakrishnan, Electrical and Computer Engineering
University Examiner

Prof. Michael Feeley, Computer Science
University Examiner

Abstract

Several communication technologies including IEEE 802.15.4g, world-wide interoperability for microwave access (WiMAX), and power line communication (PLC) have been suggested for smart grid implementation. As the successful arrival of smart grid traffic within their latency requirement is essential for the correct operation of the power grid, we focus on the optimization of different features of these communication technologies and also the development of aspects of an efficient network architecture such that the reliability requirement associated with smart grid traffic can best be assured.

We first investigate an optimized configuration of WiMAX features, in particular, the choice of frame duration, type-of-service to traffic mapping and uplink and downlink allocations, under what we call the "profile configuration". We also devise inter-class and intra-class scheduling solutions in order to prioritize time-critical traffic within both base station and customer premises equipments. We then evaluate the performance of the developed WiMAX profile configuration and scheduling scheme through our newly developed WiGrid (WiMAX for Smart Grid) module. From the performed simulations, we conclude that the proposed configurations for the WiMAX features can ensure the satisfaction of the reliability requirement.

Next, we design advanced metering infrastructures (AMIs) based on the characteristics of the PLC and the IEEE 802.15.4g technologies. We use intermediary data collectors, known as data acquisition points (DAPs), in order to efficiently collect traffic from smart meters and forward them to the utility control center. We formulate an optimization platform for efficiently placing DAPs on top of the existing utility poles or transformers, in such a way that the required reliability for smart grid traffic is ensured and also the installation cost is minimized. In order to address the QoS requirements, we derive the latency based on the characteristics of the medium access control schemes of each of these technologies. Since finding the optimal DAP locations is an integer programming problem and NP-hard, we develop several heuristic algorithms for efficiently placing DAPs within large-scale scenarios. We observe that the DAP placement algorithms, proposed here for large-scale scenarios, return near-optimal results within a much shorter time, than that of the IBM CPLEX software for small scenarios.

Lay Summary

Continuous monitoring, control and protection of the power grid elements is only possible when a two-way information flow between the utility control centres and intelligent grid devices is realized. Different wired and wireless communication technologies including power line communication (PLC), worldwide interoperability for microwave access (WiMAX) and smart utility network (SUN) technologies have been suggested for providing the communication infrastructure in different parts of the smart grid. In this thesis, we investigate the optimized configuration of these technologies for smart grid implementation such that quality of service requirements, namely latency and reliability, can best be maintained and at the same time, a cost-efficient infrastructure is designed. We apply our optimization solutions on realistic examples of smart grid infrastructures, and through numerical results, we show that the latency and reliability requirements are maintained. We show that our algorithms can provide near-optimal solutions, in terms of energy consumption and installation cost, despite their low computational complexity, which makes them powerful and efficient tools for planning reliable large-scale smart grid communication networks.

Preface

This thesis is based on the original research work that I have conducted under the supervision of Professor Lutz Lampe. I led the research for all the contributions presented in this thesis and their associated publications, including the literature review, problem formulations and required derivations, the development of methods and heuristic algorithms, and the simulation of communication systems and the evaluation of numerical results.

The contents of Chapter 2 have been published in the following papers:

- F. Aalamifar, L. Lampe, S. Bavarian, and E. Crozier, "WiMAX Technology in Smart Distribution Networks: Architecture, Modelling and Applications," *IEEE PES Transmission and Distribution Conference and Exposition*, Chicago, IL, USA, April 2014.

- F. Aalamifar and L. Lampe, "Optimized WiMAX Profile Configuration for Smart Grid Communications," *IEEE Transactions on Smart Grid*, vol. 8, no. 6, pp. 2723-2732, Nov. 2017.

The conference paper listed above presents preliminary work for the main contribution developed and presented in the journal paper. The industry collaborators, Mr. Eugene Crozier and Dr. Sara Bavarian provided the initial motivation for this work and provided information regarding specifics of distribution automation networks, and they helped with the revisions of the manuscript.

The contents of Chapter 3 have been published in the following paper:

- F. Aalamifar, G. Naddafzadeh, M. Noori, and L. Lampe, “Cost-Efficient Data Aggregation Point Placement for Advanced Metering Infrastructure,” *IEEE International Conference on Smart Grid Communications (SmartGridComm)*, Venice, Italy, November 2014.

For this paper, I conducted the literature review, formulated the optimization problem, proposed the modified K-means algorithm, and implemented the algorithm and wrote the manuscript. The post-doctoral fellows Dr. Ghasem Naddafzadeh and Dr. Moslem Noori helped with developing the idea of data aggregation point placement and the revision of the manuscript.

The contents of Chapter 4 have been submitted for publication:

- F. Aalamifar and L. Lampe, “Cost-efficient QoS-Aware Data Acquisition Point Placement for Advanced Metering Infrastructure,” Submitted 2017, under review.

The contents of Chapter 5 have been submitted for publication:

- F. Aalamifar and L. Lampe, “Optimized Data Acquisition Point Placement for an Advanced Metering Infrastructure Based on Power Line Communication Technology,” Submitted 2018, under review.

The contents of Appendix B have been published in the following paper:

- F. Aalamifar, A. Schlögl, D. Harris, and L. Lampe, “Modelling Power Line Communication Using Network Simulator-3”, *IEEE Global Communications Conference (Globecom 2013)*, Atlanta, GA, USA, December 2013.

The paper describes the project of developing a module that can emulate the behaviour of a power line communication network. Prof. Lampe initiated the project with the Master's exchange student, Mr. Alexander Schlogl, and I have supervised the overall work after starting my Ph.D. research, and I wrote the paper. Mr. Schlogl developed the concept and conducted most of the software implementation underlying the emulator. The graphical user interface has been coded by Mr. Don Harris. I extended the overall emulator and developed further modules used for the work presented in this thesis.

Table of Contents

List of Tables

List of Figures

List of Abbreviations

4G	4^{th} Generation
AMI	Advanced Metering Infrastructure
AoI	Area of Interest
ARQ	Automatic Repeat Request
AVG	Average
BC	British Columbia
BE	Best Effort
BLER	BLock Error Rate
BR	Bandwidth Request
BPSK	Binary Phase-Shift Keying
BS	Base Station
CBR	Constant Bit Rate
CAP	Contention Access Period
CDF	Cumulative Distribution Function
CFP	Contention-Free-Period
CPE	Customer Premises Equipment
CSMA/CA	Carrier Sense Multiple Access with Collision Avoidance
CTF	Channel Transfer Function
DAP	Data Acquisition Point
DL	Downlink

EDF	Earliest Deadline First
ertPS	Extended Real-Time Polling Service
ESI	Energy Services Interface
FAN	Field Area Network
FCFS	First-Come First-Serve
GUI	Graphical User Interface
HAN	Home Area Network
KD	k-dimensional
LOAD	6LowPAN Ad hoc Distance-vector protocol
LRSM	A SM that experiences Low Reliability
LTE	Long-Term Evolution
M2M	Machine-to-Machine
MAC	Medium Access Control
MB	Mega-Byte
MBB	Mobile BroadBand
MC	Mission-Critical
MCS	Modulation and Coding Scheme
MIMO	Multiple-Input Multiple-Output
MR-FSK	Multi-Regional Frequency Shift Keying
MR-OFDM	Multi-Regional Orthogonal Frequency Division Multiplex
MR-O-QPSK	Multi-Regional Orthogonal-Quadratic Phase-Shift Keying
NAN	Neighbourhood Area Network
NC	Non-Critical
NIST	National Institute of Standards and Technology
nrtPS	Non-Real-Time Polling Service

NS-3	Network Simulator-3
OFDM	Orthogonal Frequency-Division Multiplexing
OFDMA	Orthogonal Frequency-Division Multiple Access
PAP	Priority Action Plan
PER	Packet Error Rate
PL	Pathloss
PLC	Power Line Communication
PRIME	PoweRline Intelligent Metering Evolution
PSD	Power Spectral Density
QAM	Quadratic Amplitude Modulation
QoS	Quality of Service
QPSK	Quadratic Phase-Shift Keying
RPL	Routing Protocol for Low-Power and Lossy Networks
RR	Round-Robin
RS + CC/CC	Concatenated Reed Solomon with Convolutional Coding/Inner-Checksum coding
rtPS	Real-Time Polling Service
Rx	Receiver
SCP	Shared Contention Period
SM	Smart Meter
SGCN	Smart Grid Communication Network
SGLM	Smart Grid Last Mile
SINR	Signal-to-Interference plus Noise Ratio
SNR	Signal-to-Noise Ratio
SUN	Smart Utility Network

TDD	Time Division Duplex
TDMA	Time Division Multiple Access
TLT	Transmission Line Theory
TS	Terminal Station
Tx	Transmitter
UC	Utility Center
UL	Uplink
UGS	Unsolicited Grant Service
VBR	Variable Bit Rate
WAN	Wide Area Network
WLAN	Wireless Local Area Network
WiMAX	Worldwide Interoperability for Microwave Access
WiGrid	WiMAX for smart Grid
WFQ	Weighted Fair Queuing
XML	Extensible Markup Language

Notation

$\mathcal{A}$	Set of DAP locations
A, B, C, D	ABCD parameters of a two-port PLC unit
a	Installation cost of one DAP
$\boldsymbol{a}_k$	Location of k'th DAP
α	Pathloss exponent
α_x	Probability that the channel is busy at node x
β_x	Probability that the channel is idle at node x
B	Packet size in bytes
C	COST231-Hata pathloss model constant
c_0, c_1, c_2, c_3	Erceg pathloss model constants
c_{inst}	Total DAP installation cost
$C(p)$	Additional idle sensing required before transmission for traffic priority p
C_r	Data compression ratio
c_{tx}	Transmission cost
$D_x(p)$	Delay requirement for traffic priority p in time slots
d	Euclidean distance between two nodes
d_0	Reference distance for computing pathloss
d_{pmax}	SM-to-DAP transmission range
d_{smax}	SM-to-SM transmission range

d_{umax}	DAP-to-UC transmission range
δ	Penetration loss
E_{b}	Required received energy per bit
E_{tx}	Energy consumed for transmission of one packet
$\epsilon_h, \epsilon_{ij}$	Link PER
η	Fading margin
F	Noise factor
f	Channel frequency
$\Phi_x(k, m, p)$	Probability that node x senses the channel at slot k in sensing stage m for its traffic priority p
g	Energy price
$\mathcal{H}_{ij}$	Channel frequency response from transmitter i to receiver j
H	Number of hops
I	Packet size in time slots
K	Number of selected DAPs by the K-means algorithm
κ	Interference margin
χ_x	Probability of transmission failure
L	Required end-to-end latency in seconds
$\ell_{x,h}(p)$	Experienced delay for traffic priority p at the relay node at hop h
λ_0	Average traffic generation rate per node
$\lambda_x(p)$	Arrival rate of traffic class p
M	Number of sensing stages in CSMA/CA protocol
$\mu_x(p)$	Service rate of traffic class p
N_0	Thermal noise power spectral density

N'_0	Noise power spectral density at the receiver
$N_0(f_n)$	Frequency selective noise for PLC
$N_{\mathrm{f}x}$	Number of feeding nodes of node x
$N_{\max}$	Maximum number of SMs that can be connected to a DAP
N_{poles}	Number of poles
$N_{r_{hn}}$	Number of neighbouring nodes of r_{hn}
N_{SM}	Number of SMs
N_{s}	Number of available time slots for the MC or NC traffic within the delay requirement
N_{sc}	Total number of subcarriers within each subchannel
N_{tr}	Number of transformers
ν_{conv}	Convergence ratio of the iterative DAP selection algorithm
$\nu_x(p)$	Probability that node x does not have any traffic with priority higher than p for transmission
$\mathcal{P}$	Set of pole locations
p	Traffic priority index
$PL(d)$	Pathloss (in dB) at distance d
P_{tx}	Transmission power
Ψ_x	Set of neighbouring nodes of x
$\boldsymbol{p}_j$	Location of pole j
$\boldsymbol{\pi}$	Stationary distribution vector of Markov chain
$q_{ii'}$	Binary variable indicating whether SM i' is the immediate parent of SM i
R_h	Antenna height of the TS
R_i	Reliability of the MC or NC traffic at node i

r	Radius of the AoI
r_{hn}	The relay node for node n at hop h
$\bar{r}_x(p)$	Mean residual service time
$\rho_x(p)$	Probability that node x has a packet of traffic priority p for transmission
ρ_{SM}	SM density in the AoI
ϱ	Ratio of number of poles to the number of SMs in the AoI
$\mathcal{SM}$	Set of SM locations
$\boldsymbol{s}_i$	Location of SM i
$\bar{s}_x(p)$	Mean packet service time at node x for traffic priority p
$\bar{s_x^2}(p)$	Second moment of service time at node x for traffic priority p
σ_x	Expected number of packet retransmissions at node x
$\boldsymbol{T}$	Transition matrix of Markov chain
T_{F}	Frame duration
T_h	Antenna height of the BS
T_I	Transmission interval
T_m	Network lifetime
$T_{\mathrm{Q}_x}(p)$	Queuing delay at node x for traffic priority p
τ	Required reliability
$\theta_x(k)$	Probability that node x senses the channel as idle at slot k
$\boldsymbol{u}$	UC location
W_m	Size of backoff window in CSMA/CA sensing stage m
x_j	Binary variable indicating whether a DAP is installed on pole or transformer j
y_{ij}	Binary variable indicating whether SM i is directly connected

	to pole or transformer j
$Z_{\mathrm{in},i}$	Calculated impedance for the i'th unit of the two-port PLC network
Z_{L}	Load impedance of a PLC receiver device
Z_{s}	Source impedance of a PLC transmitter device
$z_{ii'}$	Binary variable indicating whether SM i' is an ancestor of SM i
$\zeta_x(k,i,m)$	Probability that node x senses the channel at slot k, in sensing stage m, and in transmission attempt i

Acknowledgments

First of all, I would like to express my sincere gratitude to Prof. Lutz Lampe for his in-depth insights, feedback and supervision during the course of my PhD studies. He always gave me a positive energy to pursue my ideas and supported me to conduct research.

I also would like to express my sincere gratitude to Mr. Eugene Crozier and Dr. Sara Bavarian, who supported part of the research presented in this thesis by providing valuable practical insights and data sets for performing simulative tests and analysis.

In this context, I also would like to thank Powertech Labs Inc. and BC Hydro for supporting part of the my research through a funded research project and for generously providing access to real-world data used in simulation experiments.

I also would like to thank MITACS internship program and the Natural Sciences and Engineering Research Council (NSERC) of Canada for providing the research fund for this thesis.

Last but not least, I would like to thank my friends in the Data Communication lab, Dr. Ayman Mostafa, Mr. Gautham Prasad, Mr. Mrinmoy Jana, and Mr. Ali Saberali, for their continuous motivation, encouragement and support.

Dedication

I would like to dedicate my thesis to my dearest family, my mother and my father, my sister and my brother and of course, my lovely husband who were always here for me in sadness and happiness. I wish all of them to be happy, healthy and successful in their endeavors too.

Chapter 1

Introduction

The notion of smart grid is a vision of the future electric power grid that integrates pervasive sensing and control systems to support distributed generation and storage, dynamic and automatic optimization of grid variables, dynamic pricing and customer choices and other advanced functionalities. This vision is tightly coupled with the deployment of a ubiquitous communications infrastructure that enables these functionalities. Since smart grids and the underlying smart gird communication infrastructure will eventually be complex systems of systems, recent standardization efforts undertaken by the U.S. National Institute of Standards and Technology (NIST) [1] and within the IEEE Project 2030 [2] have focused on architectural and reference models. For example, the IEEE 2030 reference architecture for smart grid communications includes home area networks (HANs) at the customer side, which collect the traffic from the smart electronic devices at home, neighbourhood area networks (NANs), which realize the smart grid last mile (SGLM) communication network and collect the traffic from smart meters (SMs) and transmit them to the local data acquisition points (DAPs), field area networks (FANs), which are responsible for providing the communication infrastructure within the distribution network, and wide area networks (WANs) in the transmission domain, which provide the backhaul communication and inter-connect different utilities and substations with each other, cf. [3, Chapter 1]. A simple illustration of this hierarchical architecture is shown in Figure 1.1. In this figure, we can see another component, which is called advanced metering infrastructure

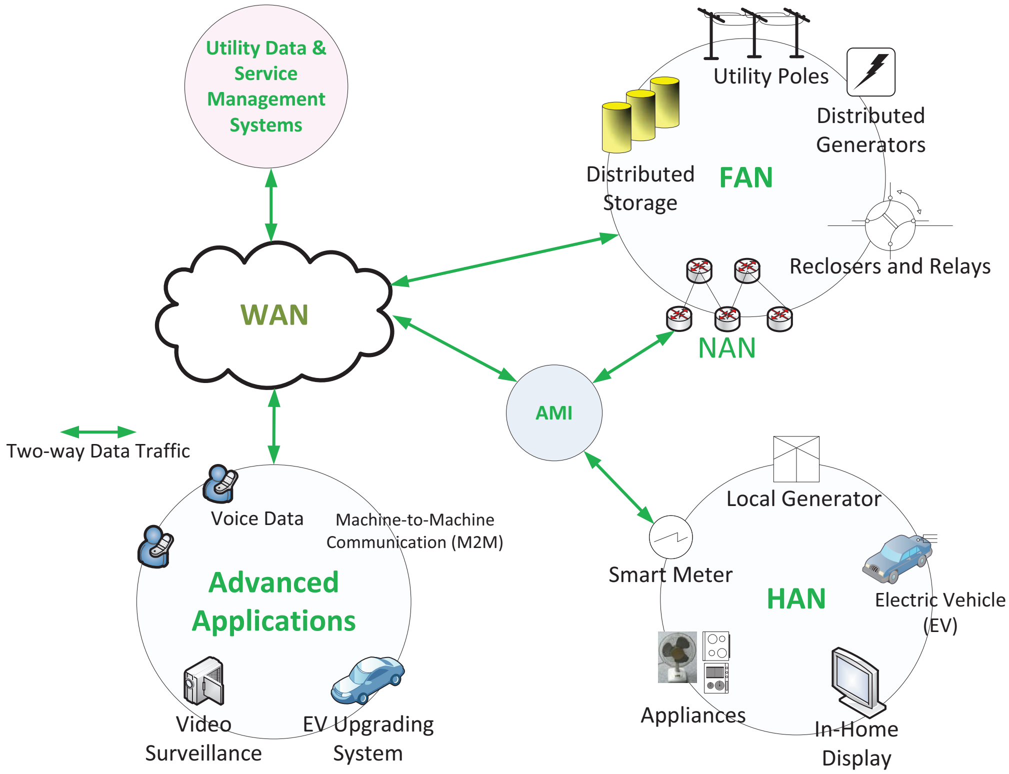

Figure 1.1: Hierarchical architecture of SGCNs.

(AMI). AMI is responsible for monitoring, controlling and protecting the automated devices located in the last mile part of the power grid network. Its main task is to transport the SM traffic to the data acquisition points through the neighbourhood area network and then transmit the aggregated traffic to the utility control center through the wide area network.

These architectural considerations are technology agnostic, and different wired and wireless technologies (often based on existing standards) compete for use in the different smart grid communication network (SGCN) domains, cf. [3, Chapter 5]. Worldwide interoperability for microwave access (WiMAX), smart utility network (SUN) and power line communication (PLC) are important communication technologies that have widely been considered and deployed in support of smart grid applications. The selection of an appropriate communication technology depends on a number of criteria among which the required network coverage and the types of data traffic with their quality of service (QoS) requirements are among the most important. These requirements are specific to the smart grid domain. For instance, HANs cover shorter links compared to FANs and WANs, and scheduling automated devices at home is not as critical as the monitoring, control and protection traffic that occurs in FANs, where incorrect or delayed information can cause major disruptions. Also, environmental characteristics such as user density, which can impact the required network capacity, and network accessibility, considering that some technologies might be unavailable in certain areas, affect the choice of technology.

WiMAX is a 4th generation broadband wireless technology and based on the IEEE 802.16 series of standards. Its features are consistent with the communication and QoS requirements occurring in FAN and WAN implementations. In particular, WiMAX offers long-range coverage, high data rate, and helps to meet the diverse service requirements from smart grid applications through its available set of service types as will be described in Section 1.4.1. On the other hand, SUN is a short-range low-cost technology, based on the IEEE 802.15.4g standard, that provides low data rate and can be used for device to device communication within HANs or NANs. Among the wired technologies, PLC is a cost-efficient solution as it uses the existing power line infrastructure. Depending on the application requirements and the type of the PLC technology (narrowband or broadband) that is considered, PLC can be used for providing the communication infrastructure within different parts of the grid, including HANs, NANs, or AMIs [4].

For the successful operation of the power grid, the data traffic should be received at the destination within the required latency. Hence, it is essential to design the underlying communication infrastructure such that the satisfaction of the QoS requirements namely latency and reliability[1] can best be ensured for different types of smart grid traffic[2]. On the other hand, many communication technologies are not primarily designed for smart grid implementation. In other words, SGCNs have their own specifications which are different from the regular Internet or mobile broadband (MBB) applications. For example, the ratio of the uplink (UL) to the downlink (DL) traffic is much higher in SGCNs and providing the network coverage is mandatory while in other types of applications, it is highly recommended. Accordingly, communication technologies should be configured differently from the case where they used for the implementations of MBB or internet applications.

To this end, NIST priority action plan (PAP) 2 provides a general guideline for assessing different wireless standards for smart grid implementation [6]. It presents different methods including mathematical models, simulation and experiments that can be used for designing and evaluating a viable wireless communication infrastructure for smart grid. All the analysis that have been provided in this guideline is for the case when only meter reading traffic is present. It has accordingly been emphasized that an extension to these types of analysis is essential in order to address the effects of other types of traffic such as the FAN traffic when designing an SGCN. Furthermore, since each wireless technology has its own set of parameters and characteristics, the development of a specific optimized profile configuration for each one is essential for constructing a reliable SGCN.

The WiMAX Forum has also approved a document on system profile require-

[1]Reliability is defined as the probability that a packet can successfully be transmitted to its destination within its required deadline [5].

[2]We note that for bursty applications such as firmware upgrade, throughput may better represent the network performance as it measures the successful arrival of a burst of packets within a certain time unit. For other types of applications such as control, protection and monitoring, since packets are independently generated from each other, according to [5], reliability best illustrates the network performance.

ment [7], also known as WiGrid (WiMAX for smart grid) that provides in depth information on network architecture, system requirements, and smart grid use cases. This document also presents a guideline for creating amendments into the WiMAX configuration in order to address smart grid specific requirements, such as uplink capacity enhancement and security considerations.

There are two types of smart grid traffic classes that are transmitted through the SGCNs namely, mission-critical and non-critical. These two traffic classes are different in their latency and reliability requirements and accordingly, different scheduling schemes are required for ensuring the satisfaction of the QoS requirements associated with these traffic classes. Mahdy *et al.* [8] have investigated the application of time division multiple access (TDMA) for scheduling smart grid traffic. However, scheduling all the traffic through TDMA limits the number of nodes that can access the medium. Gomez *et al.* [9] also investigated the mapping of different service types that has been offered by the WiMAX technology for scheduling smart metering traffic. The extension of this study is necessary so that other traffic such as distribution traffic can also be optimally scheduled and receive the required QoS. Accordingly, in the next chapters of the thesis, the application of different scheduling schemes, such as contention-free and contention-based schemes, is investigated. We then design the SGCN architecture based on the characteristics of these medium access schemes such that the required QoS is ensured.

In order to collect the traffic from thousands of SMs at the utility control center, it is suggested to forward the traffic through intermediary nodes which are known as data acquisition points (DAPs). As verified in [10], the placement of DAPs is beneficial in order to decrease the collision between SM traffic and also to increase the throughput. In a wireless infrastructure, the best possible locations for these DAPs are considered to be on top of the existing utility poles. For a PLC infrastructure, the best possible location is considered to be on the medium voltage side of the existing transformers.

The placement of collector nodes in broadband wireless access networks and sensor networks has previously been investigated [11–14]. However, there is a combination of features and requirements in SGCNs that render the problem sufficiently different from the data collector placement in other types of networks so that a new problem formulation and solution for network planning are needed. For example, in sensor networks, the collector nodes can be placed on selected endpoint nodes [15] or in arbitrary locations [11]. Different from this, in a distribution grid with overhead powerlines, the utility poles are ideal locations for DAP placement [6], since this extends network coverage and also eliminates the cost of new tower installations. Moreover, since the locations of utility poles are determined based on the power grid infrastructure, for example they are often located along roads and thus not uniformly distributed in a coverage area, it is not straightforward to apply the existing placement algorithms to place DAPs in SGCNs. Another major difference is that the on-time delivery of smart grid traffic to the utility control center and automated devices is critical for the correct operation of the electrical power grid [5, 16]. Also, due to the existence of two types of traffic classes namely, mission-critical and non-critical traffic, different scheduling schemes should be employed so that the QoS associated with both traffic classes can be maintained.

Accordingly, the main design considerations for the placement of collector nodes in AMIs are the number and location of DAPs so that 1) the network coverage is ensured, 2) the required reliabilities associated with different types of smart grid traffic classes are satisfied, and 3) existing infrastructures (utility poles, and transformers) are used. Thereby, two types of access architectures from automated devices to DAPs are possible: a) direct and b) multi-hop communication. In this thesis, both single-hop and multi-hop connectivity cases are addressed for wireless and PLC-based AMIs.

The mathematical optimization formulation for DAP placement on top of existing utility poles or transformers is an integer programming (IP) problem and is NP-hard. For cases with small number of nodes, say no more than 200, the IBM CPLEX software [17] and the GLPK solver [18] are typically used for finding optimized node locations. However, for cases with notably larger number of nodes, the development of heuristic algorithms that can find a near-optimal solution within polynomial time is desired [12, 19, 20].

In this thesis, the application of WiMAX, SUN and PLC for different smart grid applications in FAN and AMI is investigated. Our goal is to design the required communication infrastructure, in particular how to configure different system parameters and design the network architecture based on these technologies, such that the network coverage and QoS requirements associated with smart grid traffic can best be maintained. To this end, for the WiMAX technology, the optimized configuration of this WiGrid profile, i.e., the choice of frame duration, type-of-service to traffic mapping, scheduling strategies as well as the system architecture, is investigated. For the SUN and PLC technologies, we investigate the problem of data collector placement on utility poles and transformers such that the QoS requirements are maintained. Accordingly, we derive the latency based on the medium access characteristics of the PLC and SUN technologies. We then propose optimization platforms for efficiently placing data collectors in such a way that the latency and reliability requirements for the smart grid traffic are ensured and also the installation cost is minimized. Finally, we apply the solution of our proposed optimization methods to realistic examples of

SGCNs and evaluate their effectiveness through numerical results.

Based on what has been described above and also to introduce the preliminaries and definitions that are used in the next chapters, the rest of this chapter is organized as follows. We first discuss the set of traffic classes that are respectively transmitted within FANs and AMIs in Sections 1.1 and 1.2. We then describe the specifications and characteristics associated with each of the above-mentioned communication technologies in Sections 1.3, 1.4, and 1.5. Then, the pathloss models and the transmission line theory that are used for respectively calculating the attenuation within a wireless network and the channel transfer function within a PLC network are introduced in Sections 1.6 and 1.7. Finally, the contributions of this thesis are described in Section 1.8.

1.1 FAN Use Cases

In FAN, sensors and automated devices are attached to the distribution network so that the grid can automatically be monitored, controlled and protected. According to [21], the main applications of FANs are defined as follows:

- **Monitoring:** The power grid includes many major elements such as cables, circuit breakers, switches, transformers, etc. In order to be able to predict, detect and quickly respond to hazardous events, we need to monitor the status of the grid elements constantly. Accordingly, sensors need to be mounted on the main grid elements and their data should be collected, analyzed and presented to the operators.

- **Situational awareness:** It consists of the information that has been generated from the sensors, which are attached to the power lines and transformers. These information are not as critical as the one that is collected for the monitoring use case and are usually used for creating a record from the grid status.

- **Control:** This application is used for remotely controlling and configuring electrical devices such as opening a switch.

- **Protection:** The purpose of this use case is to allow for isolation of the electrical devices after a local event has happened. This is done by remote reconfiguration of the system to bypass that device. This is one of the critical use cases for smart grid which requires very low latency.

1.2 AMI Use Cases

Compared to the distribution automation network, different types of traffic are transmitted through the AMI. These traffic classes are usually collected from the SGLM communication network and are divided into two main categories, namely, mission-critical (MC) and non-critical (NC) traffic.

1. **NC traffic** includes the set of traffic classes that do not require very low latency. For example reading the home energy consumption, in a periodic or on-demand manner, is considered as an NC traffic class.

2. **MC traffic** is the set of traffic classes that are critical in their latency requirement. For example, alert notifications, including meter tampering, power theft, remote control commands, and power quality (e.g., voltage, phase or current) notifications [22] are considered as the MC traffic that is transmitted through the AMI. The MC traffic is usually modelled according to a Poisson process [23, 24].

1.3 PLC

PLC uses existing power cables or wires for data communications [25]. It has long been used by electric power utilities for voice and data communication and thus has a proven track record [26]. One of its main advantages when compared to wireless communications is that the communication medium is under the control of the utility. On the negative side, PLC has to cope with harsh transmission conditions, not unlike those experienced in wireless communications. In the recent past, there have been major research, development and standardization efforts towards the use of PLC for smart grid communications, with a focus on low-voltage and medium-voltage distribution grids, e.g., [25–27]. Several industry standards have been consolidated into new ITU-T and IEEE standards. The standards can be roughly classified into broadband (ITU-T 9960/61, IEEE 1901) and narrowband (ITU-T G.9901-G.9904, IEEE 1901.2) systems, which are different in terms of data rate, coverage, and device complexity. The systems have in common that they apply multicarrier modulation, e.g., orthogonal frequency-division multiplexing (OFDM) as the underlying communications technology, which again is similar to the wireless case, e.g., WiMAX and Long Term Evolution (LTE).

Reference [28] provides a survey on the PLC planning and implementations for deploying smart metering infrastructure. The authors present deployment strategies and optimization aspects (such as forward error correction (FEC) strategies and automatic retransmission in medium access control (MAC) layer) of using PLC for smart metering infrastructure. Low voltage and medium voltage architectures with their distinguished specifications such as the topology and their impact on the PLC infrastructure are discussed. For example, different coupler attachment strategies are required for low voltage and medium voltage part of the grid.

In Chapter 5, we develop an AMI based on the PLC, which operates based on the PRIME (ITU-T G.9904) technology. Here, we describe the main properties of the PRIME technology. The PRIME technology operates on the frequency band from 41.992 kHz to 471.6796875 kHz [29] and the maximum obtained data rate is 500 kbps.

1.3.1 MAC Scheme

In PRIME, time is divided into abstract units which are called frames and each frame is divided into smaller units which are called time slots. Each MAC frame in PRIME consists of two access periods, namely contention free period (CFP) and shared contention period (SCP). Two different medium access schemes are defined for scheduling devices within these two periods. The TDMA scheme is used for scheduling devices within the CFP period and the carrier sense multiple access/ collision avoidance (CSMA/CA) scheme is used for scheduling devices within the SCP periods.

The PRIME CSMA/CA model operates with several parameters, namely the number of transmission attempts m, sensing channel count c, the traffic priority p, and the current packet length I. When an SM has a packet with priority p and length I for transmission, it sets $m = c = 0$ and selects a random time slot within the backoff window, $W(m, p)$, with equal probability. If the channel is determined as idle at the selected time slot, the node needs to keep sensing the channel for $C(p) - 1 \doteq p - 1$ additional time slots. Each time that the channel is determined as idle, we increase c by 1. If at any of these assessments the channel is detected as busy, the node waits for I time slots, in order to allow enough time for the ongoing transmission to clear, resets c to 0 and then increments the transmission attempt m and repeats the above backoff and continuous sensing mechanism at the sensing stage $m + 1$. A transmission failure is declared if the sensing stage exceeds the number of available sensing stages, $M + 1$.

1.4 WiMAX

WiMAX is a 4th generation broadband wireless technology based on the IEEE 802.16 series of standards. WiMAX provides flexible broadband links of up to 140 Mbps (20 MHz band and 2x2 MIMO), features low latency (10-50 ms), and supports both fixed (IEEE 802.16d) and mobile (IEEE 802.16e) connections. Depending on the carrier frequency, density of users, and environment, WiMAX can realize long-range connections (e.g., more than 20 km of coverage for a 1.8 GHz link in a suburban area). WiMAX can provide point-to-point or point-to-multipoint wireless backhaul for variety of different smart grid applications. It is one of the standards identified in the NIST smart grid roadmap [30] and many electric utilities including BC Hydro, Hydro One, Power Stream, and Austrian Utility have adopted (or are in the process of adopting) WiMAX solutions for their SGCNs [31–33].

There are several papers on WiMAX SGCNs, e.g. in [9], the authors propose a traffic priority model along with WiMAX configuration setup for serving SGLM access systems traffic. The SGLM network is responsible for transporting data that occurs at the customer side (HAN). The data can either be originated from the energy services interface (ESI) or be towards the ESI. They realized that in order to improve the latency of sporadic traffic over WiMAX air interface, MAC 802.16-Service-Flow-Timeout value should be changed from 15 s to 1000 s. This eliminates the required time for re-initiating the service flow. Furthermore, they have evaluated the performance of their model by providing throughput and latency results for different customer densities. The next step to complete the work accomplished in [9] in the context of WiMAX air interface for smart grid implementation is to analyze the effect of distribution automation traffic. The questions on whether WiMAX is an appropriate selection for distribution traffic and what would be an optimized WiMAX configuration model, architecture, how it should be planned and deployed need to be answered.

1.4.1 QoS in WiMAX

WiMAX offers five classes of service known as

- **Unsolicited grant service (UGS)**: This type of service is for periodic traffic which transports fixed-size data packets and is critical in its latency and rate requirement. The bandwidth is guaranteed and assigned on a periodic basis. Therefore, no control messages are required for bandwidth assignment and the overhead is minimized.

- **Real-time polling service (rt-PS)**: This type of service is designed to reduce overhead for periodic traffic of variable size by reserving resources to transmit bandwidth requests (BRs). It is used for time critical traffic.

- **Extended real-time polling service (ert-PS)**: The operation of this type of service is similar to the UGS. However, the unsolicited grants can be used for the transmissions of both BRs as well as data. Thus, in case of changing the bit rate requirement, the request for new bandwidth can be transmitted via available unsolicited grants.

- **Non-real-time polling service (nrt-PS)**: This type of service is usually used for serving non-critical traffic as traffic is polled rarely and a minimum bandwidth is guaranteed.

- **Best effort (BE)**: In this type of service, no resource is allocated to the user, and BRs are transmitted by contention or piggybacking.

1.5 IEEE 802.15.4g (SUN)

SUN has been standardized under the IEEE 802.15.4g. It is the amended version of the wireless personal area network technology, known as ZigBee. SUN has specifically been designed to address the requirements of the smart utility network applications. Automated devices equipped with this technology, are used for monitoring and controlling the grid. The collected information is transmitted to the utility control center and it is also used for point-to-point communication between the devices placed on the grid. Three types of physical layer technologies have been defined for SUN, namely multi-rate and multi-regional frequency shift keying (MR-FSK), multi-rate and multi-regional-OFDM (MR-OFDM), and multi-rate and multi-regional offset quadrature phase-shift keying (MR-O-QPSK). This technology operates on licensed, e.g., 1.4 GHz and 2.4 GHz and non-licensed frequency bands, e.g., 901 MHz and 915 MHz. The typical data rate is around 200 kbps.

In this thesis, we assume that the IEEE 802.15.4g operates based on the OFDM physical layer. There are 4 options defined for the OFDM-based physical layer, which are different in terms of the number of active tones and their nominal bandwidth. The channel bandwidth ranges from 50 kHz up to 1094 kHz. All devices shall support the binary phase-shift keying (BPSK) and QPSK modulation and coding schemes but the support of the 16 quadrature amplitude modulation (QAM) scheme is optional. Considering different modulations and coding schemes, the channel data rate ranges from 50 kbps to 800 kbps.

1.5.1 MAC scheme

The IEEE 802.15.4g MAC protocol provides two types of medium access periods, namely CFP and contention access period (CAP), within each frame. A node stores the MC and NC traffic in different queues, and schedules the MC traffic through the CFPs using the TDMA scheme, and the NC traffic within the CAP timeslots using the CSMA/CA scheme.

Under the slotted CSMA/CA model, each node with the NC traffic, at each transmission attempt, would sense the channel at most $M+1$ times. At each sensing stage $m = 0, 1, \cdots, M$, it selects a random time slot within the backoff window, W_m, with equal probability. According to the IEEE 802.15.4g standard, in slotted CSMA/CA model, each node should identify the channel as idle for two consecutive slots before changing to transmission mode.

1.6 Pathloss Models

In this subsection, we describe two pathloss models that are typically used for estimating the attenuation within a wireless SGCN.

1.6.1 COST231-Hata Pathloss Model

This is a well-known pathloss model that is used for estimating the propagation loss in a wide-area communication network, that operates on the frequency range from 1500 MHz to 2000 MHz. The base station (BS) antenna height should be larger than the average roof top height, around 30 m to 200 m and the subscriber antenna height should be around 1 m to 10 m. The pathloss model is given by [34]

$$\begin{aligned}\mathrm{PL(dB)} &= 46.3 + 33.9\log_{10}(f) - 13.82\log_{10}(T_h) - a(R_h) + \\ &\quad \big(44.9 - 6.55\log_{10}(T_h)\big)\log_{10}(d) + 0.7R_h + C, \end{aligned} \tag{1.1}$$

where d is the path length in km, f is the frequency in MHz, and variables T_h and R_h are respectively the BS and TS antenna heights in m. For urban environments, $C = 3$ dB and

$$a(R_h) = 3.2\log_{10}^2(R_h) - 4.97, \tag{1.2}$$

whereas for suburban environments, $C = 0$ dB, and

$$a(R_h) = (1.1\log_{10}(f) - 0.7)R_h - 1.56\log_{10}(f) - 0.8). \tag{1.3}$$

1.6.2 Erceg Pathloss Model

According to [34], Erceg is one of the most applicable pathloss models that can be used for computing signal attenuation within rural and suburban areas. This model is interesting for SGCNs as the empirical measurements are taken from the areas that have specifications similar to what is desired by utility companies. The applicable frequency range is between 1800 MHz to 2700 MHz. The Erceg pathloss model is obtained as [34]:

$$\mathrm{PL(dB)} = 20\log_{10}\left(\frac{4\pi d_0}{\lambda}\right) + 10\left(c_0 - c_1 T_h + \frac{c_2}{T_h}\right)\log_{10}\frac{d}{d_0} + 6\log_{10}\frac{f}{2000} - c_3\log_{10}\frac{R_h}{2}, \tag{1.4}$$

where λ is the wavelength in meters, $d_0 = 100$ m, and c_0, c_1, c_2, c_3 are defined for each terrain type in Table 1.1.

Table 1.1: Erceg Parameters [34]

Parameter	c_0	c_1	c_2	c_3
Terrain Type A (Hilly with moderate to heavy tree density)	4.6	0.0075	12.6	10.8
Terrain Type B (Hilly with light tree density, or flat with moderate to heavy tree density)	4.0	0.0065	17.1	10.8
Terrain Type C (Flat with light tree density)	3.6	0.0050	20.0	0.0

1.7 Preliminaries on Transmission Line Theory

PLC channel modelling has usually been based on measurements and curve matching considering individual links, cf. e.g. [35, 36]. This is a perfectly valid approach when testing physical layer designs, which depend on link-characterizing parameters such as attenuation, frequency selectivity, delay spread, etc. Moving to the next level of system design, i.e., evaluation of PLC networks, a different approach for channel modelling is needed in order to capture the deterministic dependencies between different link qualities. We note that these dependencies are a result of PLC signal propagation being guided by power lines, which is a decisive difference to wireless communications, for which links between different network nodes can often be assumed independent. A methodology that is suitable for modelling mutually dependent channels in a PLC network is based on transmission line theory (TLT). This methodology relies on the knowledge of the topology, the cables/wires, and the load characteristics of the power grid underlying the PLC systems. Several works have contributed to and made use of TLT for PLC channel modelling, cf. e.g. [26, 37–42]. In TLT, power lines and all passive power-grid elements (e.g., loads, transformers, etc.) connected to it are represented as two-port networks described by their ABCD- or S-parameters. This modelling approach is immediately applicable to two-conductor networks, or it can be

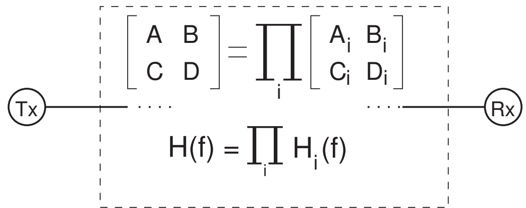

Figure 1.2: Illustration of the use of transmission line theory to compute transfer functions.

used as an approximation for multi-conductor transmission lines, cf. e.g. [25, Ch. 2].

Figure 1.2 illustrates the basic approach when analyzing a link between a PLC transmitter (Tx) and a PLC receiver (Rx) using TLT. We assume a tree-network structure and place all network elements on the path between Tx and Rx. Using the impedance carry-back method [40], the electricity grid between Tx and Rx can be transformed into a cascade of shunt impedances and other two-port networks. This cascade can then be combined into one overall ABCD matrix via multiplication of the ABCD matrices of the individual two-port networks of the cascade (see Figure 1.2). From this, the overall CTF from Tx to Rx is computed as

$$H_{\mathrm{s}}(f) = \frac{Z_{\mathrm{L}}}{AZ_{\mathrm{L}} + B + Z_{\mathrm{s}}(CZ_{\mathrm{L}} + D)} \;, \tag{1.5}$$

where Z_{s} and Z_{L} are the source and load impedance of Tx and Rx, respectively. If the transfer function without coupling losses is considered, then

$$H(f) = \frac{Z_{\mathrm{L}}}{AZ_{\mathrm{L}} + B} \;. \tag{1.6}$$

Alternatively, the transfer function can be computed as the product of the transfer functions $H_i(f)$ for the individual two-port networks of the cascade (see Figure 1.2), which are obtained similar to (1.6). Since (1.6) includes the impedance at the output of a two-port network, in this method one needs to traverse from Rx towards Tx, and the impedance used in (1.6) is updated at the ith two-port as

$$Z_{\text{in},i} = \frac{A_i Z_{\text{in},i+1} + B_i}{C_i Z_{\text{in},i+1} + D_i} \, . \tag{1.7}$$

In the case that the two-port networks connecting the shunt impedances are line pieces, (1.6) and (1.7) can also be compactly written in terms of reflection coefficients, cf. e.g. voltage-ratio approach proposed in [40]. The advantage of the second approach is that the ABCD matrix calculation is eliminated and the computational effort has been reduced. Thus, we have used the voltage-ratio approach for computing the CTF in our PLC module implementation, which has been described in Appendix A.

1.8 Contributions

In Chapter 2 of this thesis, the optimized configuration of WiMAX technology is investigated for smart grid applications. In particular, the optimized selection of frame duration, system architecture, service-type-to-traffic-mapping and scheduling schemes are investigated. We also develop a WiGrid module based on network simulator-3 (NS-3) software[3] [43], through which the optimized configuration of WiMAX technology for smart grid is evaluated. Finally, we develop a priority-based scheduler that first schedules the higher priority traffic from all the nodes, before proceeding with serving the lower priority ones. We also devise an inter-class scheduling scheme that prioritizes the bandwidth assignment to the traffic with lower remaining latency and higher current data rate.

In the process of devising an optimized profile configuration of wireless and wired

[3]NS-3 is a discrete event network simulator, which is used for emulating the behaviour of computer networks that operates based on the characteristics of the wired or wireless technologies.

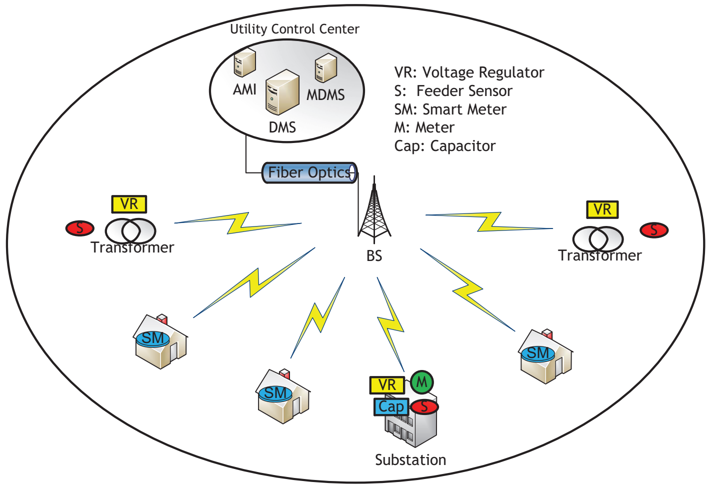

(a)

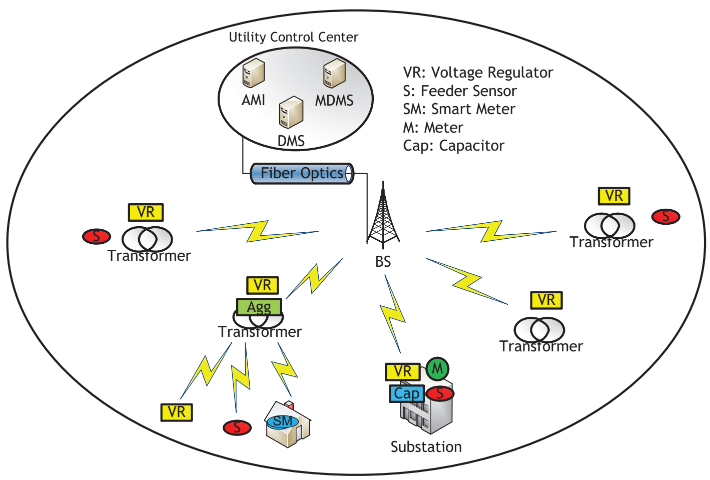

(b)

Figure 1.3: FAN architecture: (a) Direct Access Mode, (b) Aggregation Mode.

communication technologies for smart grid, we compare the performance of two access methods via which automated devices and SMs can transmit their data to the utility control center. These access methods as illustrated in Figures 1.3(a) and 1.3(b) are respectively direct access and aggregation mode [10, Figure 2]. In the direct access mode, all automated devices transmit their information directly to the BS, which backhauls the data to the utility control center. On the other hand, in the aggregation mode, a data aggregator, which is also known as a DAP, is responsible for collecting the traffic from several automated devices and forwarding it to the BS. We show that the second access method is more beneficial in terms of experiencing lower latency and higher packet success ratio. Hence, in the next chapters of the thesis, we concentrate on the aggregator architecture and investigate how to implement this architecture, i.e., what is the minimum required number of DAPs and where they should be placed, such that smart grid QoS requirements are maintained and also a cost-efficient infrastructure is obtained.

In Chapters 3-5 of this thesis, we solve the optimized DAP placement problem based on the specifications of two communication technologies. In Chapters 3 and 4, we assume that smart meter to smart meter and smart meter to data collector connections operate based on the characteristics of the 802.15.4g technology. In Chapter 5, we assume that the SGCN operates based on the characteristics of the PLC technology. We also solve the DAP placement problem for two types of access from smart meters to data collectors. In the first scenario, we consider the single-hop access of smart meters to the data collectors. In this case, we use a modified version of the K-means algorithm for efficiently placing DAPs on top of the existing utility poles while ensuring only the network coverage. In the second case, we allow the multi-hop access from smart meters to the DAPs while ensuring not only the network coverage but also the latency satisfaction. The multi-hop communication gives us the benefit of accessing more remote devices while requiring less number of DAPs. In order to ensure the latency satisfaction, we develop a delay model based on the characteristics of the MAC protocol of the 802.15.4g technology. The MAC protocol of the

SUN technology offers two medium access schemes namely: CSMA/CA and TDMA schemes. We use the CSMA/CA scheduling scheme for scheduling the non-critical traffic and TDMA for scheduling the mission-critical traffic. In order to estimate the experienced latency, we devise a Markov chain model so that we can track the nodes states in the backoff process and accordingly, we can compute the probability of latency satisfaction. For the TDMA scheduling scheme, we use the binomial distribution in order to compute the probability that the traffic of all the nodes connected to the same channel can be scheduled within the latency requirement. Finally, we devise a new analytical model for placing DAPs in a SGCN that operates based on the characteristics of the PRIME PLC technology. The devised analytical model is completely different from the one that we have first proposed for modelling the MAC protocol of the 802.15.4g technology. This is because the PRIME PLC technology operates based on the characteristics of the prioritized CSMA/CA scheduling scheme, where the traffic with lower priority should wait for a larger back off duration in order to access the medium. It should also find the channel as idle for a larger number of times, before proceeding with the packet transmission. In the PRIME PLC technology, when the node finds the channel as busy, it freezes the channel sensing for the duration of the packet size and if it finds the channel as idle, it should keep sensing the channel as idle for p consecutive times where p is the traffic priority. Overall, all these differences together necessitate the development of a new analytical model for computing the probability that the packet can be transmitted within the latency.

On the other hand, the placement of DAPs on top of the existing utility poles or transformers is an integer programming problem and is NP-hard. Accordingly, the development of heuristic algorithms is necessary in order to avoid the exponential time complexity that is needed for solving this problem. Therefore, in Chapters 3, 4, and 5 of this thesis, we devise heuristic algorithms for placing DAPs in respectively single-hop and multi-hop wireless and PLC AMIs while ensuring the network coverage and the satisfaction of the latency requirements for two types of mission-critical and non-critical smart metering traffic. We then compare the performance of our algorithms, in terms of optimality and time complexity, with the solution of the IBM CPLEX software for small-scale scenarios and with a lower bound for larger-scale ones.

Chapter 2

Optimized WiMAX Profile Configuration for Smart Grid Communications

2.1 Introduction

The viability of WiMAX technology for NANs and FANs has been investigated in the literature, several field trials [44, 45], and recent surveys [46, 47]. Under the umbrella of the NIST PAP2 guideline [6], range and capacity analyses have been conducted for different usage models to give some insights of the capability of WiMAX technology for backhauling smart metering traffic. References [48] and [49] consider a heterogeneous wireless local area network (WLAN)-WiMAX technology for collecting and backhauling smart metering traffic. This allows for extending the network coverage and improving the link quality. Aguirre *et al.* [50] formulate the capacity provided by WiMAX in order to estimate the number of SMs that can be served using this technology. References [10] and [51] investigate the performance of WiMAX technology considering different sets of FAN applications and network architectures.

The aforementioned works and others such as [52–54] generally confirm that WiMAX is a viable choice for FAN and NAN applications. Furthermore, it is implied that when wireless technologies are designed for smart grid implementation, they should be configured differently than when used for MBB applications for which they were originally designed. Pertinent discussions in the literature include [9], [53] and [49], which propose a type-of-service to traffic mapping for smart metering via WiMAX, and optimize the BS transmission power, respectively.

In light of this, the WiMAX Forum has defined a new system profile based on the IEEE 802.16 series of standards considering smart grid requirements [55]. This so-called WiGrid profile is developed in a two-phase approach known as WiGrid-1 and WiGrid-2. In the first phase, the advantages of the current features that already exist in the IEEE 802.16e and IEEE 802.16m standards are taken into account. The typical configuration of these features is modified considering smart grid network characteristics and requirements. In the second phase, the advantages of the existing amendments developed in the IEEE 802.16p and IEEE 802.16n standards, respectively, designed for enabling machine-to-machine (M2M) communication and increasing the network reliability for WiMAX networks, are taken into account. An overview of these two standard amendments has been presented in [56], where smart grid is recognized as one of the use cases which requires both greater network reliability and M2M communication. In the second phase, these two standards will further be amended with features specifically designed for SGCNs. So far, the WiMAX Forum has mostly focused on the first phase of the WiGrid development and suggested several modifications to the current WiMAX configuration. These modifications are summarized in the "WiMAX Forum System Profile Requirements for Smart Grid Applications" [21]. They include a dynamic time division duplexing (TDD) UL/DL ratio from 1 to 1.75 and the support of 64 QAM transmission.

In this chapter, we focus on the first phase of the WiGrid development and optimize the configuration and/or implementation method for several existing WiMAX features namely, frame duration, type-of-service to traffic mapping, and scheduling solution. This optimization is conducted such that the key QoS requirements namely, latency and reliability, for SGCNs are best met. In particular, our main contributions are summarized as follows.

1. We identify the characteristics and requirements associated with each smart grid traffic class and devise a scheduling solution such that on-time and reliable arrival of mission-critical traffic can better be assured. The devised scheduler also ensures that the traffic is fairly collected from automated devices within the same traffic class.

2. We investigate an optimized configuration of the above-mentioned WiMAX features under what we call "profile configuration". Different profile configurations are compared by considering both smart metering and distribution automation traffic. The latter is different from most of the literature, which only focuses on smart metering traffic, e.g., [6, 9, 22, 47–49].

3. We present a WiGrid NS-3 module [57] to facilitate the simulation of SGCNs for both the academic research and industry case studies around the world. Using this module, we evaluate the performance of the developed WiMAX profile configurations for smart grid communication scenarios with realistic parameters for the number of automated devices and their associated data traffic patterns based on [21] and [58].

The rest of this chapter is organized as follows. In Section 2.2, we discuss the advantages of using WiMAX technology for implementing SGCNs. In Section 2.3, the paradigm for optimized profile configuration for WiGrid is developed. In Section

2.4, the amendments that have been applied to the NS-3 environment in order to develop the WiGrid module are explained. In Section 2.5, WiGrid simulation results are presented and discussed. Finally, conclusions are provided in Section 2.6.

2.2 Advantages of Using WiMAX Technology for Smart Grid Implementation

According to the research conducted by [59–61], the utility applications supported by the 4^{th} generation (4G) LTE is limited compared to that of the 4G WiMAX technology. The implementation cost of the 4G WiMAX technology is lower and it has a better spectrum availability [59]. Furthermore, certain SG applications such as the protection requires the support of the layer 2, which is not provided through the solution of LTE technology. In addition, if third party networks are used for SG implementation, utilities need to pay monthly fees for each leased connection, which can lead to high operating costs. Accordingly, to avoid long term costs, being able to manage the network configuration and also to ensur high reliability and the satisfaction of the quality of service requirements, utilities typically prefer to build their own dedicated network [60].

In addition to the above-mentioned differences that favour the use of WiMAX for SG implementation, the WiMAX Forum has also developed a system profile requirement for SG traffic, which is called WiGrid-1. In WiGrid-1, the existing characteristics of the WiMAX technology has specifically been amended in order to address the QoS required for smart grid traffic. In particular, since smart grid traffic is uplink centric, the WiMAX Forum has adjusted the uplink downlink ratio such that the transmission of the uplink traffic is favored. Furthermore, to avoid the cyber security attacks within smart grid infrastructure, the integrated end-to-end security model in WiMAX technology has been enhanced. The new WiMAX system profile also supports the direct base station to base station communication for supporting the transmission of the Goose messaging and also the protection traffic which requires low latency [59].

2.3 Optimized WiMAX Profile Configuration

Considering the first phase of the WiGrid development, in this section we discuss the effects and selection of WiMAX frame duration (Section 2.3.1), types-of-service to traffic mapping (Section 2.3.2), scheduling (Section 2.3.3), unsolicited grant allocation scheme (Section 2.3.4) and system architectures (Section 2.3.5) for communication in smart grid FANs.

2.3.1 Frame Duration and Latency

In WiMAX, the physical layer frame is divided into a DL subframe and an UL subframe. Possible values for the total frame duration depend on the type of physical layer. In the OFDM physical layer, the frame duration can be either 2.5, 4, 5, 8, 10, 12.5, or 20 ms. For orthogonal frequency-division multiple access (OFDMA), 2 ms is also possible [62]. Although seven or eight different values can be considered for frame duration, 5, 10 and 20 ms are most commonly used in network configurations. This is because larger frame durations cause less fragmentation and consequently, less resources are wasted. The 20 ms frame duration is however not recommended for smart grid communication as the resources are not given fast enough for several latency-critical applications. On the other hand, scheduling resources in a relatively short frame duration of 5 ms is challenging especially when the network is almost fully loaded. Therefore, depending on the network load and the required latency for the defined applications we suggest using either a 5 ms or a 10 ms frame duration.

Table 2.1: Traffic classes and their properties and QoS requirements [21]

Flow ID[4]	Traffic class	Direction	Packet size (Bytes)	Data rate (kbps)	Active/idle (s)	Latency (ms)	Traffic Type	**Proposed scheduling type**
0	Situational awareness	UL	256	5.0	1/5	1000	Deterministic	**nrtPS**
1	Monitoring	UL	384	300	Continuous	100	Deterministic	**UGS**
2	Control	UL	128	5.0	1/5	100	Random	**rtPS**
3	Protection	UL	192	150	Continuous	20	Random	**ertPS**
4	Smart	UL	256	1.0	0.1/4.0	5000	Deterministic	**BE**

[4] For the simpler presentation of the results in Section 2.5, we have defined flow IDs to numerically refer to each traffic class.

	metering							
5	Situational awareness	DL	256	1.0	1/5	1000	Deterministic	**nrtPS**
6	Monitoring	DL	128	10.0	Continuous	100	Deterministic	**UGS**
7	Control	DL	128	1.0	1/5	100	Random	**rtPS**
8	Protection	DL	192	150	Continuous	20	Random	**ertPS**

Table 2.2: Appropriate Type of Service for Different Applications

Application Type (CBR/VBR)	Latency Requirement	Reliability	Appropriate Scheduling Type
CBR	low	high	UGS
VBR	low	high	rtPS
VBR	very low	high	ertPS
CBR/VBR	intermediate	intermediate	nrtPS
CBR/VBR	relaxed	intermediate	BE

2.3.2 Mapping WiMAX Scheduling Types to Smart Grid Traffic Classes

WiMAX offers five types of services namely unsolicited grant service (UGS), real-time polling service (rtPS), extended rtPS (ertPS), non-real-time polling service (nrtPS) and best effort (BE) to support multiple levels of QoS that are needed for serving traffic classes with different characteristics and requirements [63]. In this part, we discuss how the offered WiMAX scheduling types should be used in order to address the requirements associated with FAN applications. The characteristics of FAN traffic classes are adopted from [21] and presented in Table 2.1. The last column of this table will be explained in the following.

The UGS scheduling type is inherently suitable for serving constant bit rate (CBR) applications as it provides fixed-sized grants periodically. Furthermore, since UGS guarantees the bandwidth, it is a suitable choice for traffic that requires low latency and high reliability. Therefore, we choose the UGS scheduling type for serving the monitoring traffic which is a CBR application and requires low latency.

Whenever we have a real-time variable bit rate (VBR) traffic that requires low latency and high reliability, rtPS scheduling type can be used for serving such an application where the required bandwidth is requested through the available unicast request opportunities. For example, rtPS can be used for serving control application which is a real-time VBR traffic that requires 100 ms latency.

However, rtPS can hardly satisfy the much lower latency and higher reliability requirements associated with, e.g., protection applications compared to control traffic. This is because when rtPS scheduling type is used, many data requests should be transmitted, which adds to the latency and bandwidth overhead. In this case, we suggest using ertPS by reserving bandwidth according to the current maximum data rate associated with the traffic flow. When needed, a change of the size of UL allocations can be requested through available unicast opportunities provided by the BS, which can be used for both data transmission and bandwidth requests [63].

As the nrtPS scheduling type offers unicast request opportunities rarely, it is suitable for serving the traffic that requires partial bandwidth guarantee. Therefore, we use the nrtPS scheduling type for serving situational awareness traffic that is relaxed in its latency requirement while still requiring a latency lower than that for smart metering traffic. Since the BE scheduling type mainly offers contention-based request opportunities, it is suitable for serving the traffic with non-sensitive delay requirement such as firmware upgrades or smart metering traffic. We have also provided a general guideline in Table 2.2 which shows when to use each scheduling type for serving different types of applications.

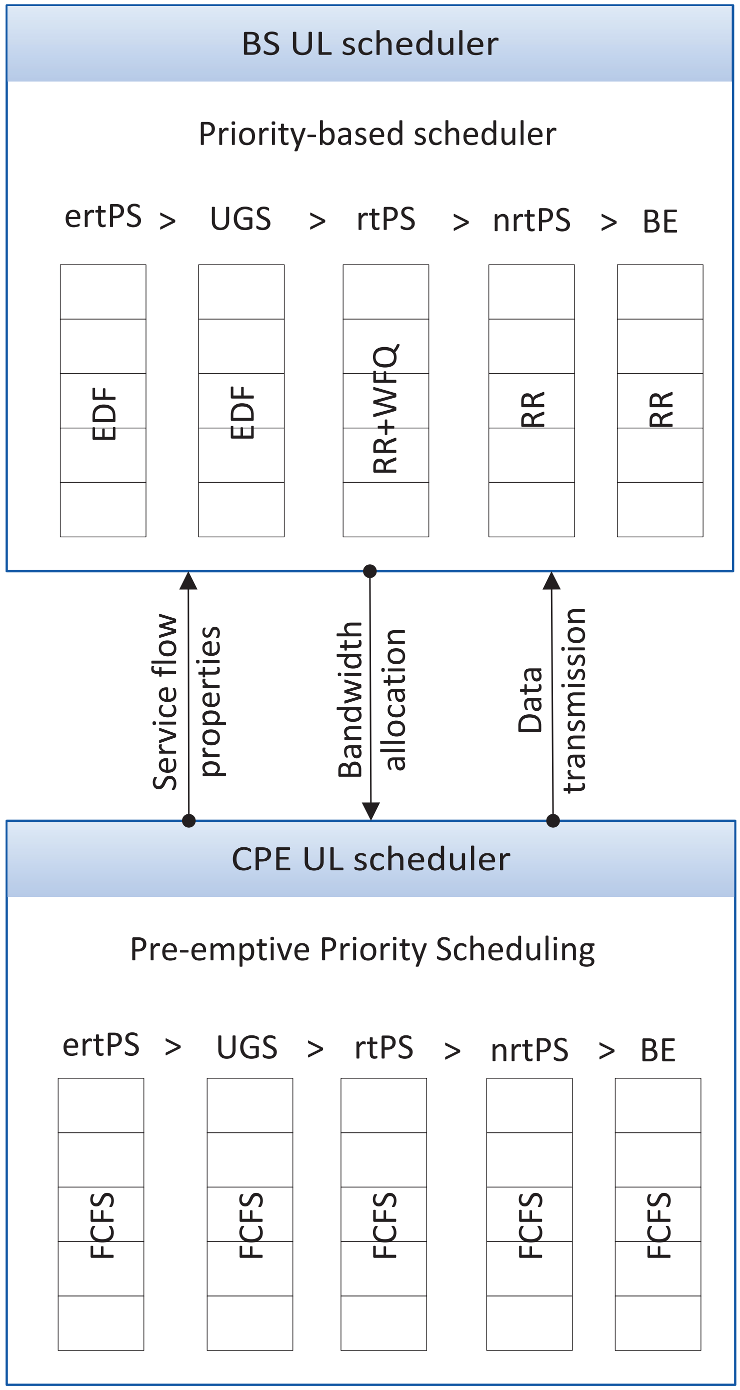

Figure 2.1: Proposed WiGrid scheduling framework.

2.3.3 Scheduler

The IEEE 802.16 standard allows vendors to implement their own schedulers in the BS and CPE devices. The BS allocates bandwidth to the CPE devices according to their connection properties. However, the user itself decides how to distribute this bandwidth among its service flows [64]. Generally, the schedulers at both the BS and CPE devices are composed of two steps: 1) inter-class scheduling and 2) intra-class scheduling methods [65]. Figure 2.1 illustrates the scheduling framework we have developed for WiGrid.

1) Inter-class Scheduling Policy: As the arrival of certain traffic classes, specifically protection and monitoring, are essential for the survivability of the power grid, we employ a priority-based scheduling strategy as the inter-class scheduling methods in both BS and CPE devices. The priority-based scheduler considers the scheduling type priorities across all the nodes with the following order: ertPS $>$ UGS $>$ rtPS $>$ nrtPS $>$ BE, where A $>$ B means scheduling type A is served before type B. In addition, a pre-emptive policy is employed by the CPEs so that by the arrival of a higher priority traffic, the transmission of a lower priority one stops immediately.

2) Intra-class Scheduling Policy: Since protection and monitoring are both receiving unsolicited grants and they require low latency, we apply an earliest deadline first (EDF) scheduling policy to advance serving traffic flows with earlier deadline. Since rtPS control traffic follows a random distribution and it also requires low latency, we poll it in a round-robin (RR) manner and serve it according to a weighted fair queueing (WFQ) scheduling policy so that no service flows are starved and at the same time, we give a higher weight to the service flows with earlier deadline and currently higher rate. For more details on the implementation of WFQ, please refer to Section 2.4 (item number 3). As the situational awareness and smart metering are deterministic traffic with low priorities, we give them a fixed bandwidth in an RR manner only if bandwidth is still available after serving the higher priority flows.

2.3.4 Unsolicited Grant Allocation Strategies

Two different algorithms namely average (AVG) and Grant/Interval have been proposed in the literature for allocating unsolicited grants to the service flows. Here, we compare the advantages and disadvantages of each method for SGCN and then, we propose the appropriate grant size that should be given to the service flows when Grant/Interval allocation algorithm is used.

1) Average (AVG) allocation algorithm: In this method, in every uplink subframe a fixed amount of resource is assigned to the connection [66]. The grant size is computed according to the minimum reserved traffic rate configured for the flow as

$$\begin{aligned} GrantSize(Byte) &\doteq BytesPerFrame \\ &\doteq MinReservedTrafficRate(bps) \\ &\quad \times FrameDuration(s)/8. \end{aligned} \tag{2.1}$$

As the AVG algorithm distributes the grants over all frames, fitting the whole packet would not be possible in the small grant size of each frame. Therefore, many packet fragmentations may occur, especially for low data rate traffic. This would in turn cause a large latency and low throughput. The AVG algorithm may also cause resource wastage since it allocates grants every frame ignoring the fact that there might be no data available for transmission.

2) Grant/Interval allocation algorithm: To overcome the fragmentation problem in the AVG algorithm, we suggest using the Grant/Interval algorithm which allocates larger grants based on the packet size and the traffic generation interval. This means that in every interval, a grant equal to the packet size is given to the service flow [63]. However, if the interval is less than one frame duration, the amount of generated data per frame would be more than one packet size and therefore, every frame a grant equal to the generated data size should be allocated for the service flow. In summary, we propose to allocate the grant size as

$$GrantSize = \begin{cases} BytesPerFrame, & \text{if } Interval < \\ & \quad FrameDuration, \\ PacketSize, & \text{otherwise.} \end{cases} \tag{2.2}$$

The Grant/Interval algorithm is more complex to implement compared to the AVG algorithm, since a timer is required for tracking the interval. Despite its complexity, there are several advantages associated with this algorithm. Firstly, it maximizes the bandwidth utilization through allocating the grants whenever needed. Furthermore, in order to avoid undesired latency, the BS can be provided with the synchronization information of the application in CPE so that the grants can be scheduled at appropriate frames [63]. According to the above discussion, we conclude that the Grant/Interval allocation algorithm is suitable for SGCNs that have several critical low data rate traffic classes.

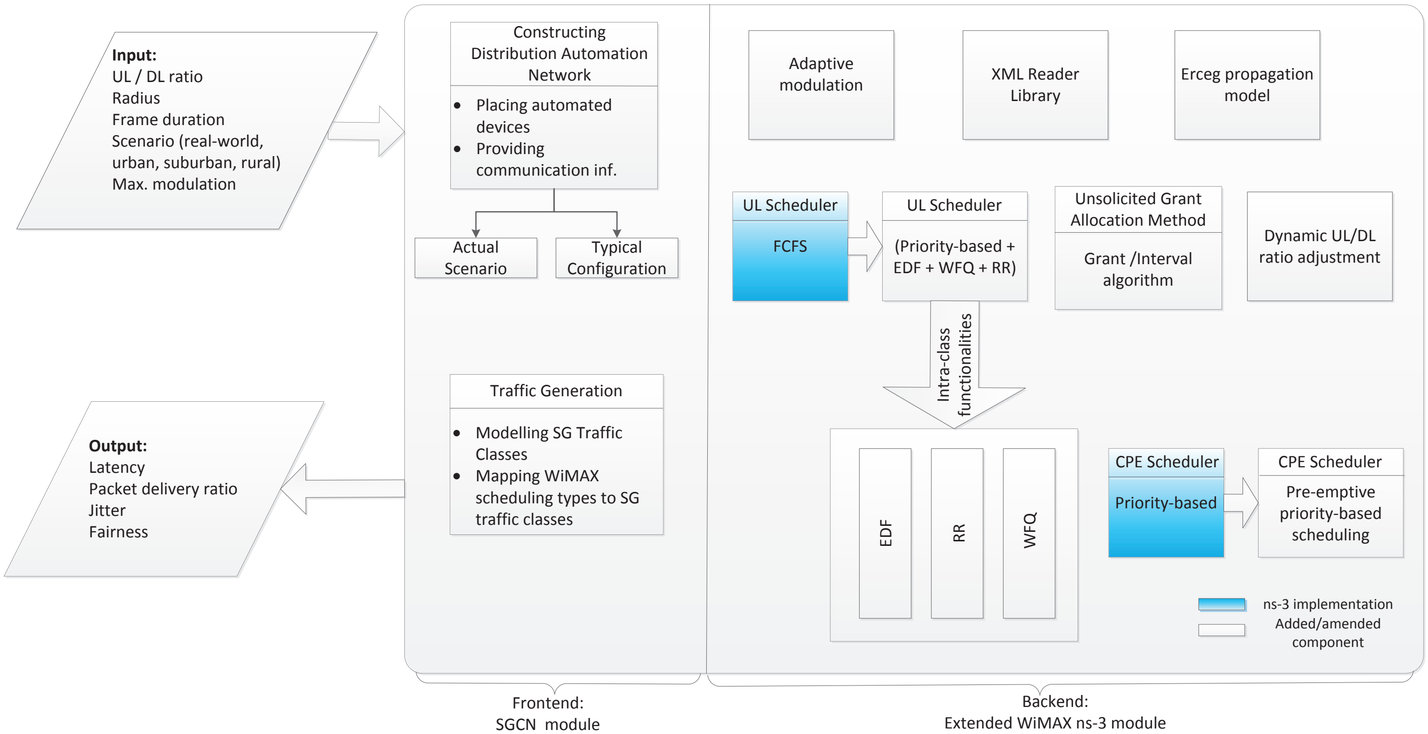

Figure 2.2: The WiGrid NS-3 module.

2.3.5 Architecture

As discussed in Chapter 1, there are two possible modes through which automated devices can transmit their information to the utility control center in a FAN: direct access and aggregation mode [10, Fig. 2]. Although the aggregator architecture is more costly and harder to deploy, it has the following merits concluded from our previous study [10] compared to the direct access mode for smart grid implementation.

1) The obtained throughput is often higher, since there are fewer active connections to the BS and therefore the collision and packet loss probabilities decrease.

2) The case that collisions among active connections to the BS happen can be dealt with better [67]. The solution for collision avoidance is to back-off and decrease link data rates. In direct access mode, the data rate associated to each device is already low and lowering it further does not make much difference. However, since the aggregate data rate is higher, decreasing it can resolve congestion faster.

3) A larger number of nodes can be supported. This is because of the data compression that is usually conducted at the data aggregators as well as the better link qualities experienced by data aggregators mounted for example, on top of transmission-line poles, and also automated devices as their link distances are decreased.

The above advantages make the aggregation mode a preferable choice for SGCNs with plenty of low data rate automated devices.

2.4 Amendments for a WiGrid Module

We have developed a software module based on the WiMAX module of the NS-3 [68, 69] which can be used for performance studies and capacity planning of WiGrid systems.

The features of this module are illustrated in Figure 2.2. The WiGrid simulator consists of a front-end SGCN module and the back-end extensions made into the WiMAX module of the NS-3.

The front-end interface constructs an SGCN topology and communication infrastructure based on the user's input. The user can either ask for a typical rural, suburban or urban scenario, or pass an XML file containing the network information of a certain actual scenario. In the typical case, the numbers of automated nodes and SMs located in each area type are set according to the BC Hydro distribution automation implementation plan [58]. Similarly, all related configurations for the base station and automated devices such as transmission power and antenna height are taken from smart grid projects conducted by BC Hydro and Powertech Labs Inc. The traffic within distribution automation networks is modelled according to the traffic patterns given by [21] and as shown in Table 2.1. Further details on this are given in Section 2.5.

The specific enhancements made into the backend module are as follows.

1) We have defined a new setSubFrameRatio function which accepts an arbitrary UL/DL ratio as an argument. This function can be called at the start of each frame for dynamic UL/DL ratio adjustments.

2) We have implemented the priority-based scheduler together with the intra-class scheduling policies at the uplink scheduler of the BS as discussed in Section 2.3. Figures 2.3(a) and 2.3(b) respectively show the flowcharts of the existing first-come first-serve (FCFS) and the new priority-based uplink schedulers in NS-3. As can be seen in the figure, at each step of the FCFS algorithm, the record of the node[5] that has registered its service flows earlier is chosen and then all its service flows are

[5] The node's record contains the information about all the node's service flows that have already been registered at the BS.

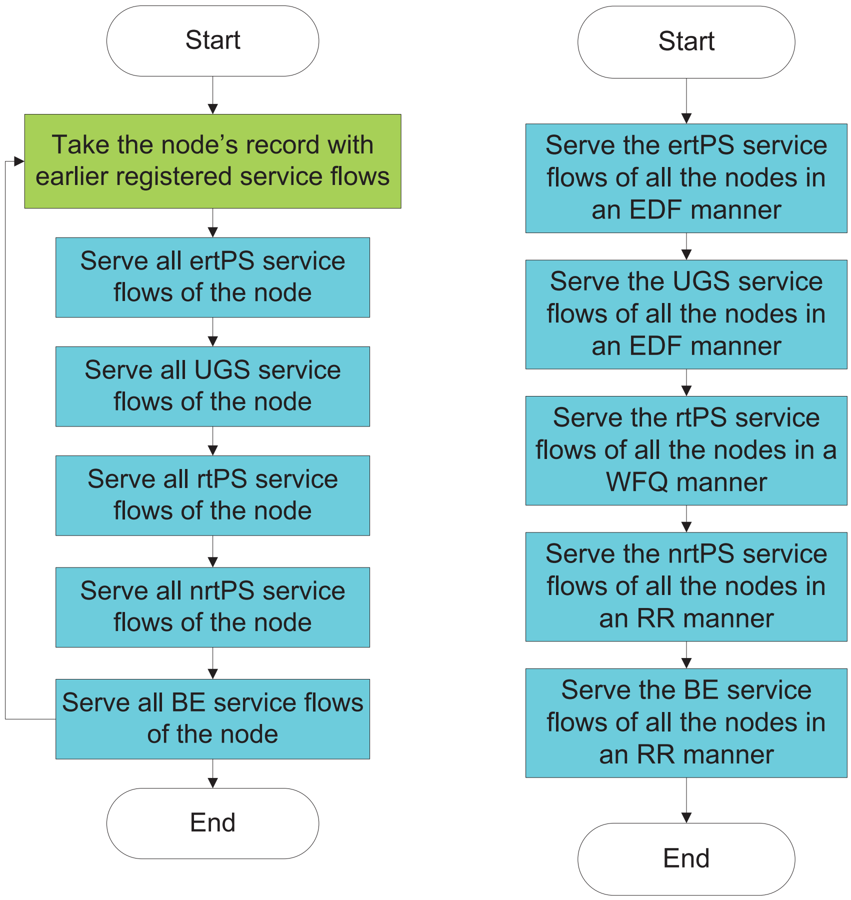

(a) (b)

Figure 2.3: The flowcharts of the (a) FCFS and (b) priority-based UL schedulers.

scheduled according to ertPS > UGS > rtPS > nrtPS > BE. In the priority-based scheduler, the service flows with the same scheduling type (starting from ertPS) from all nodes are stored in a priority queue and served according to its related intra-scheduling policy. Then, the algorithm conducts the same procedure for the service flows of other scheduling types across all the nodes with the order mentioned above.

3) In order to implement WFQ among rtPS service flows, we apply the following procedure. First, we allocate the bandwidth to the users whose latencies are going to expire in the next frame duration. For the remainder, we employ the same scheme

as proposed in [69]. In particular, the bandwidth requests from all CPE devices are added together. In case the size of the total bandwidth requests is greater than the remaining bandwidth for allocation, the difference is divided by the number of users and deducted equally from all the requesters. Hence, it is ensured that no service flow is starved and also more bandwidth is allocated to the service flow with higher current rate.

4) For allocating unsolicited grants to the traffic, we implement the Grant/Interval algorithm instead of the original NS-3 AVG algorithm. The size of the grants are determined according to Equation (2.2).

5) Adaptive modulation is not supported in the current NS-3 version. As smart grid devices are usually fixed, we assume that the channel quality stays constant and therefore, we assign each device with a constant reliable modulation at the start of the program based on its signal-to-noise ratio (SNR) characteristic. Modulation and coding rate can be selected according to the required reliability, see e.g. [5].

6) Network specifications are usually given in XML files. To this end, we have created an automatic XML reader library which reads the XML tags from the file and passes the extracted network characteristic data such as modulation, antenna height, transmission power and coordinates into the simulator.

7) The NIST PAP2 guideline [6] recommends the Erceg SUI propagation model to emulate the signal attenuation for the rural and suburban scenarios. Therefore, the implementation for this propagation model has been added to the NS-3 WiMAX module.

In addition to the modifications described here, several errors including incorrect configuration of node properties in the COST231 propagation model, incorrect mapping of SNR to block-error rate (BLER) and incorrect frame length computation have been corrected. The modified NS-3 module and the detailed list of fixed bugs and extensions has been made available at [57].

2.5 Simulation Results and Discussion

In this section, we apply the considerations and methods from Section 2.3 and use our developed simulator from Section 2.4 to quantify the effects of different system parameters to characterize an optimized WiGrid profile configuration for FAN scenarios in SGCNs.

Latency and reliability are key QoS requirements for SGCNs [45,70,71]. Therefore, we first compare the performance of different profile configurations in terms of average latency and the percentage of packets that are reliably received by the destination for different traffic classes. We also study the capability of each WiGrid-1 feature in terms of the reliability improvement that can be obtained considering different numbers of automated devices. Finally, we evaluate the fairness index for each traffic class using our proposed scheduling algorithm. Note that simulation results for comparing the direct and aggregator architectures are provided in [10].

2.5.1 Simulation Settings

We consider rural and suburban distribution networks within a circular area of 2 km radius for simulations. Typical numbers of automated nodes and SMs located in this area obtained from the BC Hydro distribution automation implementation plan [58] and the NIST PAP2 document [6], respectively, are summarized in Table 2.3 with a categorization according to the use cases from Table 2.1. Table 2.4 summarizes the default signal propagation and system settings considered for the following results. In this table, RS+CC/CC refers to Reed Solomon with convolutional

Table 2.3: Major use case categories and associated device classes and number of devices in a circular area of 2 km radius according to [6, 58]. Due to the scaling considering the area size, the number of automated devices for some use cases are float.

Use case and devices	Number of devices	
	Rural	Suburban
Monitoring	**$\approx$ 16**	**$\approx$ 32**
Recloser	6	9
Capacitor fixed	2	3
Regulator	1	1.5
Fault Circuit Indicator	5	15
Feeder meter	1	3
Feeder sensor	0.6	0.6
Situational Awareness	**$\approx$ 8**	**$\approx$ 18**
Powerline/Transformer sensor	3/2	5/4
Capacitor Switched	3	9
Control	**$\approx$ 10**	**$\approx$ 18**
Recloser	6	9
Capacitor switched	2	6
Regulator	1	1.5
Feeder sensor	0.6	1.6
Protection	**$\approx$ 3**	**$\approx$ 11**
Recloser	3	4.5
Automated switch	0	6
Smart Metering	**$\approx$ 120**	**$\approx$ 3350**

coding/inner-checksum coding [63].

The traffic classes listed in Table 2.1 are modelled according to the following

Table 2.4: Default settings for WiGrid simulations

Scenario	Suburban
Path Loss	Erceg Type-B [6]
Fading	Rayleigh
Scheduler	FCFS
Unsolicited Grant Allocation	Grant/Interval
UL/DL Ratio	1.75
Bandwidth	10 MHz
Phy Layer	OFDM
Modulation	64 QAM
Number of Sectors	3
Duplexing	TDD
FEC Code Rate/Type	3/4 / RS+CC/CC
Frame Duration	10 ms
Architecture Type	Aggregation

assumptions. The NS-3 on/off applications are used for all traffic classes. For deterministic traffic, constant values for the on-time and off-time periods are considered. In order to model the random traffic, the packet inter-arrival time (off-time) follows an exponential distribution where the mean is equal to either the idle period (e.g. for flow IDs 2, 7) or the $PacketSize/DataRate$ (e.g. for flow IDs 3, 8). It should also be noted that for the random traffic there is a small probability that the packet arrival rate exceeds the available resources. In that case, the scheduling of packets is delayed beyond the latency requirement.

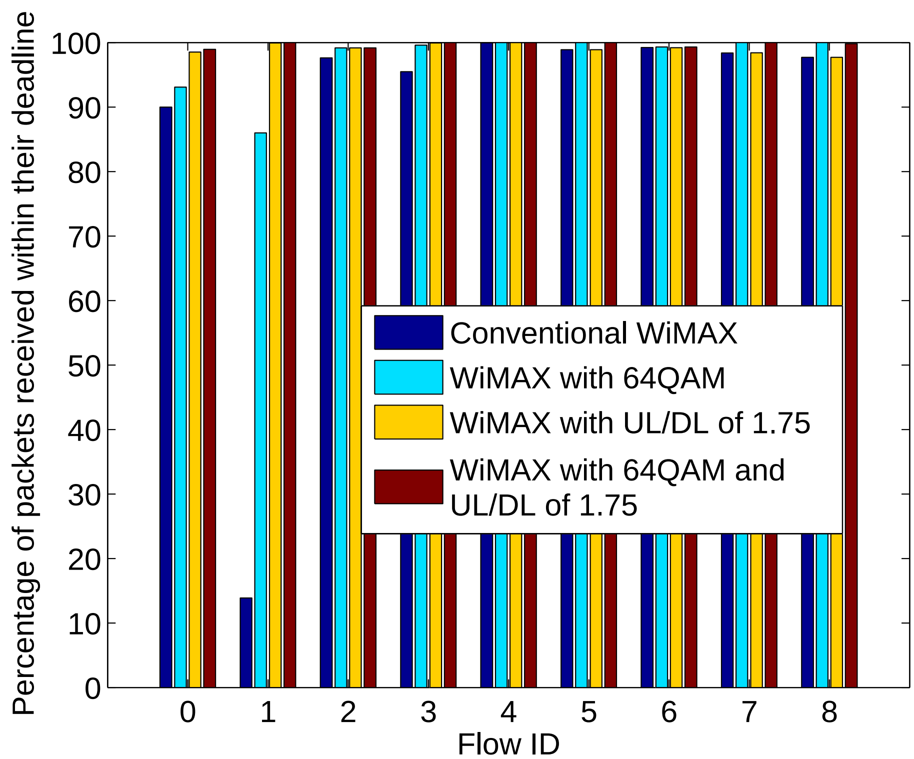

Figure 2.4: The effect of WiGrid amendments on the percentage of packets correctly received within the deadline.

2.5.2 UL/DL Ratio and Modulation Type

In conventional WiMAX, support of modulation types higher than 16 QAM is optional and the UL/DL ratio is typically configured to be close to 1. As discussed in Chapter 1, because of the larger UL traffic in SGCNs, a UL/DL ratio of 1.75 and the support of 64 QAM has been proposed by the WiMAX forum. In order to investigate the effect of these amendments on WiGrid performance, we consider the following four scenarios: i) a conventional WiMAX configuration (maximum supported modulation of 16 QAM and UL/DL ratio of 1), ii) WiMAX with support of 64 QAM, iii) WiMAX with UL/DL ratio of 1.75, and iv) WiMAX with both amendments. Figure 2.4 shows the results in terms of the percentage of packets that are correctly received within their deadline. As can be seen, the support of 64 QAM modulation increases the percentage of packets that are reliably received for both UL and DL. The increase is more significant for flow ID 1 (monitoring) which has a high data rate traffic and is associated with a higher number of automated devices. Increasing the UL/DL ratio to 1.75 also increases the percentage of packets received in the UL without compromising the DL traffic. The UL improvement due to increasing the UL/DL ratio is somewhat more pronounced compared to that when supporting a higher modulation, since it also benefits the nodes that are farther from the BS. An increase in the packet reception is also noted for flow ID 0 when both amendments are applied. For the other flows, only slight improvements are achieved with a UL/DL ratio of 1.75 and WiMAX supporting 64 QAM.

2.5.3 Scalability and Supporting Higher UL/DL Ratio and Modulation Type

Figure 2.5 illustrates the improvement of timely packet delivery that can be obtained when either resource efficiency is increased or more resources are allocated for the uplink transmission. We observe that the improvement is more significant when a higher UL/DL bandwidth ratio is applied. This is due to the uplink dominated traffic in SGCNs and the fact that the required bandwidth for remote nodes can only be provided when a higher UL/DL bandwidth ratio is employed. We also note that as the number of nodes increases, the rate of improvement decreases which indicates the bandwidth saturation for a certain number of nodes.

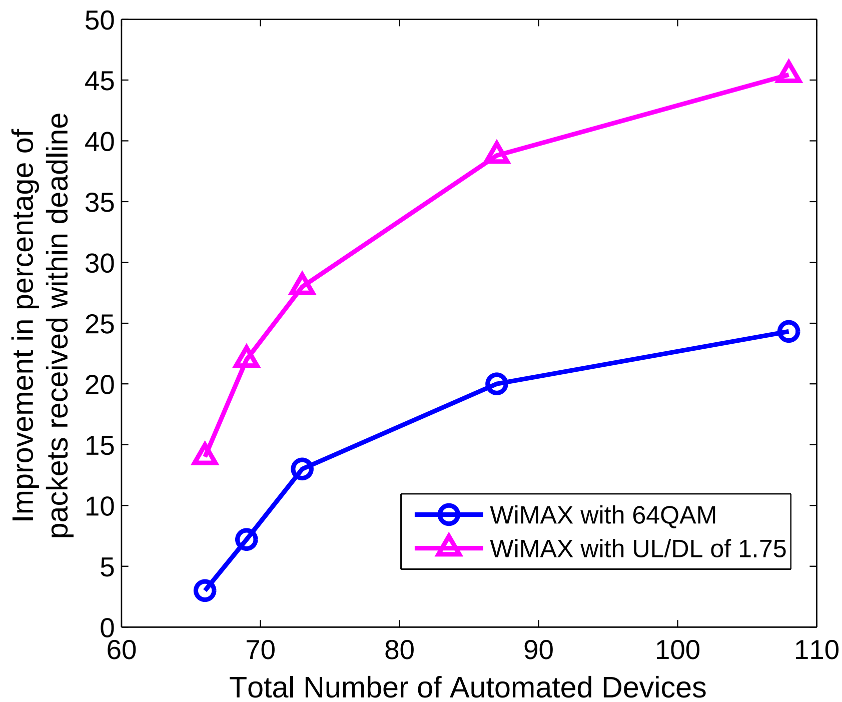

Figure 2.5: Comparing the effect of 1) supporting 64 QAM and 2) increasing UL/DL bandwidth ratio to 1.75 for the improvement of the packet delivery ratio for different numbers of automated devices.

2.5.4 Frame Duration

We now turn to the effect of different frame durations on the performance in terms of the experienced latency, latency variation and the percentage of reliably received packets. The results for the rural scenario are shown in Figure 2.6, and for the suburban scenario in Figures 2.7 and 2.8. Error bars in Figures 2.6 and 2.7 indicate the latency variations. Focusing on the rural scenario, we first note that almost all packets are received successfully (more than 99% for all service flows) under both frame durations[6]. However, as can be seen in Figure 2.6, latencies decreased notably when a 5 ms frame duration is employed. This is because of the faster allocation

[6]As the received percentages for all service flows for this case are almost the same and more than 99%, the result figure is omitted.

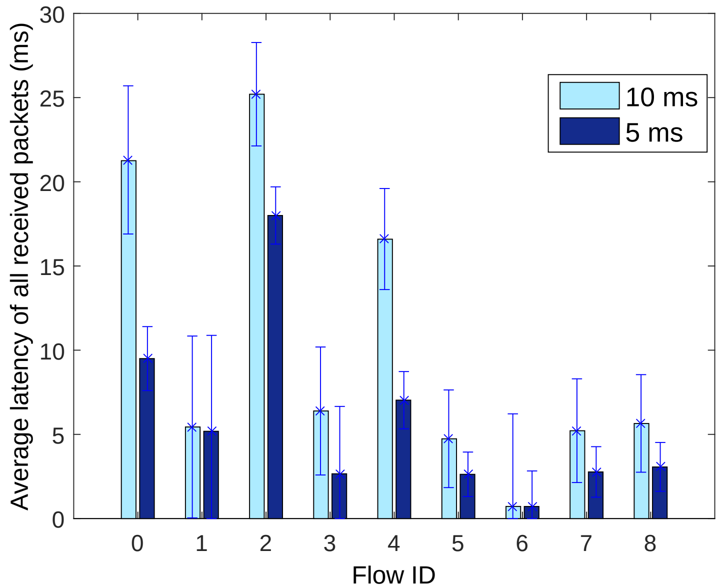

Figure 2.6: The effect of different frame durations on average latency for the rural scenario. The error bars indicate delay variations.

of resources in the case of shorter frame duration, which causes service flows to experience less waiting time when they request bandwidth. Turning now to the suburban scenario with higher device density and thus traffic demands, it can be seen from Figures 2.7 and 2.8 that the network can easily become overloaded and suffer from high latency and delay variation (e.g. flow ID 1[7]) and packet loss (e.g., flow IDs 1 and 3) if the relatively short frame duration of 5 ms is used. This is due to the fact that fewer number of grants are available in each frame, leading to frequent packet fragmentation. We conclude that the 10 ms frame duration is preferred for heavily loaded FANs as considered in the suburban scenario. We also note that the delay variations for all flows in stable scenarios (suburban with 10 ms and rural with both frame durations) are small.

[7] Flow ID 0 experiences 400 ms latency which is still within the deadline.

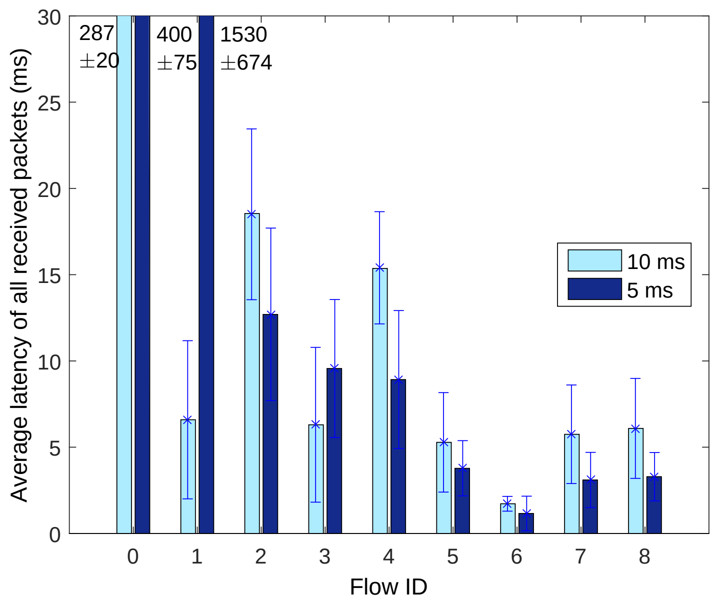

Figure 2.7: The effect of different frame durations on average latency and delay variations for the suburban scenario. We note that due to the scaling of the figure, the latency values for flow IDs 0 and 1 are written as text beside to their latency bars. For example, flow ID 0 experiences 287 ms latency with 20 ms delay variation when traffic is transmitted using 10 ms frames.

2.5.5 Unsolicited Grant Allocation Strategies

The different allocation methods for scheduling unsolicited grants, presented in Section 2.3.3, are now compared considering the rural FAN scenario. Figure 2.9 shows the percentage of reliably received packets for the AVG and Grant/Interval allocation algorithms for the rural scenario. We observe that the AVG algorithm causes packet loss for the traffic in flow IDs 1 and 3. The AVG algorithm wastes resources through allocation when there is no traffic. Furthermore, the required grants are distributed over all the UL subframes, so that only a few symbols are granted at each UL subframe. This causes extra overhead due to packet fragmentation. This is prevented by the application of the Grant/Interval algorithm in the scheduler implementation, which thus appears to be preferable.

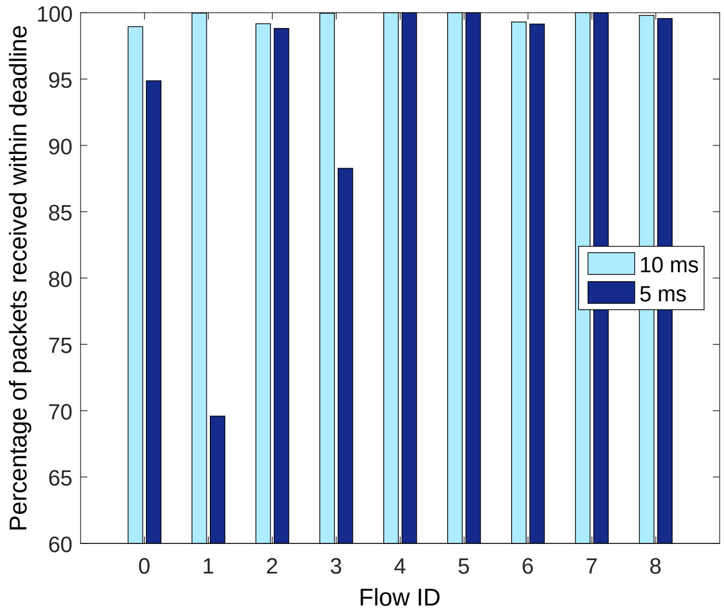

Figure 2.8: The effect of different frame durations on the percentage of packets correctly received within their deadline for the suburban scenario.

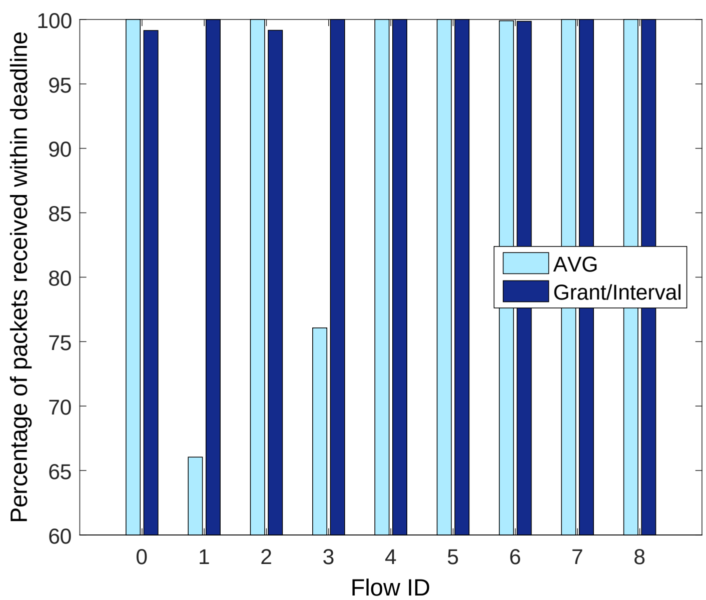

Figure 2.9: Comparing AVG and Grant/Interval unsolicited grant allocation strategies.

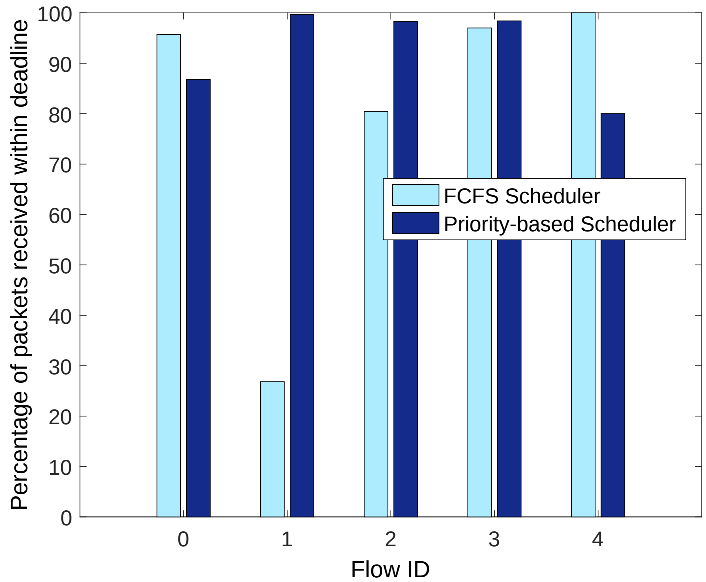

Figure 2.10: Comparing FCFS and priority-based uplink schedulers for the suburban scenario with radius of 2.2 km.

2.5.6 Comparing two Schedulers

Finally, in order to show the importance of scheduling smart grid traffic classes based on their priorities, we consider a higher load circular suburban area of 2.2 km radius where the number of monitoring nodes is increased to 39. As can be seen in Figure 2.10, the priority-based scheduler at both the BS and CPE devices improves the percentage of the packets that are reliably received for higher-priority flow IDs, namely flow IDs 1 (UGS), 3 (ertPS) and 2 (rtPS) by de-prioritizing lower-priority ones, namely flow IDs 0 (nrtPS), and 4 (BE). We have also computed the fairness indices that can be obtained from both schedulers according to Jain's fairness index [72] and compared them in Table 2.5. Fairness here is defined as the percentage of packets that have successfully delivered to the destination from each automated device. We observe that the intra-scheduling methods we have employed in the priority-based scheduler notably improve the fairness among different automated devices. For exam-

Table 2.5: Fairness indices for the FCFS and priority-based schedulers

Scheduler / Flow ID	0	1	2	3	4
FCFS	1.0	0.78	0.86	0.98	1.0
Priority-based	0.99	1.0	0.97	1.0	1.0

ple, the EDF scheduling method we have applied for scheduling monitoring traffic, flow ID 1, ensures the latency satisfaction of the packets originated from different devices. The marginal difference seen for flow ID 0 is due to the logic of the priority-based scheduler, which de-prioritizes lower priority traffic and therefore, a few nrtPS nodes did not receive the same bandwidth as others.

Table 2.6: Optimized profile configuration for the FAN traffic

Scheduler	Priority-based
Unsolicited Grant Allocation Strategy	Grant/Interval
Maximum Supported Modulation Type	64 QAM
UL/DL Ratio	1.75
Frame Duration	5 ms (normal load, rural), 10 ms (high load, suburban)
Traffic Class	**Scheduling Type**
Situational awareness	nrtPS
Monitoring	UGS
Control	rtPS
Protection	ertPS
Smart metering	BE

We conclude from the above scenarios that the combination of all the optimized features as summarized in Table 2.6 leads to an optimized profile configuration that better meets the latency and throughput requirements of FAN traffic.

2.6 Conclusions

In this chapter, an optimized WiMAX profile configuration that consists of the selection of scheduling strategies, type-of-service to traffic mapping, and frame duration was investigated. Our conceptual considerations were complemented through simulations enabled by modifications to the WiMAX NS-3 module that includes WiGrid amendments. Our numerical results for two SGCN scenarios suggest that a 5 ms frame duration is advisable for rural areas while, for higher density areas a 10 ms frame duration is suggested as it can still satisfy network requirements but avoids many packet fragmentations that would occur with a shorter frame duration. We have also shown that priority-based scheduler is consistent with smart grid objectives where the reliable reception of mission-critical traffic must be assured.

Chapter 3

Cost-Efficient DAP Placement for a Single-Hop AMI

3.1 Introduction

From the discussion provided in the previous chapter, we observed that the aggregator architecture outperforms the direct transmission. Accordingly, within the next chapters of the thesis, we focus on the development of the aggregator architecture based on different communication technologies. In this chapter, we solve the problem considering a simple scenario, where only single-hop communication is allowed. We construct the infrastructure once based on the WiMAX technology and once based on the 802.15.4g SUN technology. The two infrastructures are compared in terms of the implementation cost and the required number of data collectors (DAPs). In the next chapter, we devise a new approach for developing the wireless aggregator architecture considering a more complicated scenario, where multi-hop communication from devices to the data collectors are allowed and also the latency requirements for different types of smart grid traffic are maintained. Finally, in Chapter 5, we derive a new analytical method and devise a new network planning solution for developing the aggregator architecture based on the physical and medium access control characteristics of the PLC technology.

Figure 3.1 illustrates a possible metering infrastructure with DAPs using wireless

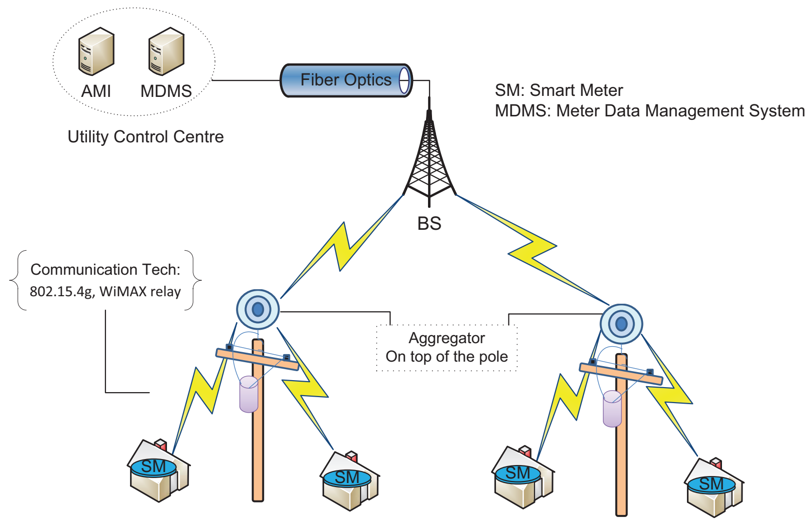

Figure 3.1: Aggregation model in the AMI for a smart grid.

communications to collect data from a set of SMs. For power distribution networks with overhead powerlines, utility poles are ideal locations for DAP placement. This helps to eliminate the cost of new tower installations as well as getting extended coverage for wireless systems. For example, Canada's BC Hydro mounts DAPs on top of the existing poles [73]. Accordingly, an interesting challenge is the *pole selection* for DAP placement. In particular, the required number of DAPs should be minimized while providing sufficient network coverage.

The mathematical optimization formulation for DAP placement on top of existing utility poles is an integer programming (IP) problem and is NP-hard. For cases with small number of nodes, say no more than 200, the IBM CPLEX software [17] and the GLPK solver [18] are typically used for finding optimized node locations. However, for cases with notably larger number of nodes, a heuristic algorithm needs to be developed [12, 19, 20].

Reference [74] provides a distributed minimum packet forwarding algorithm for finding suitable locations at which packet aggregation for a certain destination should be performed in order to minimize transmission cost. It assumes a mesh infrastructure in which aggregation can be performed at the SM itself. This however is not usually the case in AMI, where aggregation is done at separate nodes. Optimal DAP placement problem can also be viewed as a facility location problem [75]. The objective is to minimize facility costs, which depend on the opening (installation) price of facilities as well as how nodes are assigned to the facilities, for example based on the their distance. Since finding the optimal configuration in a facility location problem is NP-hard in general, heuristic algorithms such as K-means and K-median [76] or convex relaxations [77] have been applied for solving this type of problem.

Kekatos *et al.* [77] consider a convex relaxation for the placement of K phasor measurement units (PMUs) on smart grid buses such that the network's synchronization error is minimized. The algorithm is designed according to the PMU-specific functionalities, such as the sampling rate, and assumes a fixed K. In the context of cellular networks, a two-phase combined genetic and K-means algorithm has been used for the optimal placement of radio ports in order to minimize the maximum pathloss experienced by the worst case users as well as minimizing the average pathloss tolerated over the entire set of users [78]. The genetic algorithm provides the initial placement of the radio ports, then K-means is used for updating the initial solution and obtaining the optimal locations.

In this chapter, in order to compute the required number of DAPs and optimally select their locations for a single-hop communication infrastructure, we apply a modified version of the K-means algorithm. To this end, we adapt K-means algorithm and optimize both installation and transmission cost. Minimizing the transmission cost is especially beneficial for the black out scenarios when SMs should operate based on their own batteries. As a main constraint, we restrict the locations of DAPs to be from a set of existing utility poles. Additional constraints is derived from the network coverage.

To validate our proposed algorithm, we run extensive simulations based on smart metering parameters presented in [6]. We also compare the results of our solution in small scenarios to the optimal solution obtained from brute-force search, which demonstrates a near-optimal performance of the proposed method.

The rest of this chapter is organized as follows. Section 3.2 introduces the details of system model. The DAP placement problem is derived in Section 3.3, followed by the solution of this problem using the K-means algorithm in Section 3.4. Performance results are presented and discussed in Section 3.5. Finally, Section 3.6 concludes this chapter.

3.2 System Model

Consider a distribution grid using overhead distribution lines suspended from utility poles delivering electricity to homes or businesses equipped with SMs. Some utility poles host DAPs, each of which is wirelessly connected to a subset of the SMs. The DAPs themselves are also wirelessly connected to a utility center (UC). To model this, let us consider a network of N_{SM} SMs, K DAPs and one UC, and assume that N_{poles} utility poles are located within this network. The (2D) locations of SMs, utility poles, and the UC are known and given by $\mathcal{SM} = \{\boldsymbol{s}_i\}_{i=1,\cdots,N_{SM}}$, $\mathcal{P} = \{\boldsymbol{p}_j\}_{j=1,\cdots,N_{\text{poles}}}$, and $\boldsymbol{u}$, respectively, whereas the value of K and the location of DAPs, $\mathcal{A} = \{\boldsymbol{a}_k\}_{k=1,\cdots,K}$, are to be optimized. The SMs and DAPs can be equipped with different communication technologies such as WiFi, WiMAX, IEEE 802.15.4 (ZigBee), and the 802.15.4g standard specifically developed by IEEE for smart utility networks (SUNs) [79]. The number of SMs is obtained based on their densities for different environments using [6]

$$N_{SM} = \rho_{SM} \pi r^2,$$

where r is the radius of the area-of-interest (AoI) and ρ_{SM} is the SM density in that area. The value of ρ_{SM} depends on the AoI being rural, urban or sub-urban [6].

3.2.1 Data Aggregation Model

DAPs are placed on top of the utility poles, and their task is to collect the data from SMs and send them to the UC. In this chapter, we assume a one-hop communication from SMs to the DAPs (SM-DAP) and from DAPs to the UC (DAP-UC). We note that single-hop communication is of interest for the cases that minimum latency is desired.

DAPs also combine and compress the received data from SMs before transmission to the UC. We denote the compression ratio by C_r. The value of C_r can be between 1/2 to 2/3 depending on correlation between data and the algorithm employed in the DAP [80].

Different numbers of SMs, from a few up to 2000 [6], can be connected to one DAP. Usually, a relatively large number of SMs can be supported by a single DAP due to the low frequency and amount of data messages sent from the meters. In the following, we denote the maximum number of SMs that can be connected to one DAP by $N_{\max}$. Furthermore, we define the ratio between the number of available utility poles and the number of SMs in a given service area as $\varrho = \frac{N_{\text{poles}}}{N_{SM}}$. It is reasonable to assume that for a denser environment (e.g. an urban area), a utility pole contributes to the energy distribution over a larger number of SMs, and hence, ϱ is smaller.

3.2.2 Transmission Model

We assume that the SMs adjust their transmission power P_{tx} according to the link reliability to ensure that they can connect to the DAP with a given transmission success probability. The energy consumed for transmitting B bytes of data over distance d can be represented as

$$E_{\mathrm{tx}} = 8\ B\ \gamma\ E_{\mathrm{b}}\ \eta\ PL(d)\ , \tag{3.1}$$

where γ is the ratio of the total power consumption in the modem and the power consumed for transmission, E_{b} is the required received energy per bit, η is the fading margin, and $PL(d)$ represents the pathloss at distance d. The pathloss can be modeled as

$$PL(d) = PL(d_0)\left(\frac{d}{d_0}\right)^{\alpha}\ , \tag{3.2}$$

where $PL(d_0)$ is the pathloss at the reference distance d_0 and α is the pathloss exponent. Note that the factor 8 in (3.1) accounts for B being packet size in bytes and E_{b} denoting energy per bit.

3.3 Problem Formulation

Given the DAP and transmission model above, we now formulate the DAP placement problem. The basic objective is to select a subset of pole locations from $\mathcal{P}$ to install DAPs on top of them such that required number of DAPs is minimized while providing radio coverage for all SMs. This objective minimizes the installation cost, which is defined as the purchase and labor price for the initial placement of a DAP. In addition, we are interested in minimizing the communication cost, which we measure in terms of the consumed energy for transmitting data. Note that the power model (3.1) implies a transmission cost proportional to d^α, which we consider a more realistic model compared to the transmission-cost function being linear in d adopted in [81].

Assume that the network is supposed to work for a duration of T_m. To mathematically formulate our cost function, let a denote the installation cost (in dollars) of one DAP. The total installation cost, c_{inst}, is then a times the number of poles selected for DAP placement. Also, let g denote the energy price (e.g., the price for consuming 1 kWh of energy). Then, the transmission cost can be computed as

$$c_{tx} = gE_{\mathrm{tx}}\frac{T_m}{T_I} \; , \tag{3.3}$$

where T_I is the time interval between the transmissions, so that the third term represents the total number of transmissions that one SM sends during T_m.

For radio coverage we require each SM to be connected to at least one DAP, which means that the SM-DAP distance needs to be smaller than the SM transmission range d_{pmax}. Furthermore, up to a maximum of $N_{\max}$ SMs can be connected to a single

DAP. Hence, the DAP-placement problem can be written as

$$\begin{aligned}
\underset{\{x_i\},\{y_{ij}\}}{\text{minimize}} \quad c_{inst} + c_{tx} \quad &= \sum_{j=1}^{N_{\text{poles}}} a x_j \\
&+ b \sum_{i=1}^{N_{\text{SM}}} \sum_{j=1}^{N_{\text{poles}}} y_{ij}(PL(d_{ij}) + C_r PL(d'_j)) \qquad (3.4a)
\end{aligned}$$

subject to

$$d_{ij} \leq d_{\text{pmax}}, \qquad 1 \leq i \leq N_{\text{SM}}, 1 \leq j \leq N_{\text{poles}} \qquad (3.4b)$$

$$d'_j \leq d_{\text{umax}}, \qquad 1 \leq j \leq N_{\text{poles}} \qquad (3.4c)$$

$$\sum_{j=1}^{N_{\text{poles}}} y_{ij} = 1, \qquad 1 \leq i \leq N_{\text{SM}} \qquad (3.4d)$$

$$\sum_{i=1}^{N_{\text{SM}}} y_{ij} \leq N_{\text{max}}, \qquad 1 \leq j \leq N_{\text{poles}} \qquad (3.4e)$$

$$y_{ij} \leq x_j, \qquad 1 \leq i \leq N_{\text{SM}}, 1 \leq j \leq N_{\text{poles}} \qquad (3.4f)$$

$$x_j \in \{0, 1\}, \qquad 1 \leq j \leq N_{\text{poles}} \qquad (3.4g)$$

$$y_{ij} \in \{0, 1\}, \qquad 1 \leq i \leq N_{\text{SM}}, 1 \leq j \leq N_{\text{poles}}, \qquad (3.4h)$$

where $b = g8B\gamma E_{\text{b}}\eta T_m/T_I$, d_{ij} and d'_j denote the distance between SM i and pole j and between pole j and the UC, respectively. The values of d_{pmax} and d_{umax} correspond to the transmission range of SMs to the DAPs and DAPs to the UC, respectively. The binary variable x_j is an indicator for whether a DAP is installed on pole j, and the binary variables y_{ij} indicate whether the SM i is connected to the DAP on the pole j. The first term in the objective accounts the installation cost of DAPs, and the two terms in the second sum in the objective represent the total cost of transmission from SMs to their corresponding DAPs and from DAPs to the UC, respectively. Constraints (3.4b), (3.4c), and (3.4d) ensure radio coverage, and constraint (3.4e) limits the maximal number of SMs per DAP. Furthermore, constraint (3.4f) ensures that the relation between DAP selection and placement is maintained, i.e., a SM can only be connected to a pole which is selected for DAP installation.

The optimization in (3.4a) is a type of integer programming and solving it optimally incurs an exponential time complexity. For large networks, a lower complexity algorithm is required to solve the placement problem. The optimization in (3.4a) can also be viewed as a clustering problem with additional constraints on the cluster size and head locations. This motivates the use of a modified K-means algorithm, as will be explained in the next section.

3.4 K-means Approach

In this section, we show how the K-means algorithm can be adapted to find a near-optimal DAP placement based on the optimization problem (3.4a). In the K-means algorithm, the number of clusters, K, is a parameter whose value should be known. In our problem, finding an appropriate value for K which provides the AMI coverage is a challenging task. Therefore, we start from a minimum initial estimate for K,

$$K_0 = \left\lceil \frac{N_{\mathrm{SM}}}{\min\{A, \rho_{SM}\pi d_{\mathrm{pmax}}^2\}} \right\rceil , \tag{3.5}$$

and then increment it. The initial estimate in (3.5) provides a (loose) lower bound for the value of K. This is because in higher densities ($\rho_{SM}\pi d_{\mathrm{pmax}}^2 \geq A$) the constraint (3.4e) cannot be satisfied for any values $K < K_0$ and the placement problem would be infeasible. Similarly, in lower densities ($\rho_{SM}\pi d_{\mathrm{pmax}}^2 < A$), we need at least K_0 DAPs to ensure that all SMs get at least one DAP in their transmission range.

In each iteration of the conventional K-means algorithm, the nodes (here, SMs) choose their nearest cluster head. Accordingly, we set $y_{ik} = 1$ if the ith SM belongs to the kth cluster, and $y_{ik} = 0$ otherwise. Then, the cluster head locations are updated to the centroid of their connected SMs. The K-means algorithm terminates when the difference in the updated cluster head locations in two consecutive iterations is less than a threshold. Since we need to account for both the SM-DAP and DAP-UC transmission costs, we modify the K-means algorithm and incorporate the utility center location, $\boldsymbol{u}$, in the update equation of the cluster heads as

$$\boldsymbol{a}_k = \frac{\omega \boldsymbol{u} + \sum_{i=1}^{N_{\mathrm{SM}}} y_{ik} \boldsymbol{s}_i}{\omega + \sum_{i=1}^{N_{\mathrm{SM}}} y_{ik}}. \tag{3.6}$$

where $\omega \doteq C_r \frac{d_{\mathrm{pmax}}}{d_{\mathrm{umax}}}$ is a function of both the compression ratio C_r, to consider the effect of data compression on DAP-UC links, and the coverage ratio, i.e. $\frac{d_{\mathrm{pmax}}}{d_{\mathrm{umax}}}$, so that the cluster heads which have few SMs are not pulled towards the UC and consequently lose their connection to the SMs.

The K-means procedure may violate constraint (3.4e) in our problem, i.e., more than $N_{\max}$ SMs could be placed into a single cluster. In this case, we find the SMs that have other cluster heads in their communication range, and reconnect them to the new cluster head. To this end, every DAP has a tag which indicates the current number of its connected SMs. When a node tries to connect to a DAP which has a connected tag larger than $N_{\max}$, the SM chooses its next available DAP. After the modified K-means finishes, the final cluster heads are mapped to the nearest poles. If due to the mapping a constraint could not be satisfied, the current run is declared infeasible.

The optimization procedure is summarized in Algorithm 3.1. Starting from K_0, we run the modified K-means with "NumTries" different initial placements, map the final cluster-head locations to their nearest poles and check if all the constraints are satisfied; If due to the mapping a constraint could not be satisfied, the current run is declared infeasible. Then, the solution with the lowest cost is chosen. Since initial placements in the K-means algorithm affect its final solution, different runs are needed for exploring different configurations and finding a solution closer to the optimum. Finally, we stop when the cost for the best solution found for $K+1$ clusters is larger than that with K clusters by a given "tolerance" value. Setting tolerance to 0 forces the algorithm to terminate as soon as the optimized cost increases when incrementing K. There might be some cases where further increasing K drives the cluster heads to be much closer to the SMs so that the transmission cost savings compensate the added installation cost. In these cases, a positive value of tolerance enables our algorithm to search for more cluster head configurations, and possibly finding a better solution, at the cost of increased runtime complexity.

Algorithm 3.1 Iterative K-means algorithm for DAP placement optimization.

Require: $\mathcal{SM}, \mathcal{P}, \boldsymbol{u}, a, b, \alpha, \beta, \gamma, M$.

Get K_0 from (3.5).
$k \leftarrow 0$
do
    $K \leftarrow K_0 + k$.
    for $i = 0$: NumTries-1 **do**
        Uniformly-randomly initialize the cluster head locations.
        Run the modified K-means algorithm.
        Map $\boldsymbol{a}_k$s to their nearest poles.
        $F_i \leftarrow$ Achieved cost from (3.4a). Or, $F_i \leftarrow \infty$ if any of (3.4b)-(3.4e) are not satisfied.
    end for
    $C_k \leftarrow \min\{F_i\}$.
    diff $\leftarrow C_k - C_{k-1}$.
    $k \leftarrow k + 1$.
while diff $<$ tolerance
return $\min\{C_k\}$

3.5 Performance Evaluation

In this section we test the efficiency of our proposed DAP placement algorithm in different scenarios, namely urban, suburban, and rural environments, whose pertinent parameters are obtained from [6]. As explained in Section 3.2, there are also several choices for selecting the communication technology. A common choice for the DAP-UC links is WiMAX, due to its coverage of a few kilometers with a good reliability [82]. WiMAX technology can also be used for the SM-DAP links. In this case all SMs are equipped with the WiMAX transceivers with a transmission range of about 1 km [83]. Another choice for these links are IEEE 802.15.4g transceivers [79], for which the transmission range is limited to a few hundred meters.[8]

Table 3.1 summarizes the parameters used in our simulations for the above-mentioned environments and transmission technologies. The location of SMs and poles are uniformly randomly chosen in the AoIs with radii of 1, 2, and 5 kilometers as examples for urban, suburban and rural environments, respectively. We assume a required signal-to-noise ratio (SNR) of $E_{\mathrm{b}}/N_0' = 10$ dB, where $N_0' = N_0 F$. N_0 and F are the receiver noise power spectral density and noise factor, respectively. As suggested in [6], we use the COST231 pathloss model for the urban and suburban environments and the Erceg type C model for the rural areas. The parameters chosen for the SM-DAP links are as follows: SM height is 2 m, DAP height is 10 m, center frequency is 1800 MHz (WiMAX) and 1400 MHz (802.15.4g). The parameters chosen for the DAP-UC links are: DAP height is 10 m, WiMAX base-station antenna height is 30 m, and center frequency is 1800 MHz. For distances less than 100 m, the ITU-R M.2135 (NLOS) model has been used. We also let $A = 2000$ [6].

Figure 3.2 shows the results of optimization of the DAP locations using Algo-

[8]We recall that we only consider single-hop transmission in this chapter.

Table 3.1: Simulation parameters.

Parameter	Value	Parameter	Value
ρ_{SM}	2000 (per km^2, urban) [6] 800 (per km^2, suburban) [6] 10 (per km^2, rural) [6]	r	1 km urban 2 km suburban 5 km rural
d_{pmax}	100 m (802.15.4g) [79] 1 km (WiMAX) [82]	ϱ	$\frac{1}{3}$ (sub)urban $\frac{1}{10}$ rural
d_{umax}	5 km (WiMAX) [82]	C_r	$\frac{1}{2}$
T_m	15 years	T_I	15 min
B	1024 bytes	g	0.1 \$/kWh [84]
N_0	-174 dBm/Hz	η	10 dB
F	7 dB	η	10 dB
PL model	COST231 (sub)urban [6] Erceg Type C rural [6]	a	\$2000 [85]
$N_{\max}$	2000	γ	2

rithm 3.1 for different topologies and transmission technologies. Furthermore, Table 3.2 compares the values of N_{SM}, K, and the minimum, maximum and average number of SMs served by a DAP for different topologies, including those considered in Figure 3.2.

The sub-figures on the left and right side of Figure 3.2 correspond to the use of, respectively, WiMAX and 802.15.4g for the SM-DAP links. Figures 3.2(a) and 3.2(b) (corresponding to the second row of Table 3.2) show the optimized DAP placement in a suburban area, and Figures 3.2(c) and 3.2(d) (corresponding to the third row of Table 3.2) show the optimized placements for a rural area. We observe that for the 802.15.4g technology, due to the limited transmission range, more DAPs are required than when WiMAX is applied. In fact, the results in Table 3.2 show about three (rural) to 150 (urban) times fewer DAPs for WiMAX. This suggests that relaying should be applied for reducing the cost of DAP installation when using 802.15.4g. This would come with an increase in delay, which would not be critical for meter data though.

We can also observe from Figures 3.2(c) and 3.2(d) that since the SMs are placed sparsely in a rural setting, there are on average much fewer (3-10) SMs connected to one DAP, compared to the suburban and urban scenarios where on average 402 and 1570 SMs are connected via WiMAX to one DAP.

Figures 3.2(e) and 3.2(f) (corresponding to the last row of Table 3.2) consider a mixed urban, suburban, and rural area scenario, with different densities over radii of 1, 2, and 5 km, respectively. This model gives a simple representation of cities, with larger SM densities in downtown and surrounding residential areas, and sparse SM distributions in rural parts around them. We can again observe that a single-hop 802.15.4g-based DAP supports typically 10 SMs, while a WiMAX can serve 255 on average, and up to 1000, SMs in the urban and suburban areas. Also note that the total number of DAPs placed in the mixed scenario is smaller than the sum of DAPs needed for each of the individual scenarios, mainly because the areas overlap in the mixed topology.

Finally, Figure 3.3 compares the runtime and optimality of the DAP placement the proposed algorithm (using 50 runs of K-means) and a brute-force search in a topology with 1005 SMs, 20 poles and 4 to 8 DAPs. As can be seen, our algorithm finds placements within 15% of the optimal costs, with a notably lower complexity. We note that the complexity of the brute-force search is proportional to $\binom{N_{\text{Poles}}}{K}$, while for the proposed (K-means) algorithm complexity increases linearly with N_{SM}, K, and NumTries. In Figure 3.3, the low runtime ratio for larger K suggests that we can also increase number of runs for obtaining better results. For example, running the

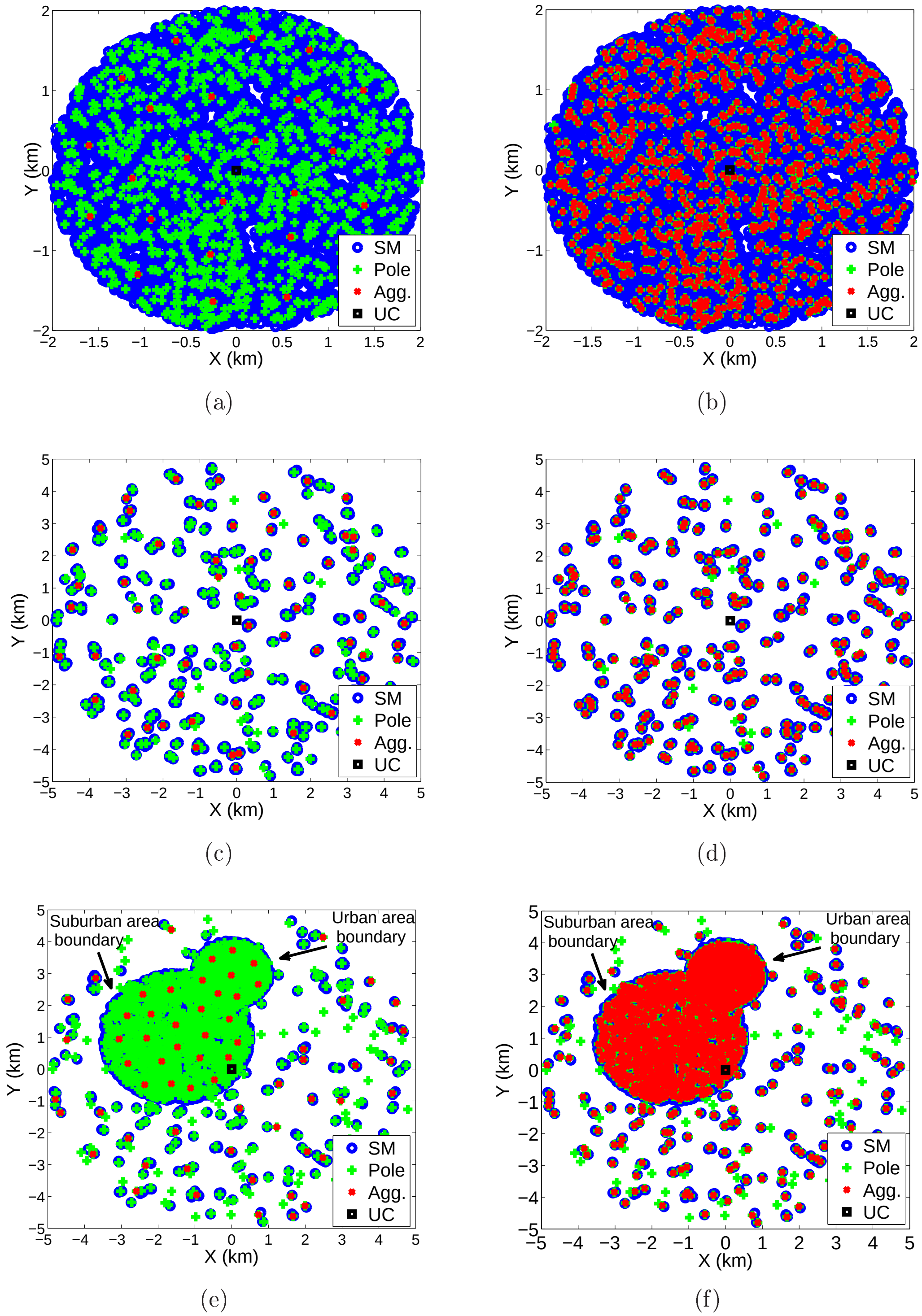

Figure 3.2: DAP placement for different environments and transmission technologies. The SM-DAP links of the sub-figures on the left and right side use WiMAX and 802.15.4g transmission technology, respectively. Sub-figures (a) and (b): suburban area. Sub-figures (c) and (d): rural area. Sub-figures (e) and (f): mixed urban, suburban, and rural areas.

Table 3.2: DAP placement optimization results for different topologies.

Topology	SM-DAP link	N_{SM}	K^*	min./avg./max. SMs per DAP
Urban	WiMAX	6283	4	1528 / 1570.75 / 1626
	802.15.4g	6283	618	1 / 10.17 / 32
Suburban	WiMAX	10053	25	301 / 402.12 / 488
	802.15.4g	10053	999	1 / 10.06 / 35
Rural	WiMAX	785	73	2 / 10.75 / 42
	802.15.4g	785	248	1 / 3.17 / 10
Mixed	WiMAX	17121	67	1 / 255.54 / 1000
	802.15.4g	17121	1814	1 / 9.44 / 35

$K = 8$ case for 500 times reduces the optimal cost ratio to 1.05 with a runtime ratio of 0.2. As the values of K and N_{poles} increase, the brute force search (or solving (3.4a) by integer programming) becomes intractable, while the proposed algorithm can still provide a solution, as shown in Figure 3.2 and Table 3.2.

3.6 Conclusions and Future Work

In this chapter, we have considered the problem of DAP placement in single-hop wireless-based AMIs. To this end, we have identified the top of the existing utility poles as possible DAP locations. We have formulated the placement problem as an integer program. Noting the relation to clustering problems, we have adapted the well-known K-means algorithm for obtaining suboptimal solutions to the placement problem. Numerical results for different wireless communication technologies and SM densities have emphasized the effect of transmission range of the wireless technology for data aggregation with relatively few DAPs. Comparing to the brute-force search

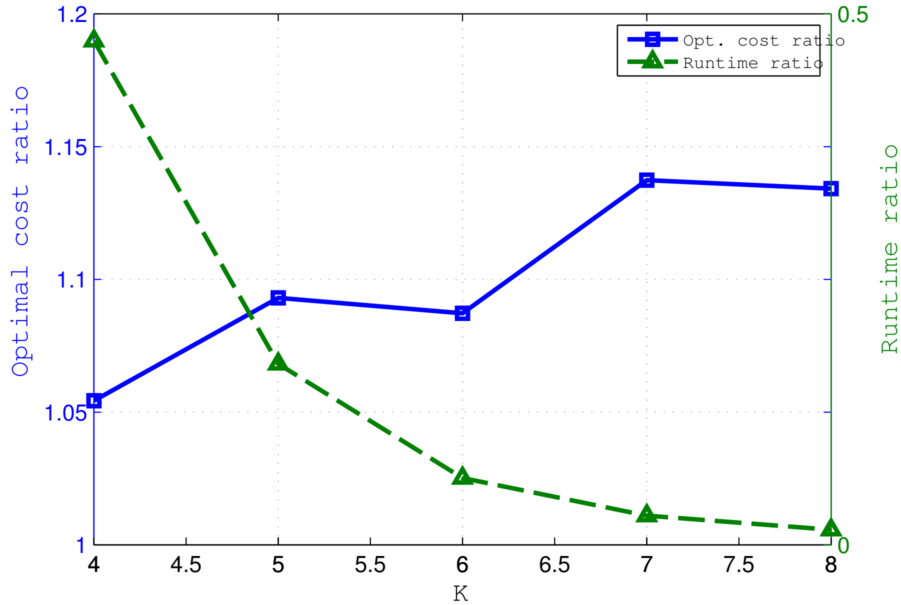

Figure 3.3: Cost and runtime ratio of the proposed modified K-means algorithm compared to a brute-force strategy for finding the optimal DAP placements. $N_{\text{SM}} = 1005, N_{\text{poles}} = 20$.

for finding the optimal placement, we have demonstrated for small-scale examples that proposed method can be used with a low time complexity to achieve a near-optimal cost.

Chapter 4

Cost-Efficient QoS-Aware DAP Placement for a Multi-Hop AMI

4.1 Introduction

In the previous chapter, we proposed a modified K-means algorithm for DAP placement in the single-hop communication scenario only considering network coverage, assuming SMs and poles are uniformly distributed through the area. In this chapter, we consider a more realistic scenario, where the location of SMs and poles are driven from the actual implementations. We solve the problem of DAP placement problem for a multi-hop communication infrastructure while ensuring not only the network coverage but also the satisfaction of the QoS requirements. We use the characteristics of the IEEE 802.15.4g technology for connecting SMs to SMs and SMs to DAPs.

The K-means algorithm chooses random locations as primary potential locations for DAP placement and all the network construction is conducted based on these locations. These random locations are eventually mapped to the closest pole. However, there is a higher possibility that such a mapping would result in the violation of QoS constraints when a realistic data set is considered, for example when poles are aligned with the road structure. Therefore, in this chapter, we apply a different and more suitable heuristic algorithm by which the network is constructed from pole locations.

Heuristic algorithms proposed for relay placement are typically based on cover-set or facility-location algorithms. For example, references [15] and [86] propose weighted cover-set algorithms for respectively gateway and reader placement for wireless sensors and radio-frequency identification nodes. Reference [20] applies the minimum-cover-set algorithm for finding the optimal location of DAPs for both single and multi-hop access in SGCNs. When the network becomes large, their heuristic algorithm breaks the area into smaller squares which can be handled by the optimizer. Their post-optimization step involves merging the solution of smaller squares by removing the redundant poles located in square edges. This step of their heuristic algorithm has a high complexity, because every pole that is not selected is checked to see if it can replace a subset of two or more selected poles.

In [19], the authors develop a K-means based algorithm for placing a fixed number of aggregators on selected utility poles with the objective of minimizing the total number of hops SMs require to access the selected data aggregators. This work is among the first to consider multi-hop communication and minimize the experienced delays by minimizing the total number of hops. However, limiting the number of hops only addresses the effect of transmission delay and ignores the effect of congestion delay which explicitly depends on the number of competitors and their arrival rates at each hop.

References [23] and [87] propose aggregator placement solutions for respectively maintaining and maximizing the obtained QoS in an AMI. They use M/D/1 and M/G/1 queuing models for computing the expected latency over the designed infrastructure. However, the mission-critical and non-critical smart grid traffic need the guarantee of certain latency requirements with certain probabilities (i.e., ensuring certain reliabilities), which is not provided through the solutions in [23], [87]. In order to improve reliability in SGCNs, several approaches such as automatic repeat request (ARQ) and other error control methods [88–90], utilizing multiple path routing [91, 92] and redundancy design [93] are proposed. In this chapter, we investigate the effect of employing ARQ on improving the obtained reliability.

In this chapter, we do not adopt the average latency model with fixed or minimum number of hops criteria considered in [19,20,23,87]. Instead, to meet latency requirements of smart grid traffic, in Section 4.2, we compute the probability of achieving a certain latency requirement for both mission-critical and non-critical traffic. To this end, we employ the IEEE 802.15.4g MAC protocol [94] with the CFP and the CAP for scheduling critical and non-critical smart grid traffic. Then, we devise an optimization problem in Section 4.2 and propose a novel heuristic algorithm for solving the problem in Section 4.3. The heuristic algorithm approximates the minimum required number of DAPs through the use of a greedy algorithm for selecting potential pole locations for aggregator placement. In order to connect nodes through reliable routes, we use the Dijkstra algorithm for identifying transmission paths with the maximum packet success ratio. In Section 4.4, we provide performance results based on realistic locations for SMs and poles, which we have obtained from BC Hydro. The results show that the paths found by our algorithm satisfy the latency requirements for both types of traffic to a specified level. We also compare the optimality and complexity of our solution for small-scale scenarios with the branch and cut algorithm offered by the IBM CPLEX software [17]. For larger-scale scenarios, we compute a lower bound solution for the placement problem and compare the optimality of our algorithm with this lower bound. Finally, we conclude the chapter in Section 4.5.

Table 4.1: Mission critical and non-critical traffic properties [70].

Traffic Class	**Traffic Name**	**Packet Size (Bytes)**	**Arrival Frequency**	**Traffic Type**	**Required Latency (s)**
NC	Periodic Meter Reading (MR)	250	15 min	Deterministic	5
NC	On-demand MR Request	50	5 days	Poisson	30
NC	On-demand MR Response Data	250	5 days	Poisson	30
MC	Power Quality Notifications	100	5 min	Poisson	1
MC	Remote Control Commands	100	1 day	Poisson	1
MC	Alert Notifications	50	1 week	Poisson	3

4.2 System Model and Problem Formulation

We consider a distribution grid with overhead power lines suspended from utility poles delivering electricity to homes or businesses equipped with SMs. Some utility poles host DAPs, each of which is wirelessly connected to a subset of the endpoints (SMs) either in a single-hop or multi-hop manner. The multi-hop communication utilizes IEEE 802.15.4g [94] for connecting SMs to each other or to the DAPs. We also assume two types of traffic classes, namely MC and NC, as listed in Table 4.1, are passing through the grid. For the MC traffic, we only consider the events that are locally and independently from other meters generated.

According to the OpenSG Forum [5], reliability is defined as the probability that a packet can successfully be received at the destination within its required latency. Therefore, in order to meet the reliability requirements of the smart grid traffic, both the route quality in terms of the packet success rate and the probability of exceeding the latency requirement over the route should be taken into account. We formulate the link quality in Section 4.2.1 and the probability of latency satisfaction for NC and MC traffic in Section 4.2.2. Using these expressions, we formulate the obtained reliability over a certain route in Section 4.2.3.

4.2.1 Link Quality

The link quality, defined as the probability of a successful packet transmission on the link between nodes i and j, is obtained as

$$1 - \epsilon_{ij} = 1 - \mathcal{Q}(\gamma_{ij}), \tag{4.1}$$

where ϵ_{ij} is the link packet error rate (PER), γ_{ij} is the signal-to-interference plus noise ratio (SINR) and $\mathcal{Q}$ maps the SINR to the PER based on the modulation and coding scheme. The SINR is given by

$$\gamma_{ij} = \frac{P_{\text{tx}}}{(N_0' + \kappa)\ PL(d_{ij})\ \eta\ \ \delta}\ , \tag{4.2}$$

where P_{tx} is the transmit power, PL is the distance-dependent path loss, the variable d_{ij} denotes the distance between nodes i and j, η is the fading margin, and $N_0' = N_0F$ where N_0 and F are respectively the receiver noise power spectral density and noise factor. The variable κ denotes the interference margin, which accounts for the inter-operator interference when operating in the unlicensed band or when the same block of frequency is used by other operators or applications as well as cell-to-cell interference [34]. Furthermore, δ is the penetration loss which is present when SMs are located inside the building. The pathloss component $PL(d_{ij})$ depends on the area type. According to the NIST PAP2 guideline [34], the Erceg SUI propagation model best emulates the channel propagation for rural and suburban scenarios. For urban areas, the ITU-R M.2135-1 (outdoor) and ITU-R M.1225 (indoor) propagation models are suggested.

4.2.2 Delay Model

The IEEE 802.15.4g MAC protocol provides two types of medium access periods, namely CFP and CAP, within each frame. A node stores the MC and NC traffic in different queues, and schedules the mission-critical traffic through the CFPs using the TDMA scheme, and the non-critical traffic within the CAP time slots using the CSMA/CA scheme. We hereafter denote the number of available time slots per frame in the CFP and CAP by N_{T} and N_{C}, respectively.

Let us assume that the traffic from each node should be received at the destination within a time period of L seconds. In order to compute the probability that an NC or MC packet can be transmitted within this delay requirement, we need to translate L to its equivalent number of available slots via[9]

$$N_{\mathrm{s}} = (\mathrm{MC\ or\ NC}) = \frac{L}{T_{\mathrm{F}}} \times N_{\mathrm{T}} \text{ or } N_{\mathrm{C}} \ , \tag{4.3}$$

where T_{F} is the frame duration in seconds. As we are dealing with a multi-hop communication system, the cumulative waiting time during all the hops should be less than the required latency. Let us assume node n is located at depth H_n of the network and r_{hn} is the relay node which forwards the message of node n at hop h

[9] We assume L is a factor of T_F.

where $1 \leq h \leq H_n$. To meet the required delay for node n we allow

$$S = \left\lfloor \frac{N_{\mathrm{s}}}{H_n} \right\rfloor \tag{4.4}$$

time slots to be consumed at each of its forwarding nodes. This conservative assumption allows us to guarantee the required reliability. It should be noted that in practice, a larger delay may be consumed at some hop, while the total delay is still maintained.

There are several components included in the total packet delay, namely transmission, queuing, medium access, and propagation delay. Propagation delay is usually ignored for links with short distances [34]. In the following, we first compute the queuing delay. We then formulate the latency requirement that should be met for QoS satisfaction at each hop by deducting the queuing and transmission delay from the total allowed delay. For the transmission delay, we assume each packet can be transmitted within one time slot. Next, we mathematically derive the probability of meeting this required delay based on the MAC protocol specifications of the 802.15.4g standard.

4.2.2.1 Queuing Delay

For tractability of computing the queuing delay, we assume all sources generate Poisson traffic, which has been shown to be a sufficiently accurate approximation for mixed traffic as considered in our work [23]. We further assume that the Poisson traffic model also applies to nodes forwarding packets, which is justified if the traffic load at each node is low [95–98] and will also be verified numerically in Section 4.4.3 for typical traffic scenarios of our application. Hence, according to the Pollaczek-

Khinchin formula [99], the waiting time in time slots is given by

$$T_{\mathrm{Q}_x} = \frac{\lambda_x \bar{s_x^2}}{2(1 - \frac{\lambda_x}{\mu_x})} , \tag{4.5}$$

where

$$\lambda_x = \sigma_x \lambda_0 (N_{\mathrm{f}x} + 1) \tag{4.6}$$

is the aggregated arrival rate at the node, $N_{\mathrm{f}x}$ denotes the total number of feeding nodes that are directly or indirectly connected to node x, λ_0 is the average traffic generation rate per node, and σ_x gives the expected number of times that the packet should be re-transmitted, which will be calculated later in this section. μ_x is the packet service rate and $\bar{s_x^2}$ denotes the second moment of the service time for both NC and MC traffic, which is given by

$$\bar{s_x^2} = \frac{N_{\mathrm{C}} + N_{\mathrm{T}}}{N_{\mathrm{C}} \text{ or } N_{\mathrm{T}}} \sum_{k=1}^{S} \Big(R_x(k) - R_x(k-1) \Big) k^2, \tag{4.7}$$

where $R_x(k)$ is the probability that the packet can successfully be transmitted within k CAP or CFP slots. Variables μ_x and $R_x(k)$ are obtained later in this section.

4.2.2.2 Medium Access Delay

Consider that r_{hn} has $N_{r_{hn}}$ neighbours, which we collect in the set $\Psi_{r_{hn}}$, and let $\mathcal{P}_{r_{hn}} = \{p_x : x \in \Psi_{r_{hn}}\}$ be the probabilities that these neighbours have a packet for transmission, given by $p_x = \frac{\lambda_x}{\mu_x}$ [99], where λ_x has been defined in (4.6) above, and μ_x is the service rate. μ_x is obtained later in the following section.

Here, we describe how the probability of exceeding a certain delay is computed for the traffic generated by node n for the above-mentioned scheduling schemes as a function of S and $\mathcal{P}_{r_{hn}}$. In order to increase the obtained reliability, for each packet, we allow up to N_{ARQ} transmission attempts. For computing the probability of not exceeding a certain latency for CSMA/CA scheduling scheme, we use the analysis given in [100] for computing the probability that the channel is busy and also the method given in [101] for computing the probability that a node senses the channel at a certain slot k in a certain stage m.

- **Non-critical traffic:** Under the slotted CSMA/CA model, each node with the NC traffic, at each transmission attempt, would sense the channel at most $M+1$ times. At each sensing stage $m = 0, 1, \cdots, M$, it selects a random time slot within the backoff window, W_m, with equal probability. According to the IEEE 802.15.4g standard, in slotted CSMA/CA model, each node should identify the channel as idle for two consecutive slots before changing to transmission mode. If two nodes sense the channel as idle at the same time, there would be a collision.

  Figure 4.1 shows the Markov chain model associated with the CSMA/CA procedure. We define $\alpha_{1_{r_{hn}}}$ as the probability that the channel is busy when sensing for the first time, $\alpha_{2_{r_{hn}}}$ as the probability that the channel is busy when sensing for the second time, provided that the channel was idle for the first time, and

$$\beta_{r_{hn}} = (1 - \alpha_{1_{r_{hn}}})(1 - \alpha_{2_{r_{hn}}}) \tag{4.8}$$

  as the probability that the channel is determined as idle for two consecutive time slots. The channel is determined as busy if the channel was idle for two consecutive time slots and at least a node had sensed the channel in those slots.

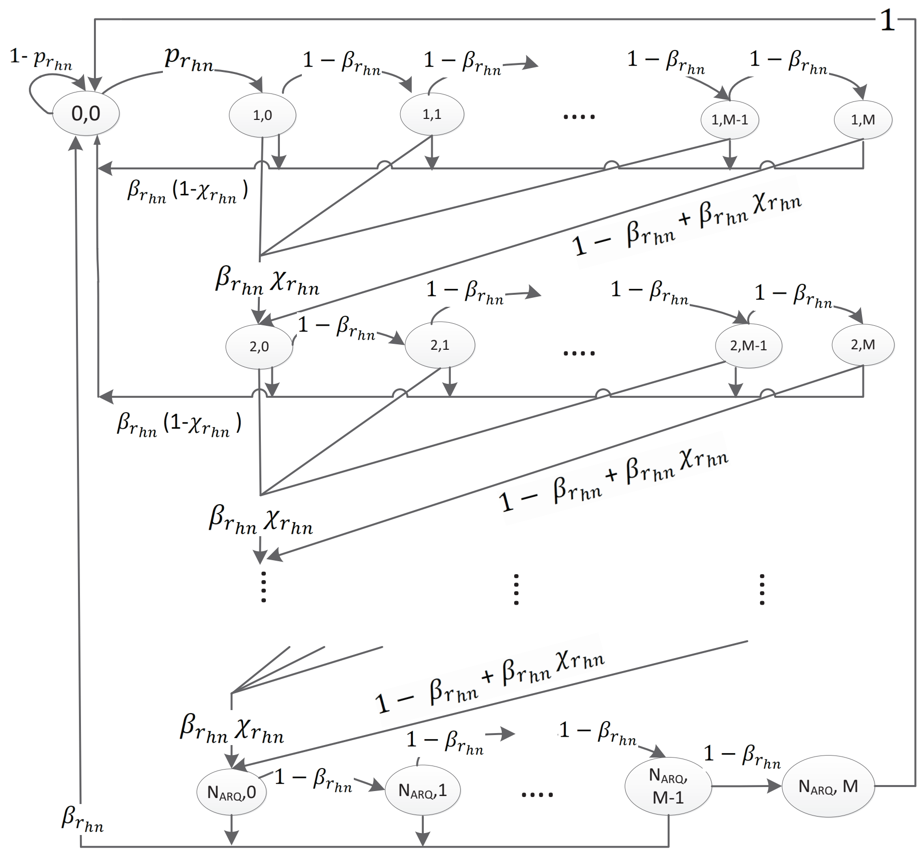

Figure 4.1: Markov chain for the CSMA/CA process. State (i, m), $1 \leq i \leq N_{\text{ARQ}}$, $0 \leq m \leq M$ represents the sensing stage m in the ith transmission attempt, and $(0, 0)$ is the state of having no packets for transmission. $p_{r_{hn}}$ is the probability that the node has a packet for transmission, $\beta_{r_{hn}}$ is the probability that the channel is idle and $1 - \chi_{r_{hn}}$ is the probability that the packet has successfully been transmitted.

Hence, the probability of $\alpha_{1_{r_{hn}}}$ is obtained from [100]

$$\alpha_{1_{r_{hn}}} = (1 - \alpha_{1_{r_{hn}}})(1 - \alpha_{2_{r_{hn}}}) \left(1 - \left(\prod_{x \in \Psi_{r_{hn}}} (1 - \xi_x)\right)\right), \tag{4.9}$$

where ξ_x is the probability that a neighbour node senses the channel in an arbitrary time slot. The probability that the channel is determined as busy when sensing for the second time, given that the channel was idle for the first time is obtained from [100]

$$\alpha_{2_{r_{hn}}} = (1 - \alpha_{2_{r_{hn}}}) \left(1 - \left(\prod_{x \in \Psi_{r_{hn}}} (1 - \xi_x)\right)\right). \tag{4.10}$$

In order to compute ξ_x, we use the stationary probabilities associated with the Markov chain shown in Figure 4.1. Let $\boldsymbol{\pi}$ and $\mathbf{T}$ respectively denote the stationary distribution vector and transition matrix of this Markov chain. Solving the stationary state equation $\boldsymbol{\pi}\mathbf{T} = \boldsymbol{\pi}$ subject to $\sum_j \boldsymbol{\pi}_j = 1$, we can compute the probability that a neighbour node senses the channel in an arbitrary time slot as

$$\xi_x = \sum_{i=1}^{N_{\text{ARQ}}} \sum_{m=0}^{M} \frac{\boldsymbol{\pi}_{g(i,m)}}{W_m}, \tag{4.11}$$

where $g(i,m) = (i-1)(M+1) + m + 1$, $\boldsymbol{\pi}_{g(i,m)}$ is the probability of being in sensing stage m in transmission attempt i, and $\frac{1}{W_m}$ gives the probability of sensing the channel in an arbitrary time slot in stage m.

In order to compute the probability that a node can transmit its packet within the required latency, we need to compute the probability that the node senses the channel within the latency and also the channel is idle. Let us define $\theta_{r_{hn}}(k)$ as the probability that node r_{hn} senses the channel in time slot k and also the channel is idle [101]. Since slot k can be sensed at any of the N_{ARQ} transmission attempts and $M+1$ backoff stages, $\theta_{r_{hn}}(k)$ is obtained as

$$\theta_{r_{hn}}(k) = \sum_{i=1}^{N_{\text{ARQ}}} \sum_{m=0}^{M} \zeta_{r_{hn}}(k,i,m)\ \beta_{r_{hn}}, \tag{4.12}$$

where $\zeta_{r_{hn}}(k,i,m)$ is the probability of sensing the channel at slot k, in sensing stage m, in transmission attempt i. The variable $\zeta_{r_{hn}}(k,i,m)$ is computed based on the probability of having an unsuccessful transmission attempt (due to either finding the channel as busy during all $M+1$ backoff stages or due to packet transmission failure) in one of the previous d slots in the previous try and then sensing the channel at slot $k-d-2$ in the current try,

$$\zeta_{r_{hn}}(k,i,m) = \begin{cases} \sum_{d=3(i-2)+1}^{k-2} \sum_{m'=0}^{M} \zeta_{r_{hn}}(d,i-1,m') \\ \Delta_{m'}\ \phi_{r_{hn}}(k-d-2,m),\ i>1, \\ \phi_{r_{hn}}(k,m), \quad i=1, \end{cases} \tag{4.13}$$

where at least 3 slots are consumed at each attempt (2 slots for sensing and 1 for transmission),

$$\Delta_{m'} = \begin{cases} \beta_{r_{hn}}\chi_{r_{hn}}, & m' < M, \\ \beta_{r_{hn}}\chi_{r_{hn}} + (1-\beta_{r_{hn}}), & m' = M, \end{cases} \tag{4.14}$$

and $\phi_{r_{hn}}(k,m)$ is the probability that node r_{hn} assesses the channel at slot k in sensing stage m. The value of $\phi_{r_{hn}}(k,m)$ is also recursively computed as a cumulative probability of sensing the channel at slot j in the previous sensing stage, finding the channel as busy in either the first or second slot and accordingly, backing off for $k-j$ slots with probability $\frac{1}{W_m}$ in the current sensing stage m [101]. In other words, $\phi_{r_{hn}}(k,m)$ can be calculated as

$$\phi_{r_{hn}}(k,m) = \begin{cases} \sum_{j=1}^{k-1} \phi_{r_{hn}}(j,m-1)\ \alpha_{1_{r_{hn}}}\ \frac{1}{W_m} \\ + \sum_{j=1}^{k-2} \phi_{r_{hn}}(j,m-1)\ (1-\alpha_{1_{r_{hn}}})\ \alpha_{2_{r_{hn}}} \frac{1}{W_m},\ m \geq 1,\ k \geq 1, \\ \frac{1}{W_0}, \qquad m = 0, \quad k \geq 1, \\ 0, \qquad k < 1. \end{cases} \tag{4.15}$$

Finally, using (4.8)-(4.13), the probability that node r_{hn} can successfully transmit the packet within the required latency is obtained as

$$R_{r_{hn}}(S) = \sum_{k=1}^{S-T_{\mathrm{Q}}-1} \theta_{r_{hn}}(k)(1-\chi_{r_{hn}}), \tag{4.16}$$

where $1-\chi_{r_{hn}}$ is the probability that the packet can successfully be transmitted, i.e., the packet transmission does not fail due to a collision (given that the channel is determined as idle, at least one other node senses the channel at the same time as r_{hn}) or due to a link error. It is obtained as

$$1-\chi_{r_{hn}} = (1-\epsilon_h)\left(\prod_{x\in\Psi_{r_{hn}}} (1-\xi_x)\right), \tag{4.17}$$

where ϵ_h is the link PER between r_{hn} and the relay node at the next hop as defined in (4.1).

- **Mission-critical traffic:** In this section, we compute the probability that all the bandwidth requests from the neighbour nodes, can be scheduled within the latency requirement. According to [34], this probability is computed as

$$\Pr(\ell_{r_{hn}} \leq S) = \sum_{i=0}^{S-1} \left(\sum_{\psi \in \Psi_{r_{hn},i}} \prod_{j \in \psi} p_j \prod_{k \in \Psi_{r_{hn}} \setminus \psi} (1 - p_k) \right), \tag{4.18}$$

where $\ell_{r_{hn}}$ is the experienced delay at relay node r_{hn} over one transmission attempt, $\Psi_{r_{hn},i}$ is the set of all subsets of $\Psi_{r_{hn}}$ with size i. For Poisson traffic assumed here, the expression in (4.18) has the closed-form solution [102]

$$\Pr(\ell_{r_{hn}} \leq S) = \sum_{i=0}^{S-1} \frac{1}{N_{r_{hn}} + 1} \sum_{\kappa=0}^{N_{r_{hn}}} \mathrm{e}^{\mathrm{j}\frac{-2\pi\kappa i}{N_{r_{hn}}+1}} \prod_{k=1}^{N_{r_{hn}}} \left(p_k \mathrm{e}^{\mathrm{j}\frac{2\pi\kappa}{N_{r_{hn}}+1}} + (1 - p_k) \right), \tag{4.19}$$

where j is the imaginary unit. Let us define $\mathcal{L}_{r_{hn},i}$ as the cumulative sum of delays over i transmission attempts. We can compute the obtained reliability at hop h after N_{ARQ} transmission attempts as

$$R_{r_{hn}}(S) = \sum_{i=1}^{N_{\mathrm{ARQ}}} \Pr(\mathcal{L}_{r_{hn},i} \leq S - T_{\mathrm{Q}})\ (\epsilon_h)^{i-1}\ (1 - \epsilon_h), \tag{4.20}$$

where similar to the NC traffic, the probability of latency satisfaction at each attempt can be recursively computed based on the time that has elapsed in the previous attempts, i.e.,

$$\Pr(\mathcal{L}_{r_{hn},i} \leq S) = \sum_{k=i-1}^{S-1} \Pr(\mathcal{L}_{r_{hn},i-1} = k) \Pr(\ell_{r_{hn}} \leq S - k), i > 1, \tag{4.21}$$

where

$$\Pr(\mathcal{L}_{r_{hn},i} = k) = \sum_{d=i-1}^{k-1} \Pr(\mathcal{L}_{r_{hn},i-1} = d) \Pr(\ell_{r_{hn}} = k - d), i > 1, \tag{4.22}$$

and

$$\Pr(\ell_{r_{hn}} = u) = \frac{1}{N_{r_{hn}}+1} \sum_{\kappa=0}^{N_{r_{hn}}} \mathrm{e}^{\mathrm{j}\frac{-2\pi\kappa(u-1)}{N_{r_{hn}}+1}} \prod_{k=1}^{N_{r_{hn}}} \left(p_k \mathrm{e}^{\mathrm{j}\frac{2\pi\kappa}{N_{r_{hn}}+1}} + (1-p_k) \right). \quad (4.23)$$

- **Computing service rates:** As mentioned earlier, in order to compute p_x, we need to compute the average service rate for the NC and MC traffic for node x. The average service rate for node x can be obtained as $\mu_x = \frac{1}{\bar{s}_x}$, where $\bar{s}_x$ is the mean packet service time, which is calculated as

$$\bar{s}_x = \begin{cases} \frac{1}{N_\mathrm{C}+N_\mathrm{T}} \sum_{i=1}^{N_\mathrm{T}} i + \sum_{m=0}^{M} (1-\beta_x)^m \frac{W_m+2}{2} + \\ \qquad \sum_{m=1}^{M} (1-\beta_x)^m \left(\frac{W_m+2}{2N_C} N_\mathrm{T} \right) + 1, \quad \text{CSMA/CA}, \\ \frac{1}{N_\mathrm{C}+N_\mathrm{T}} \sum_{i=1}^{N_\mathrm{C}} i + \left\lfloor \frac{\frac{1}{2} \sum_{x' \in \Psi_x \cup \{x\}} \lambda_{x'} \frac{L}{H_x}}{N_\mathrm{T}} \right\rfloor (N_\mathrm{T}+N_\mathrm{C}) + \\ \qquad \bmod \left(\frac{1}{2} \sum_{x' \in \Psi_x \cup \{x\}} \lambda_{x'} \frac{L}{H_x}, N_\mathrm{T} \right), \quad \text{TDMA}, \end{cases} \quad (4.24)$$

that is, for the NC traffic $\bar{s}_x$ is computed based on whether the packet has arrived during the CFP and accordingly, the corresponding CFP duration should be added to the service time. Also, we need to consider the expected time that is needed for backoff based on the derivation given in [101], plus adding another CFP if the channel is busy and the remaining CAP slots are not sufficient for a new backoff. Finally, one time slot is added for packet transmission. For the MC traffic, $\bar{s}_x$ is computed based on whether the packet has arrived during the CAP and accordingly, the corresponding CAP duration should be added to the service time. Also, we need to consider the expected CFP time that is required for serving packets that have been generated by the node and neighbours during the time period $\frac{L}{H_x}$.

- **Computing expected number of retransmissions:** The value of σ_x gives the expected number of retransmissions that is required for a successful transmission of a packet generated by node x, which is located at hop h. This value is obtained as [103]

$$\sigma_x = \begin{cases} \frac{1}{1-\epsilon_h}, & \text{for MC traffic,} \\ \frac{1}{(1-\chi_x)(1-(1-\beta_x)^{M+1})}, & \text{for NC traffic.} \end{cases} \tag{4.25}$$

4.2.3 Obtained Reliability over the Path

Based on the derivation of reliability for each hop in (4.16) and (4.18), the obtained reliability over each path can be calculated as

$$R_n = \prod_{h=1}^{H_n} R_{r_{hn}}(S). \tag{4.26}$$

4.2.4 Problem Formulation

In order to collect the traffic from SMs either in a single-hop or multi-hop structure, aggregators are placed on top of the existing utility poles. The placement should be conducted such that coverage for all automated devices is ensured, the required latency for critical and non-critical traffic is satisfied, and at the same time, a cost-efficient infrastructure in terms of installation and maintenance is obtained.

To formulate the associated optimization problem let us assume N_{SM} is the number of SMs in the area which need to be covered and N_{poles} is the number of poles from which a subset should be selected for DAP placement. The binary variable x_j

indicates whether a DAP is installed on pole j. Also let the binary variables y_{ij}, $q_{ii'}$ and $z_{ii'}$ indicate whether an SM i is directly connected to the DAP located on pole j, whether a node i' is the immediate parent[10] of another node i, and whether node i' is an ancestor of another node i, respectively.

Using these variables and the expressions from Sections 4.2.1 to 4.2.3, we can formulate the optimization problem for the DAP placement in (4.27) (on the next page). According to [20, 104], DAPs are very costly to be installed. Therefore, in order to have a cost-efficient infrastructure, we define the objective (4.27a) as the minimization of the installation cost, c_{inst}, which we consider linearly proportional to the total number of DAPs that should be mounted on top of the poles. Assuming that discovering one route is enough for each SM, constraint (4.27b) ensures that it is either directly connected to a DAP or it has an immediate connection to another SM, which becomes its parent node. Constraint (4.27c) provides the relation between the parent of a node, $q_{ii'}$, and its ancestors, $z_{ii'}$. Constraints (4.27d) and (4.27e) ensure that only one of the nodes i or i' can be the parent or an ancestor of the other one. Constraint (4.27f) enforces the connectivity of all nodes to a DAP, via single or multi-hop communication. Accordingly, constraint (4.27g) as previously obtained in (4.26), ensures the satisfaction of the reliability constraint as a cumulative effect of packet success ratio and the latency requirement for both MC and NC traffic, where τ is the specified required reliability in percentage. Constraint (4.27h) ensures that the aggregated traffic from the connected nodes to each DAP is less than the offered service rate by the DAP, μ. Constraint (4.27i) ensures that the relation between DAP selection and placement is maintained, i.e., an SM can only be connected to a pole which is selected for DAP installation.

[10] Any node which is on the route from the source to the destination is defined as the ancestor of the source. The ancestor node directly connected to the source is called the source's parent.

$$\min_{\{x_j\},\{y_{ij}\},\{q_{ii'}\},\{z_{ii'}\}} \quad c_{\text{inst}} = \sum_{j=1}^{N_{\text{poles}}} x_j \tag{4.27a}$$

Subject to

$$\sum_{j=1}^{N_{\text{poles}}} y_{ij} + \sum_{i'=1}^{N_{\text{SM}}} q_{ii'} = 1, \qquad 1 \le i \le N_{\text{SM}}, \tag{4.27b}$$

$$q_{ii'} \le z_{ii'}, \qquad 1 \le i, i' \le N_{\text{SM}}, \tag{4.27c}$$

$$q_{ii'} + q_{i'i} \le 1, \qquad 1 \le i, i' \le N_{\text{SM}}, \tag{4.27d}$$

$$z_{ii'} + z_{i'i} \le 1, \qquad 1 \le i, i' \le N_{\text{SM}}, \tag{4.27e}$$

$$\sum_{j=1}^{N_{\text{poles}}} y_{ij} + \sum_{j=1}^{N_{\text{poles}}} \sum_{i'=1}^{N_{\text{SM}}} z_{ii'} y_{i'j} = 1, \qquad 1 \le i \le N_{\text{SM}}, \tag{4.27f}$$

$$R_i \ge \tau, \qquad 1 \le i \le N_{\text{SM}}, \text{ for MC and NC}, \tag{4.27g}$$

$$\sum_{i=1}^{N_{\text{SM}}} y_{ij} \lambda_i \le \mu, \qquad 1 \le j \le N_{\text{poles}}, \tag{4.27h}$$

$$y_{ij} \le x_j, \qquad 1 \le i \le N_{\text{SM}}, \quad 1 \le j \le N_{\text{poles}}, \tag{4.27i}$$

$$x_j, y_{ij}, z_{ii'}, q_{ii'} \in \{0, 1\}, \qquad 1 \le i, i' \le N_{\text{SM}}, \quad 1 \le j \le N_{\text{poles}}, \tag{4.27j}$$

A *relaxed* version of the optimization problem in (4.27) can be formulated in order to obtain a lower bound on the optimal solution of the DAP placement for a given scenario. In particular, we can assume perfect links by setting $\epsilon_h = 0$ for all links in (4.16) and (4.20) when calculating the reliability constraint (4.27g), which also means that all SMs are connected to DAPs through single hops. Hence, we can eliminate variables $q_{ii'}, z_{ii'}$ and drop the constraints (4.27c)-(4.27f). This lower bound only addresses the latency constraints (4.16) and (4.19). The resulting problem is still an IP problem, however, it can be solved as follows. The latency constraint (4.27g) in the resulting problem is equivalent to the system of exponential equations (4.8)-(4.16) for CSMA/CA and (4.19) for the TDMA which can be solved using a numerical solver by assuming continuous variables. The solution obtained from solving these system of

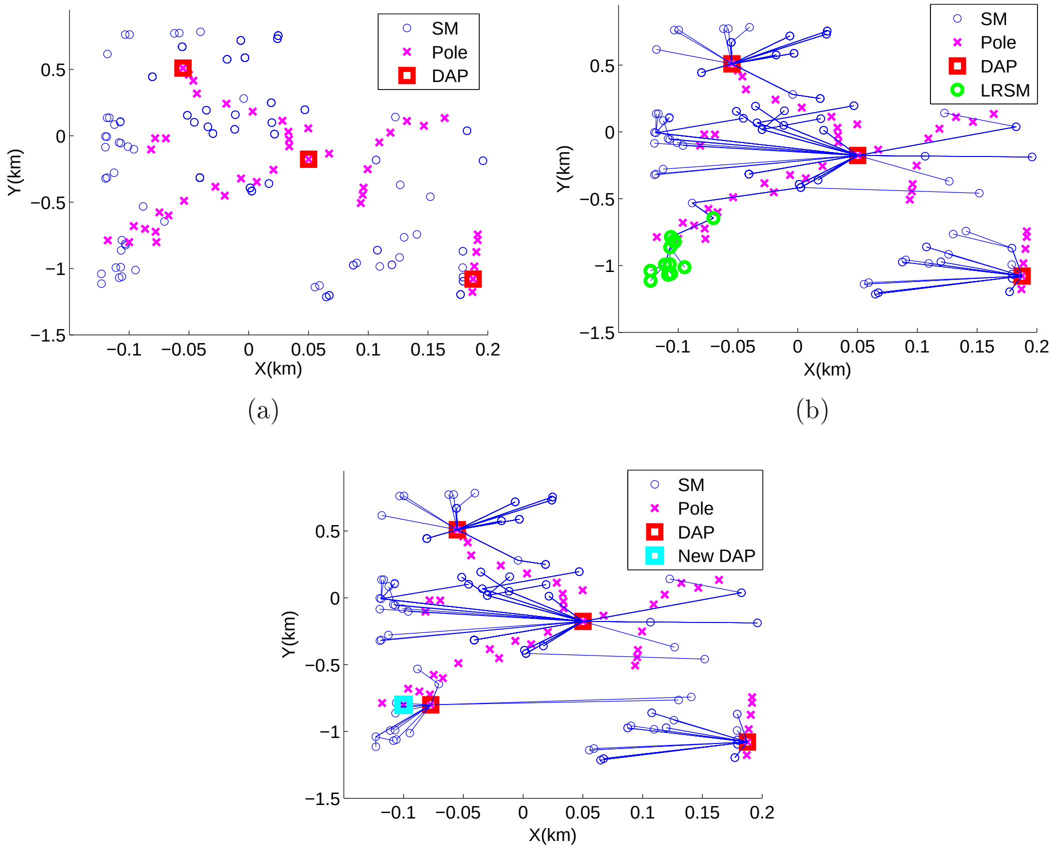

(a) (b) (c)

Figure 4.2: Sample scenario for illustration of the steps of the heuristic algorithm. (a) First phase pole selection, (b) Second phase - step I, with initial shortest paths (LRSM denotes an SM which experiences low reliability) and second phase - step II (DAP locations have not been changed in this case), (c) Second phase - step III, placing a new DAP at $(-0.1, -0.8)$ and re-running second phase - step I for reconstructing the tree, and second phase - step II, relocating each aggregator closer to the center-point of its current cluster members (the new aggregator is moved to $(-0.07, -0.8)$).

equations gives the maximum number of nodes that can be connected to a DAP such that latency constraints are met, N_{lat}. Then, the optimal solution to the relaxed optimization problem is obtained by $\lceil \frac{N_{\text{SM}}}{N_{\text{lat}}} \rceil$. This lower bound can be used as a benchmark for evaluating the performance of our heuristic algorithm derived in the next section.

4.3 DAP Placement Algorithm

The optimization in (4.27) is an IP problem and directly solving it has an exponential time complexity with regards to the problem size, i.e., number of variables and constraints [105]. Optimization solvers such as CPLEX [17] and GLPK [18] employ the branch and cut method for solving IP problems. However, the complexity of such algorithms is still high and exponential in the worst case scenario. Therefore for large networks, a lower complexity algorithm is desired [12, 13, 106]. In this section, we propose a new heuristic algorithm, which is partly inspired from [15] and [12], where a greedy approach is used for identifying potential locations for relay placement. In order to address the QoS requirements, we consider a second phase for the algorithm as described later in this section. We later on, through the results presented in Section 4.4, show that our proposed algorithm can provide a good solution to the DAP placement problem with a relatively low computational complexity.

The proposed DAP placement algorithm consists of two phases. In the first phase, we address the objective (4.27a) through approximating the minimum required number of aggregators and their initial locations. This is done through selecting poles that cover the largest number of uncovered SMs through multi-hop communication as per (4.27b)-(4.27f)[11]. In the second phase, based on the initial location of DAPs, we explore shortest path routes for the SMs to connect them to the DAPs and ensure that their network coverage, and QoS and capacity requirements as per (4.27g) and (4.27h) are maintained.

[11]We note that if the locations of some of the DAPs had already determined, their corresponding values for x in the optimization problem 4.27 should be considered as 1. Accordingly, in the first phase of our heuristic algorithm, these locations should be considered as part of the potential pole locations for DAP placement.

4.3.1 Phase 1: Pole Selection

In this phase, through a greedy approach, we select the poles that have the largest number of connectivities to the uncovered SMs as candidates for DAP installation. In order to identify the set of SMs that can be covered by a certain pole through multi-hop communication as per (4.27b)-(4.27f), we construct a k-dimensional (KD) tree[12] over the set of SMs and perform range search operations, considering the effective coverage range of poles and SMs, d_{smax} and d_{pmax}.

We repeat the above step for the remaining SMs that are not yet connected to a selected pole until all SMs are connected to a DAP or there is no solution for the remaining nodes, i.e. there is no pole or SM in their communication range.

4.3.2 Phase 2: Tree Construction

In this phase, we connect endpoints to the aggregators that have been selected in phase 1 and ensure that the capacity and QoS requirements (4.27g) and (4.27h) are satisfied. We perform the following steps.

Step I (route discovery): We use the Dijkstra algorithm to connect each SM through single or multi-hop communication, to the DAP that its capacity has not yet exceeded as per (4.27h) and also results in obtaining the maximum packet success

[12] A KD tree is a data structure for organizing k-dimentional data points in a binary search tree [107]. Performing range search operation over this tree (data structure) helps to identify the set of nodes that are in the communication range of certain locations.

rate. To this end, we use the link PERs obtained from (4.1) and (4.2) via[13]

$$c_{ij} = \log\left(\frac{1}{1-\epsilon_{ij}}\right)$$

as the link costs. This step determines the clusters, i.e., the set of SMs that are connected to each DAP.

Step II (relocating each aggregator to the center-point of its cluster members): As the first phase of the algorithm only addresses the coverage constraint, in this phase we move each DAP to the pole nearest to the center-point of its cluster members, so that on average fewer hops would be required for SMs within the cluster to access the DAP and accordingly, a better reliability can be provided for them. Note that all the SMs should be able to connect to the newly selected location for the DAP, otherwise, this re-location would not be conducted.

Step III (adding new aggregators): In this step, we compute the obtained reliability as per (4.27g) for all the nodes and disconnect those that experience low reliability for either of their MC or NC traffic. Then, we re-run the first phase of the algorithm for finding new aggregators for covering the disconnected nodes. As there might be some already connected nodes whose reliability would improve if they connected to the newly added aggregators, we repeat the second phase of the algorithm over the whole set of SMs in order to re-connect them to the new set of DAPs. Adding new aggregators can only increase satisfaction of the reliability constraint, and thus this step is re-iterated until the required reliability is met for all

[13]We note that since in the first phase of the algorithm, the locations of the DAPs are selected considering only the network coverage and the latency is ensured in the last phase of the algorithm, it may lead to selecting few DAPs more than what is necessary. The reason that we have not considered latency in the first phase of the algorithm is because the network load impacts the experienced latency and for tracking the latency, we need to connect nodes one by one. This by itself adds a factor of $O(N_{\mathrm{SM}})$ to the run-time complexity of the algorithm, which makes it impossible to effectively solve the problem for large-scale scenarios.

nodes or no solution can be found (i.e., no solution exists for meeting the required reliability).

Figure 4.2 shows an example of the phases of our algorithm in an SGCN with 425 SMs and 45 poles. The SMs are shown as circles, poles are marked with crosses and the selected DAPs are represented as squares. As it can be seen, the first phase of the algorithm selects three poles for DAP installation (Figure 4.2(a)). The second phase of the algorithm constructs initial shortest paths for all the nodes and computes their obtained packet success ratio and reliability. We can observe that 13 nodes become disconnected during step III of phase 2 (marked as larger (green) circles in Figure 4.2(b)) as their obtained reliability with the current set of DAPs is less than the specified reliability of $\tau =\ 98\%$. Then, through repeating the first phase of the algorithm, a new pole is selected for the DAP placement (new DAP in Figure 4.2(c)) and steps I and II of the second phase are repeated for reconstructing the shortest paths and moving poles to the center-point of their currently allocated cluster members.

We now provide details on the performance of the proposed algorithm in terms of optimality and convergence speed.

4.3.3 Optimality Analysis

The DAP placement is an instance of the set cover problem [108, Theorem1] and we have applied a greedy approach for solving it. It is well-known that the approximation factor of greedy algorithms for solving a set cover problem in the worst-case scenario is $\ln(N)$, where N is the number of nodes to be covered [108]. Moreover, there is no approximation algorithm that can provide a significantly better approximation factor than what is provided by a greedy algorithm for solving a set cover problem [109].

Therefore, the solution provided by the proposed heuristic algorithm in the worst case differs from the optimal solution by a factor of $\ln(N_{\mathrm{SM}})$, and this is the best approximation factor that a polynomial solution can achieve.

4.3.4 Convergence Analysis

According to the global convergence theorem, an algorithm converges to a desired solution if we can define a descent function on the solution set [110]. Since in each iteration of our algorithm, the number of nodes that are not covered by a DAP are decreasing (adding new DAPs improves the experienced reliability), we can conclude that our algorithm converges.

In terms of the convergence ratio, assume r_k is the number of DAPs in the kth iteration of the algorithm, and r^* is the number of DAPs when the algorithm converges. Since in our algorithm, $\nu_{\mathrm{conv}} = \lim_{k\to\infty} \frac{r_{k+1}-r*}{r_k - r^*}$ is a value between 0 and 1 (as the distance to the required number of DAPs is decreasing), according to [111] we can conclude that the algorithm linearly converges to the desired solution with ratio ν_{conv}. The value of ν_{conv} is different for different scenarios. For a smaller value of ν_{conv}, the algorithm converges faster.

4.4 Numerical Results and Discussion

In this section, we test our proposed DAP placement algorithm using realistic smart meter and pole locations information from the area of Kamloops, BC, Canada.

Table 4.2: Simulation parameters [6, 70].

Parameter	**Value**	**Parameter**	**Value**
Req. reliability, τ	90%	PL model	Erceg Type B
SM height	2 m	DAP height	10 m
N_{ARQ}	4	Modulation and coding scheme (MCS)	QPSK code rate of $\frac{3}{4}$
Noise Factor (F)	7 dB		
Interference Margin (κ)	6 dB	Fading Margin (η)	12.3 dB
Transmission power (P_{tx})	30 mW	Receiver Noise PSD (N_0)	-174 dBm/Hz

4.4.1 Simulation Settings

Table 4.2 summarizes the parameters we have used for running our simulations. Figure 4.3(a) presents the geographical locations of SMs and poles over the map of Kamloops, BC, Canada. The SMs and poles are marked with blue circles and magenta crosses, respectively. It is important to note that the poles are mostly aligned with the roads on the map and their location do not follow a uniform-random distribution model. As suggested in [6], the Erceg Type B best models the signal propagation for the smart grid infrastructure in rural and suburban areas. Therefore, we have used this model for emulating the pathloss in the considered Kamloops suburban area, which is a hilly environment with light to moderate number of trees. The area size is 20×2 km^2 which includes 8053 SMs and 776 poles. The traffic specifications are derived from [5] as presented in Table 4.1 in Section 4.2.

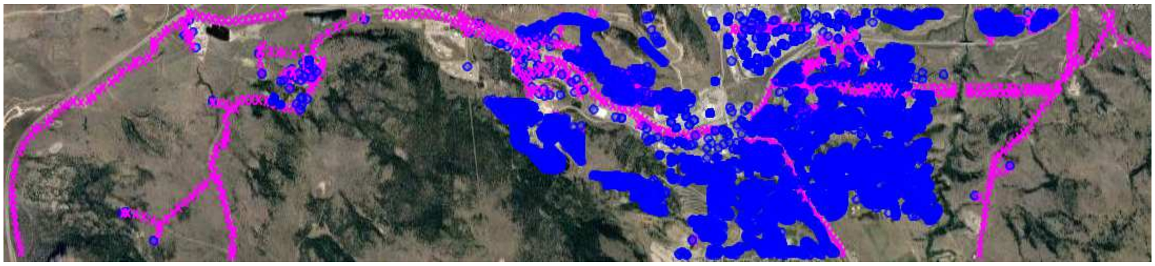

(a)

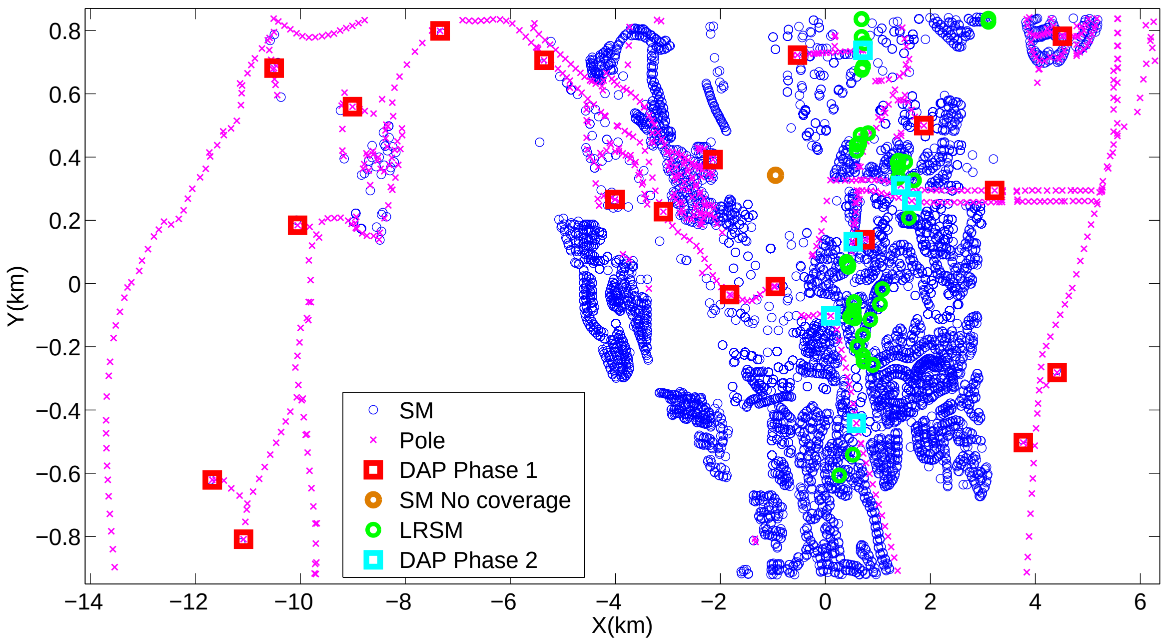

(b)

Figure 4.3: (a) The geographic location of smart meters and poles in the Kamloops suburban area. (b) Results of the proposed DAP placement algorithm for the Kamloops scenario. The red and cyan squares show the poles that are selected for DAP placement respectively in the first and second phase of the algorithm. The green circles show the low-reliability SMs (LRSMs) for which the poles in the second phase were added. The larger (orange) circle identifies the 19 SMs that are not connected to any DAP.

4.4.2 Performance Comparison with CPLEX

We first compare the optimality and complexity of our devised algorithm with the results obtained based on the CPLEX software for solving (4.27)[14]. To this end, since

[14]We have used the CPLEX software for finding optimal solutions to our IP problem using the branch and cut algorithm. For cases with large number of variables and constraints, sub-optimal

CPLEX is not able to solve the large-scale scenarios, we select smaller scale scenarios considering different area densities from the Kamloops scenario. The performances of our algorithm and the CPLEX software are compared in Table 4.3. As the number of aggregators indicates the optimization objective, we can observe that our algorithm returns near-optimal results and at the same time, our algorithm offers much lower run-time complexity and memory requirement. We further observe from Table 4.3 that more aggregators are required for the scenarios with lower SM density.

solutions can be obtained by defining additional bounds to the branches with depth larger than a certain threshold. One of the pioneer works for automatic configuration of the features of the IBM CPLEX software in order to improve the run-time complexity of the associated heuristic algorithms has been conducted by Hutter *et al.* [112]. In particular, they have proposed two automatic configuring algorithms namely BasicILS and FocusedILS that are trained by 50 instances of the problem. The best configuration which results in low run-time complexity is selected for finding solutions for larger scale scenarios.

Table 4.3: Comparing the optimality and complexity of proposed DAP placement algorithm and CPLEX for solving problem (4.27) for several small-scale scenarios within Kamloops

Scenario	Method	Memory (MB)	Time (s)	Number of Iterations	Number of Aggregators	Max. hops
47 SMs 43 Poles Rural (23.5 SMs per km^2)	CPLEX (13009 Non-zero coeffs.)	358.2 4487 Variables 6746 Constraints	25.0	NA	4	2
47 SMs 43 Poles Rural (23.5 SMs per km^2)	DAP placement algorithm	0.7	5.0 4.3 First phase 0.7 Second phase	1	4	2
60 SMs		481.1				

12 Poles Suburban (155.2 SMs per km^2)	CPLEX (12942 Non-zero coeffs.)	4124 Variables 7841 Constraints	77.0	NA	1	10
60 SMs 12 Poles Suburban (155.2 SMs per km^2)	DAP placement algorithm	0.9	6.1 5.1 First phase 1.0 Second phase	2	2	6
74 SMs 37 Poles Suburban (513.9 SMs per km^2)	CPLEX (34290 Non-zero coeffs.)	1094.6 9554 Variables 15140 Constraints	1860.0 (Stopped at 6% optimality gap)	NA	1	5
74 SMs 37 Poles	DAP placement	1.2	7.3 6.5 First phase	1	1	5

Suburban (513.9 SMs per km^2)	algorithm		0.8 Second phase			
161 SMs 24 Poles Urban (958.3 SMs per km^2)	CPLEX (135888 Non-zero coeffs.)	854.3 38117 Variables 64335 Constraints	840.0	NA	1	6
161 SMs 24 Poles Urban (958.3 SMs per km^2)	DAP placement algorithm	2.3	14.3 10.3 First phase 4.0 Second phase	1	1	6

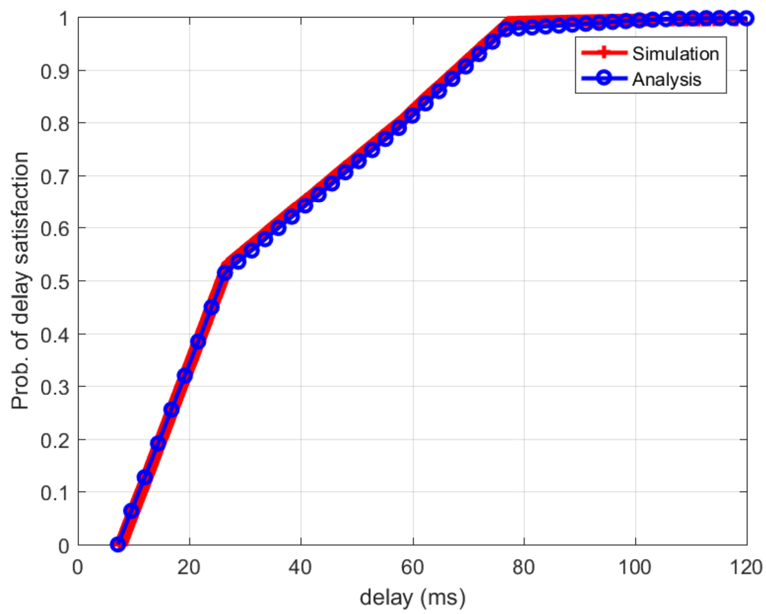

Figure 4.4: Comparison of the analysis and simulation for the probability of delay satisfaction as a function of deadline.

4.4.3 Validation of the Delay Model

In order to validate our assumptions and delay model derived in Section 4.2, we use the NS-3 software [43] to simulate the SM-to-relay transmissions in the Kamloops scenario. Each SM generates packets based on the traffic classes listed in Table 4.1. We measure the total delay experienced by each packet as the difference between the time it is successfully received by the destination and its generation time. Figure 4.4 compares the empirical delay distribution with the analytical probability of delay satisfaction for the packets that have been generated from an SM, which has 124 feeding nodes and 126 neighbour nodes. Nine of the neighbours have respectively 1244, 330, 319, 233, 108, 58, 53, 26, 5 feeding nodes and the other 117 nodes do not have any. As it can be seen from Figure 4.4, the probability of latency satisfaction obtained from simulations closely matches the values obtained from the analysis in Section 4.2.2. This verifies that the assumptions made in the system model are valid for the traffic classes listed in Table 4.1. Specifically, under the mixed traffic model the distribution of packet generations in each SM can be well approximated with a Poisson distribution, and the distribution of packet arrival in the forwarding nodes can be also assumed to follow a Poission distribution.

4.4.4 Number of DAPs

Figure 4.3(b) shows the result of the DAP placement algorithm for the whole Kamloops scenario. In the first iteration of the algorithm, 19 poles, marked with red squares, are selected for DAP placement such that the network coverage can be ensured. In the next 3 iterations, 6 additional poles, marked with cyan squares, are added in order to enforce the required reliability for the SMs that do not satisfy the reliability requirement. These SMs are marked with green circles in the figure. For the 19 SMs which are located in the same building at location $(-1.0, 0.35)$, there is no connectivity solution, as there is no pole or SM in their connectivity range.

Figure 4.5 compares the result of our heuristic algorithm with the lower bound on the required number of DAPs which only addresses the latency constraint, as explained in Section 4.2.4. On the x-axis of this figure, the number of SMs and poles are shown in separate lines. The scenarios shown in columns 1-7 are from the smaller scale scenarios in Kamloops, and scenarios 8 and 9 are taken from two other rural and suburban locations in BC, Canada. Scenario 10 illustrates the entire Kamloops scenario. We can observe from Figure 4.5 that the solution of our heuristic algorithm is relatively close to the lower bound, which suggests that it is not far from the optimal solution. For example, for the Kamloops scenario with 8053 SMs, the ratio between the obtained solution by our heuristic (25 DAPs) and the lower bound (19 DAPs) is much less than the worst-case approximation factor ($\ln(8053) \simeq 9$).

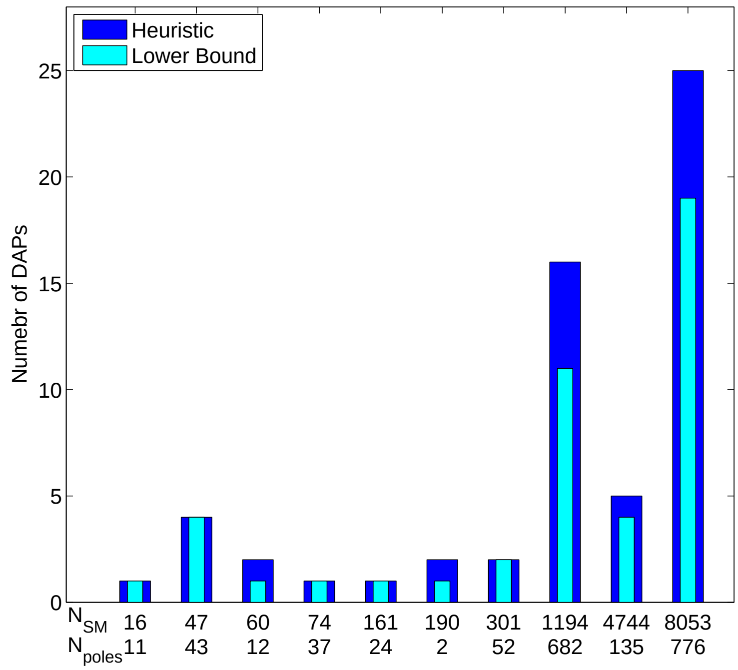

Figure 4.5: Comparison between the heuristic solution and the lower bound. For each scenario, the number of SMs and poles are shown in separate lines on the x-axis.

4.4.5 Connections per Pole

Figure 4.6 shows the empirical cumulative distribution function (CDF) of the number of connections to the DAPs for the Kamloops scenario. It is observed that around 80% of the DAPs have less than 623 SM connections. We also note that about 35% of the DAPs have less than 5 connections which is due to the several rural areas with sparse location of smart meters, e.g. for $x < -6.0$ in Figure 4.3. To reduce the number of DAPs with few connectivities, the installation of range extenders would be beneficial.

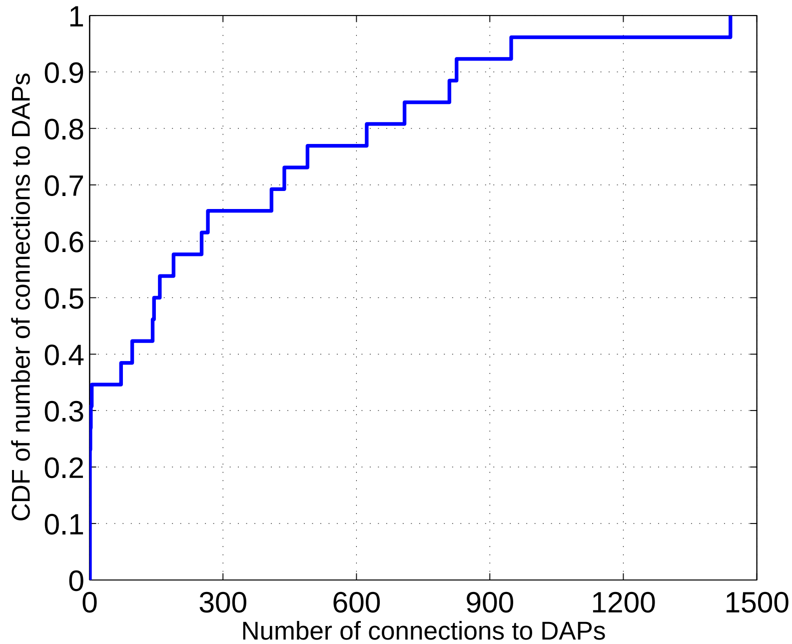

Figure 4.6: CDF of total number of connections to DAPs (the mean value is 322).

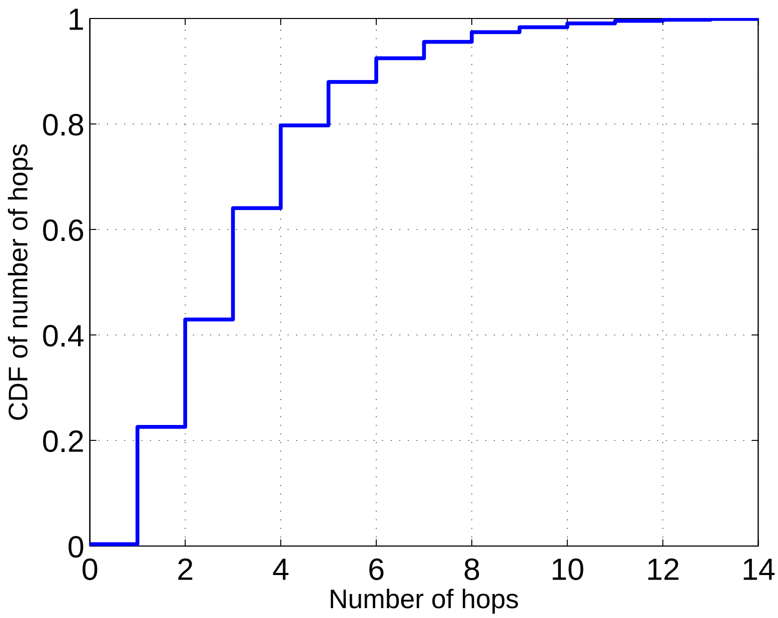

Figure 4.7: CDF of the number of hops (the mean value is 3.2).

4.4.6 Number of Hops

Figure 4.7 shows the distribution of the number of hops for SM-DAP connections in the network for the Kamloops scenario. As can be seen, around 22% of the nodes are directly connected to DAPs, and 90% of the nodes are within a 6-hop connectivity from a DAP. For the farther nodes, our algorithm ensures that their obtained reliability is still within what is required. This shows the flexibility of our algorithm compared to [15] and [19], where they address latency through considering a fixed number of hops, while our algorithm selects the DAP locations and number of hops based on the network topology, SM to SM and SM to pole distances and number of competitors at each hop. The dynamic selection of number of hops based on these parameters makes it possible to access farther SMs with the lowest number of DAPs, without compromising the required latency.

4.4.7 Queuing Delay

Figure 4.8 shows the CDF of the queuing delays observed for the mission-critical and non-critical traffic for the Kamloops scenario. The maximum queuing delay observed for mission-critical traffic is 0.1857 ms and the maximum queuing delay observed for non-critical traffic is 0.30 ms. The small queuing delay observed is due to the low data rate at the nodes.

4.4.8 Complexity Analysis

4.4.8.1 Proposed algorithm

Here we estimate the complexity of each step in our algorithm to derive its overall complexity.

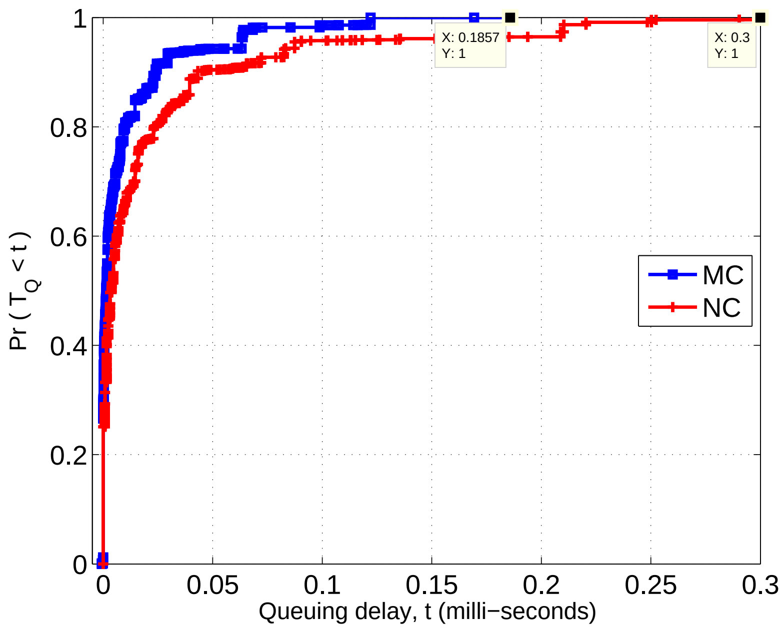

Figure 4.8: CDF of queuing delay for the MC and NC traffic.

KD tree construction and range search: In the first phase of our placement algorithm, we use the KD tree data structure for storing SM locations. Then, we perform a range search operation over this tree in order to identify the set of SMs which are in the communication range of a certain pole. The runtime and memory complexity of KD tree construction are respectively $O(N_{\mathrm{SM}} \log(N_{\mathrm{SM}}))$ and $O(N_{\mathrm{SM}})$. The range search operation complexity is $O(N_{\mathrm{poles}} \log(N_{\mathrm{SM}}))$.

Shortest path: In order to identify optimal routes for each SM, shortest paths are constructed from each DAP using the Dijkstra algorithm. The associated time and memory complexity are $O(N_{\mathrm{SM}}^2)$ and $O(N_{\mathrm{SM}}^2)$, respectively.

Since the shortest-path search has the higher complexity of the above two steps, the total algorithm run-time and memory complexities are of the orders of $N_{\mathrm{DAP}}O(N_{\mathrm{SM}}^2)$ and $N_{\mathrm{DAP}}O(N_{\mathrm{SM}}^2)$, respectively. For the specific Kamloops scenario with 8053 SMs considered above, we measured a memory usage of 83 MB.

4.4.8.2 CPLEX

CPLEX uses a branch and cut algorithm for finding the optimal solution to the IP problem. In the worst case, the complexity of such an algorithm is exponential, and the actual mean time-complexity depends on many factors and is evaluated empirically [113, 114]. Another limiting factor when optimization solvers are used for solving IP problems is the required RAM. According to [115], for every 1000 constraints, at least 1 MB RAM is required by CPLEX in order to solve an IP problem. Since the presented DAP problem in (4.27) considering 8053 SMs and 776 poles has around 140,000,000 constraints, an estimated 140 GB RAM would be needed to solve it by CPLEX.

4.4.9 Comparison with Other Works

In this section, we compare the optimality and time-complexity of our algorithm with the work presented in [20] and [87]. For a fair comparison with [20], we limit the number of hops to $H = 4$ and compare the solution of our algorithm with the second scenario in [20, Table II] that has a similar number of SMs and poles as the Kamloops scenario. We observe from our simulations results, which are omitted here due to space constraints, that our algorithm finds a more cost-efficient solution as it only selects 37 out of 776 poles and ensures coverage and latency constraints, while the algorithm from [20] selects 426 poles for DAP placement and only ensures SM coverage. Furthermore, the complexity of their algorithm is higher. In particular, the method from [20] requires to calculate the multi-hop connectivity matrix as part of the pre-processing method, which has a computational complexity of $H \cdot O((N_{\text{poles}} +$

$N_{\mathrm{SM}})^3)$. Then, the coverage matrix is passed to the GLPK software for obtaining the minimum number of cover sets, which in the worst-case scenario has a complexity of $O(2^{(N_{\mathrm{poles}}+N_{\mathrm{SM}})})$. When the network becomes large, their heuristic algorithm breaks the area into smaller squares which can be handled by the optimizer. Their post-optimization step involves merging the solution of smaller squares, solved by GLPK software, by removing the redundant poles located in square edges. This step has the complexity of $O(N_{\mathrm{SM}}N_{\mathrm{poles}}^2)$. In terms of the memory complexity, the method from [20] would require 2-306 MB depending on the selected square size.

Reference [87] utilizes the divide and conquer algorithm for identifying the set of SMs that can relay traffic in an AMI. In the procedure of relay selection, the maximization of QoS is considered in the objective by minimizing packet loss and average latency, which are calculated based on the link distance and M/D/1/k queueing theory. The algorithm focuses on single-hop connectivity of endpoints to the aggregator and finally, connects every 10-15 endpoints to one aggregator. This is not a feasible solution in practice, since at least around 533 aggregators would then need to be installed and maintained.

4.5 Conclusion

In this chapter, the problem of DAP placement for an AMI with overhead power lines has been investigated. We proposed a mutli-phase heuristic algorithm for selecting the optimized pole locations for DAP placement such that smart grid QoS requirements can be met. We maximized the obtained reliability for the smart grid traffic through discovering routes with minimum packet error rates and scheduling the mission-critical and the non-critical traffic using TDMA and CSMA/CA protocols, respectively. The probability of exceeding a certain latency is computed based on the specific characteristics of these two protocols. Comparing the results of our algorithm with the literature and solutions obtained by the IBM CPLEX software for small-scale examples, we believe that our algorithm is competitive in terms of performance for the problem at hand, albeit at much lower complexity. The complexity advantage allows us to successfully tackle larger-scale problems as shown in this chapter.

Chapter 5

Network Planning for Smart Utility Networks Using PLC

5.1 Introduction

In order to facilitate communication within the AMI, several solutions such as long-range wireless technologies, e.g., WiMAX and cellular networks [24, 53, 116], short-range low-data rate wireless technologies, such as IEEE 802.15.4g SUN technology [94] and Wi-Fi [117], and wired solutions such as Ethernet [49, 54] and PLC [54, 118, 119] have been employed. Among the wired communication technologies, PLC has the advantage that the required cable infrastructure is already in place, which greatly reduces installation cost and also allows for an easier access to remote areas.

The placement of intermediary DAPs between the SMs and the utility control center is necessary in order to avoid the high possibility of congestion between the traffic flows generated from thousands of SMs. The placement of DAPs is also helpful for decreasing the distance to the utility control center and consequently, achieving a higher packet success ratio and throughput at the SMs.

In the PLC AMI, DAPs are installed on the distribution transformers residing on utility poles or pad-mounted transformers when respectively an overhead or underground power line infrastructure is used [120]. In North American countries, only a few SMs are served by a single distribution transformer and it would be costly to install DAPs on all of them. To reduce the installation and maintenace cost, DAPs are placed on the medium-voltage side of a distribution transformer so that SMs served by other transformers can share the same DAP [118, 120, 121]. The selection of the location of these DAPs is critical so as to meet the QoS requirements associated with the different traffic types, namely, regular meter reading, alert notifications, power quality and on-demand meter reading [6, 21, 70]. In particular, the location of DAPs affects the number of hops and contenders that data traffic from each SM would experience when accessing the communication medium.

Although the problem of data collector placement for smart grids has been investigated in several papers, there are only a few which designed the AMI based on QoS requirements. In [8], the authors developed a genetic based algorithm for a single-hop AMI. They connect SMs to the DAPs through the IEEE 802.15.4g technology and schedule all the traffic through a TDMA scheduling scheme, which limits the number of nodes that can access the medium and the network utilization. In [87], the authors proposed a divide-and-conquer solution for optimally placing DAPs in a single-hop AMI. They designed the AMI based on the maximization of the obtained QoS but not its satisfaction, which leads to an overdesign in terms of number of DAPs. In [122], the authors investigated which network nodes should be chosen for access point installation in a medium voltage distribution network based on PLC such that the capacity and link quality requirements can be maintained. However, latency requirements have not been taken into account. The authors in [123], based on several experiments, proposed a general guideline for designing the AMI based on PLC technology. They place DAPs in secondary substations and use narrowband PLC over the low-voltage distribution grid for connecting SMs to the DAPs. In order to meet latency requirements, they limit the maximum number of hops to a certain limit. However, limiting the maximum number of hops only addresses the transmission delay but not the medium access delay.

In our previous works [124] and [104], we have developed a heuristic algorithm for placing the DAPs on top of the existing utility poles for a large-scale *wireless* AMI. In particular, we have assumed SMs are equipped with SUN mesh technology and transmit their traffic to the DAPs using multi-hop communication. We note that the model derived for SUN in [124] and [104] can not directly be applied to a PLC-AMI because of the different physical and MAC layer properties of the wireless and wired technologies. In particular, the transmission and propagation properties are different in SUN and PLC. Moreover, unlike SUN, the PLC technology considered in this work accommodates traffic priorities when scheduling traffic through CSMA/CA, which requires a completely different analysis for the medium access delay.

In this chapter, we complement the analyses and designs presented in [8, 87, 104, 122–124]. We study the design of an AMI infrastructure using the popular PRIME PLC technology [29] for the aggregation of SM traffic in DAPs, which can be placed on pad-mounted or overhead transformers. Multi-hop communication is enabled to access distant nodes in the network and to reduce the required number of DAPs [125]. We derive an analytical model for computing the obtained reliability considering the priority-based CSMA/CA MAC scheme in the PRIME standard. Based on this model, we formulate an optimization problem for obtaining the minimum number of DAPs and their locations while meeting the reliability requirement. We then propose a heuristic method for finding a solution to the NP-hard optimization problem in large-scale AMI scenarios.

The remainder of this chapter is organized as follows. We first present the system model in Section 5.2 and then formulate the probability of latency satisfaction based on the PRIME CSMA/CA MAC procedure in Section 5.3. As the problem of optimal DAP placement with the QoS constraint is a non-linear integer programming problem and is NP-hard, we apply a heuristic method and formulate the simplified network planning optimization problem in Section 5.4. In Section 5.5, we test our proposed optimization approach on realistic scenarios, where SMs and network nodes locations are obtained from BC Hydro, a Canadian power utility company. Numerical results show that our approach can efficiently compute the minimum required number of DAPs and their optimized locations while ensuring the satisfaction of the QoS requirements for the SM traffic.

5.2 System Model

In this section, we first describe all the assumptions that we have considered for the power grid infrastructure, as well as for the traffic model in Section 5.2.1. Next we elaborate the differences that exist between CSMA/CA procedures of the IEEE 802.15.4g standard and PRIME in Section 5.2.2. We note that the components of the PLC module that we have developed for estimating the channel behaviour and SINR within the PLC networks are explained in Appendix B.

5.2.1 Power Grid Infrastructure and Traffic Assumptions

We consider a power grid infrastructure with N_{SM} SMs and N_{tr} pad-mounted or overhead transformers that are connected together through an existing power line network. We assume that the communication between SMs and DAPs are conducted through PRIME PLC technology in a single-hop or multi-hop manner. PRIME technology operates within the frequency band from 41 kHz to 471 kHz. This bandwidth is separated into eight subchannels. Each device may communicate over one or N_{ch}

of these subchannels. The transmission over each subchannel is conducted through 97 equally spaced subcarriers using OFDM [29].

We assume each SM, which operates either as a source or a relay node, forwards P different traffic flows, each based on a Poisson arrival process [126]. A lower value of $p \in \{1, 2, \ldots, P\}$ is given to the traffic that has a higher priority. The assumption that the traffic arrival at each intermediary SM follows a Poisson process is justified when the traffic load at each traffic class is low [95–98]. The traffic flows need to be collected by DAPs that are placed with selected transformers. We assume that DAPs with overlapping coverage use different channels for communication [123]. As discussed in [123], this assumption is practical for PLC and has the benefit of avoiding co-channel interference and traffic congestion between DAPs.

As different traffic flows have different reliability requirements, we use the priority-based CSMA/CA proposed in PRIME for scheduling the traffic. Here, we assume all nodes connected to the same DAP are within the sensing range of each other. This assumption helps us to avoid the hidden node problem. We should note that the required SINR for detecting a carrier is much less than what is required for decoding a packet correctly. Accordingly, as also confirmed through our simulations, even the nodes that require multi-hop access can detect the carrier of other nodes.

In PRIME, time is divided into abstract units which are called frames and each frame is divided into smaller units which are called time slots. The CSMA/CA back off procedure is conducted based on the concepts of these time slots. Accordingly, in the next sections, all the time-related variables are derived in units of time slots.

5.2.2 Comparing the CSMA/CA Procedures of the IEEE 802.15.4g standard and PRIME Specifications

As can be seen from the CSMA/CA procedures described in Sections 1.3.1 and 1.5.1, the CSMA/CA scheduling scheme in the PRIME technology has several differences compared to the the IEEE 802.15.4g standard. First, a differentiated access has been defined in PRIME for traffic with different priorities. Traffic classes with lower priorities should wait longer to access the medium. Second, each traffic flow should sense the channel as idle for a certain number of times, which is determined according to its traffic priority. Third, if the SM senses the channel as busy, it has to wait for the duration that it takes for the packet to be transmitted fully, i.e. I, before going to the next backoff stage. These differences necessitate the development of a new analytical model for the medium access delay, which is different from the one proposed in [124] for the IEEE 802.15.4g transmission.

In the following section, we derive an analytical model for computing the probability of latency satisfaction based on the characteristics of the priority-based CSMA/CA scheme, described in Section 1.3.1, and the channel behaviour of the PLC networks, described in Section 1.7, for each smart grid traffic flow.

5.3 An Analytical Model for Computing Reliability

The reliability for transmitting smart grid data is defined as the probability that a data packet can successfully be received at the destination within its required latency [70]. Therefore, the reliability depends on both the experienced latency and the quality of the route, i.e., the obtained SINR ratio and packet error rate over the route. Accordingly, in this section, we first derive the probability of latency satisfaction based on the medium access characteristics of the PRIME technology in Section 5.3.1. Then, we derive the packet error rate and overall reliability in respectively Sections 5.3.2 and 5.3.3.

5.3.1 Delay Model

There are several components that affect the amount of the delay that a packet experiences at each hop. It includes the queuing delay, medium access delay, transmission delay and the propagation delay. The propagation delay has a very small value and its effect is usually ignored. In this section, we first derive the queuing delay for each traffic priority at node x, T_{Q_x} in time slots. Then, we deduct the queuing and transmission delay from the total packet deadline and compute the probability that the packet can successfully access the medium within its deadline.

Let us assume that the link from node x to the DAP is through H_x hops. In order to meet the delay requirement, denoted as $D(p)$ and measured in time slots, for a traffic priority p, we allow

$$S_x(p) = \frac{D(p)}{H_x} \tag{5.1}$$

time slots to be consumed at each hop h. This conservative assumption allows us to guarantee the required latency at each hop. It should be noted that in practice, a larger delay may be consumed at some network segment while the total delay is still maintained.

5.3.1.1 Queuing Delay

We assume traffic is transmitted according to a priority queuing system. Applying the Pollaczek-Khinchin equation, the average waiting time of traffic flow p is given by [127]

$$T_{\mathrm{Q}_x}(p) = \frac{\bar{r}_x}{\left(1 - \sum_{p'=1}^{p-1} \rho_x(p')\right)\left(1 - \sum_{p'=1}^{p} \rho_x(p')\right)}, \tag{5.2}$$

where $\rho_x(p)$ is the probability of having a packet of traffic priority p for transmission. It can be expressed as

$$\rho_x(p) = \frac{\lambda_x(p)}{\mu_x(p)}, \tag{5.3}$$

where $\lambda_x(p)$ is the arrival rate of traffic class p, and $\mu_x(p)$ is the inverse of the packet service time of traffic class p. Also, $\bar{r}_x$ is the mean residual service time which can be derived as

$$\bar{r}_x = \frac{1}{2} \sum_{p=1}^{P} \lambda_x(p) \bar{s_x^2}(p), \tag{5.4}$$

where $\bar{s_x^2}(p)$ is the second moment of service time of traffic priority p. The expressions for $\mu_x(p)$ and $\bar{s_x^2}(p)$ are derived later in this section.

Having computed the queuing delay, we now compute the probability that the packet can be transmitted within the deadline.

5.3.1.2 Medium Access Delay

The probability that a packet of node x at hop h can successfully be transmitted within the deadline is obtained as

$$\Pr(\ell_{x,h}(p) \leq S_x(p)) = \sum_{k=1}^{S_{x,\max}(p)} \theta_x(k,p), \tag{5.5}$$

where $\ell_{x,h}(p)$ is the experienced latency at hop h for traffic priority p, $S_{x,\max}(p) = S_x(p) - T_{\mathrm{Q}_x}(p) - I - C(p)$, and $\theta_x(k,p)$ is the probability that the channel is determined

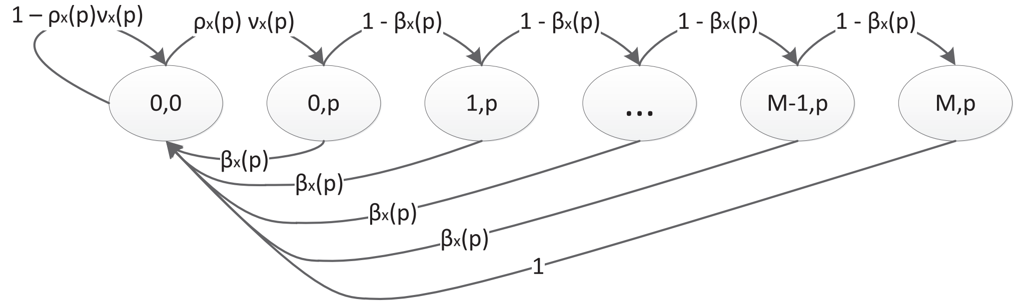

Figure 5.1: The Markov chain of the CSMA/CA for traffic priority p.

as idle at slot k for traffic priority p. The latter is given by

$$\begin{aligned}\theta_x(k,p) &= \zeta_x(k,p)\ \beta_x(p) \\ &= \zeta_x(k,p) \prod_{j=1}^{C(p)} \left(1-\alpha_x\left(j\right)\right),\end{aligned} \tag{5.6}$$

where $\zeta_x(k,p)$ is the probability that the traffic priority p senses the channel at slot k and $\beta_x(p)$ is the probability that the channel is idle, when sensed for $C(p)$ consecutive times. $\alpha_x(j)$ is the probability that the channel is busy when it is sensed for the jth time, which is obtained later in this section.

As each slot can be sensed at either of the $M+1$ stages, the probability of assessing a certain slot is obtained as a cumulative effect of sensing the channel at different backoff stages,

$$\zeta_x(k,p) = \sum_{m=0}^{M} \Phi_x(k,m,p), \tag{5.7}$$

where $\Phi_x(k,m,p)$ gives the probability that the node senses the channel in slot k and sensing stage m for its traffic priority p. The values of $\Phi_x(k,m,p)$ are computed in Appendix A.

The variable $\alpha_x(j)$ in (5.6) gives the probability that the channel is busy when node x senses the channel for the jth time, given that the channel was idle for $j-1$

times. This happens if in one of the previous $t(j)$ slots the channel was idle for p consecutive times and at least one node had sensed the channel for its traffic priority p. Therefore, variable $\alpha_x(j)$ is computed as

$$\alpha_x(j) = t(j) \sum_{p=1}^{P} \prod_{j'=j}^{p} \Big(1 - \alpha_x(j')\Big)\Big(1 - \prod_{x' \in \Psi(x)} \big(1 - \xi_{x'}(p)\big)\Big). \tag{5.8}$$

Here, $\Psi(x)$ is the set of nodes that are connected to the same DAP as node x,

$$t(j) = \begin{cases} I & j = 1 \\ 1 & j > 1 \end{cases}, \tag{5.9}$$

and $\xi_{x'}(p)$ is the probability of assessing the channel by a neighbour node in an arbitrary slot, which is obtained as

$$\xi_x(p) = \sum_{m=0}^{M} \frac{P_x(m,p)}{W(m,p)}, \tag{5.10}$$

where $P_x(m,p)$ is the probability that node x is in backoff stage m for its traffic priority p. This probability can be obtained from the corresponding Markov chain that has been illustrated in Figure 5.1 for the CSMA/CA procedure. Variable $\nu_x(p) = \prod_{p'=1}^{p-1} (1 - \rho_x(p'))$ denotes the probability that the node does not have any traffic with priority higher than p for transmission. The transition probabilities for this Markov chain can be derived as

$$\begin{bmatrix} 1-\rho_x(p)\nu_x(p) & \beta_x(p) & \dots & \beta_x(p) & \beta_x(p) & 1 \\ \rho_x(p)\nu_x(p) & 0 & \dots & 0 & 0 & 0 \\ 0 & 1-\beta_x(p) & 0 & \dots & 0 & 0 \\ \dots & \dots & \dots & \dots & \dots & \dots \\ 0 & 0 & \dots & 0 & 1-\beta_x(p) & 0 \end{bmatrix} \cdot \begin{bmatrix} P_x(0,0) \\ P_x(0,p) \\ P_x(1,p) \\ \dots \\ P_x(M-1,p) \\ P_x(M,p) \end{bmatrix} = \begin{bmatrix} P_x(0,0) \\ P_x(0,p) \\ P_x(1,p) \\ \dots \\ P_x(M-1,p) \\ P_x(M,p) \end{bmatrix}. \tag{5.11}$$

and from (5.11) the stationary distributions of the CSMA/CA states can be obtained as

$$\begin{aligned} P_x(0,0) &= \frac{\beta_x(p)}{\beta_x(p)+\rho_x(p)\nu_x(p)\left(1-(1-\beta_x(p))^{M+1}\right)}, \\ P_x(m,p) &= P_x(0,0)\rho_x(p)\nu_x(p)(1-\beta_x(p))^m. \end{aligned} \tag{5.12}$$

Probability of Collision: A collision would only occur if at least one contender node senses the channel at the same time as the transmitter for either of its traffic priorities [128, 129]. The probability of collision for traffic priority p, knowing that the channel was idle for p consecutive time slots, is denoted as $\chi_x(p)$ and is obtained as

$$\chi_x(p) = \sum_{j=1}^{P} \prod_{j'=p+1}^{j} \Big(1-\alpha_x\left(j'\right)\Big)\Big(1-\prod_{x'\in\Psi(x)}\left(1-\xi_{x'}(j)\right)\Big). \tag{5.13}$$

Computing service times: In order to compute the probability of having a packet for transmission and also to compute the queuing delay, the first and second moments of the service time are needed. These are given by

$$\bar{s}_x(p) = \sum_{m=0}^{M} \left(1-\beta_x\left(p\right)\right)^m \left(\frac{1}{2}W(m,p) + 1 + \sum_{j=2}^{C(p)} \prod_{j'=1}^{j-1} (1-\alpha_x(j')) + I\right), \tag{5.14}$$

and

$$\bar{s_x^2}(p) = \sum_{k=1}^{S_x(p)} \Pr(\ell_{x,h}(p)=k)\ k^2\ , \tag{5.15}$$

where the expected service time of traffic priority p is computed based on the time that is consumed at each backoff stage. The term $\left(1-\beta_x\left(p\right)\right)^m$ is the probability of moving to the sensing stage m, and the last two terms respectively represent the time consumed for $C(p)$ consecutive channel sensings and the transmission. Accordingly, the service rate is obtained as

$$\mu_x(p) = \frac{1}{\bar{s}_x(p)}. \tag{5.16}$$

5.3.2 Route Quality

The route quality is obtained through multiplying the link packet error rates over the whole path. To this end, we first compute the obtained SINR for each link and then, we translate it to the PER. The SINR of each link is computed according to

$$\gamma_{ij} = \frac{\sum_{n=1}^{N_{\text{ch}}} \sum_{k=1}^{N_{\text{sc}}} P_{\text{tx}}(f_{nk}) |\mathcal{H}_{ij}(f_{nk})|^2}{\sum_{n=1}^{N_{\text{ch}}} \sum_{k=1}^{N_{\text{sc}}} (N_0(f_{nk}) + \kappa(f_{nk}))}, \tag{5.17}$$

where N_{ch} is the total number of subchannels used for transmission and N_{sc} is the total number of subcarriers within each subchannel, and f_{nk} is the corresponding central frequency for each subcarrier. Variable N_0 stands for the power spectral density of the background noise and the frequency selective noise at the low voltage and medium voltage cables, P_{tx} denotes the transmission power spectral density, and $\mathcal{H}_{ij}$ is the channel frequency response from transmitter i to receiver j. Variable κ denotes the co-channel interference. The packet error rate between nodes i and j can be written as

$$\epsilon_{ij} = \mathcal{Q}(\gamma_{ij}), \tag{5.18}$$

where $\mathcal{Q}$ maps the SINR to the PER based on the modulation and coding scheme.

5.3.3 Reliability

The reliability over the whole path is obtained as the multiplication of the link reliabilities, each of which is computed as the multiplication of the probability of latency satisfaction and the probability of successful packet reception at each link h:

$$R_x(p) = \prod_{h=1}^{H_x} \left(1 - \epsilon_{x,h}\right)\left(1 - \chi_x(p)\right) \Pr\left(\ell_{x,h}(p) \leq S_x(p)\right), \tag{5.19}$$

where $\epsilon_{x,h}$ denotes the packet error rate between the relay node located at hop $h-1$ and the relay node located at hop h as derived in (5.18). These relay nodes forward the packets of node x. The reliability constraint can then be expressed as

$$R_x(p) \geq \tau, \tag{5.20}$$

where τ is the desired reliability requirement for the network.

5.4 Optimization Problem

In this section, we formulate an optimization problem for computing the minimum required number of DAPs and their optimized locations such that the installation cost is minimized and the reliability requirement that has been derived in the previous section can be met. The placement of data collectors on certain network node locations is an integer programming problem. While such problems can efficiently be solved using the IBM CPLEX software [17] when the solution space is small (e.g., for linear constraints with small number of variables and constraints), for scenarios with non-linear constraints, which involve searching a larger space for checking the conflicts [130], and large number of variables, we usually require a low-complexity heuristic method to obtain a solution [12].

The reliability constraint given in (5.20) is non-linear. Therefore, in order to decrease the complexity of the optimization problem, in Section 5.4.1, we first decompose the reliability constraint into two constraints, namely latency satisfaction and route quality. The latency constraint is then further simplified into a linear constraint. In Section 5.4.2, we deal with the route quality constraint by proposing a pre-processing algorithm that obtains routes with high packet success ratio. Finally, we formulate the simplified optimization problem with all linear constraints in Section 5.4.3.

5.4.1 Decomposition Method

We decompose the non-linear reliability constraint (5.20) into two constraints, namely route quality and delay satisfaction,

$$\prod_{h=1}^{H_x} \left(1-\epsilon_{x,h}\right) \geq \tau_r, \qquad 1 \leq x \leq N_{\mathrm{SM}}, \tag{5.21}$$

$$\prod_{h=1}^{H_x} \left(1-\chi_x(p)\right) \Pr\left(\ell_{x,h}(p) \leq S_x(p)\right) \geq \tau_d, \; 1 \leq x \leq N_{\mathrm{SM}}, \; 1 \leq p \leq P \tag{5.22}$$

where $\tau_r \tau_d = \tau$. We note that while replacing (5.20) by (5.21) and (5.22) is done to reduce the complexity of the optimization problem, it also limits the solution space as the problem is solved for specific values of τ_r, and τ_d.

Next, we approximate (5.22) by constraining the maximum number of nodes that can be connected to a DAP while ensuring the latency satisfaction. This will indeed be equivalent to (5.22), if we assume that each node generates the same amount of traffic and accordingly, the probability that each node senses the channel, i.e., ξ_x is equal for all these nodes. The maximum number of nodes that can be connected to the same DAP, denoted as $N_{\max} = |\Psi_x|$, is then obtained from the non-linear system of equations (5.2)-(5.16), and (5.22). In order to write the corresponding constraint, we define the binary variable y_{ij} to indicate whether an SM i is connected to the DAP located on transformer j. We then have

$$\sum_{i=1}^{N_{\mathrm{SM}}} y_{ij} \leq N_{\max}, \quad 1 \leq j \leq N_{\mathrm{tr}}. \tag{5.23}$$

To account for the fact that the assumption that each node generates the same amount of traffic can be violated, especially for multi-hop communication, we consider a final step for our heuristic algorithm to ensure that the obtained topology indeed satisfies the original constraint (5.22). This will be explained in Section 5.4.3.

5.4.2 Finding Valid Routes

The route quality constraint (5.21) is non-linear as the quality of all the links in a multi-hop route should be taken into account. However, as suggested in [20, 122], we can reduce the complexity of a solver such as CPLEX by pre-computing the set of valid routes, which are the ones whose packet success ratio is higher than the required threshold, as per (5.21). Algorithm 5.1 shows the pseudo-code for calculating these routes. The inputs to this algorithm are the SM-to-transformer and SM-to-SM link error rates, respectively denoted by ϵ_{ij} and $\epsilon_{ii'}$, the maximum allowed number of hops $H_{\max}$, and the desired route quality threshold τ_r. This algorithm finds the path qualities Q_{ij} and the number of hops for each node, denoted by H_{ij}, as follows. In the first step, the SMs that have link qualities larger than the desired route quality threshold are directly connected to the transformer. Then, the algorithm checks whether the SMs that are not yet connected to the transformer have link qualities to the connected SMs that can satisfy the desired route quality. After the algorithm execution is finished, the SM i is connected to transformer j directly or via multi-hop, respectively if $H_{ij} = 1$ or $2 \leq H_{ij} \leq H_{\max}$, or not connected if $H_{ij} = 0$.

Algorithm 5.1 Finding SM-to-transformer paths

Require: $\epsilon_{ij}, \epsilon_{ii'}, H_{\max}, \tau_r$.

$Q_{ij} \leftarrow 1 - \epsilon_{ij}$ if $1 - \epsilon_{ij} \geq \tau_r$ else 0.

$H_{ij} \leftarrow 1$ if $1 - \epsilon_{ij} \geq \tau_r$ else 0.

for $h = 2 : H_{\max} + 1$ **do**

    for each SM i and transformer j which $H_{ij} == 0$ do

        $Q^* \leftarrow \max_{i' \colon 0 < H_{i'j} < H_{\max}} ((1 - \epsilon_{ii'}) Q_{i'j})$

        $i^* \leftarrow \arg \max_{i' \colon 0 < H_{i'j} < H_{\max}} ((1 - \epsilon_{ii'}) Q_{i'j})$

        $Q_{ij} \leftarrow Q^*$ if $Q^* \geq \tau_r$ else 0.

        $H_{ij} \leftarrow H_{i^*j} + 1$ if $Q^* \geq \tau_r$ else 0.

    end for

end for

return Q, H

5.4.3 The Simplified DAP Placement Problem

Using the results from Sections 5.4.1 and 5.4.2, in this section, we formulate the simplified optimization problem as follows. Let us define the binary variable x_j to indicate whether a DAP is installed on transformer j. As stated in [126], DAPs are costly to be installed and maintained. Therefore, we define the objective as finding the minimum required number of DAPs that can ensure the satisfaction of the reliability requirement. After finding $N_{\max}$ as explained in Section 5.4.1 and obtaining the set of valid routes from Algorithm 5.1, the DAP placement optimization problem can be written as

$$\underset{\{x_j\},\{y_{ij}\}}{\text{minimize}} \quad c_{\text{inst}} = \sum_{j=1}^{N_{\text{tr}}} x_j \ , \tag{5.24a}$$

subject to

$$\sum_{j=1}^{N_{\text{tr}}} y_{ij} = 1, \qquad 1 \le i \le N_{\text{SM}} \tag{5.24b}$$

$$\sum_{i=1}^{N_{\text{SM}}} y_{ij} \le N_{\max}, \qquad 1 \le j \le N_{\text{tr}}, \tag{5.24c}$$

$$\sum_{i=1}^{N_{\text{SM}}} y_{ij}\lambda_i \le \mu_j, \qquad 1 \le j \le N_{\text{tr}}, \tag{5.24d}$$

$$y_{ij} \le x_j,\, 1 \le i \le N_{\text{SM}}, 1 \le j \le N_{\text{tr}}, \tag{5.24e}$$

$$x_j, y_{ij} \in \{0,1\}, \quad 1 \le i \le, 1 \le j \le N_{\text{tr}}. \tag{5.24f}$$

Problem (5.24) is a linear integer program since the objective function (5.24a) and all of the constraints are linear functions of binary variables x_j and y_{ij}. The numbers of variables and constraints for this problem are respectively $N_{\text{SM}}N_{\text{tr}}+N_{\text{tr}}$ and $N_{\text{SM}}N_{\text{tr}}+2N_{\text{tr}}+N_{\text{SM}}$. These are significantly lower than those for the original problem, which has a structure similar to (4.27), with $3N_{\text{SM}}N_{\text{tr}}+N_{\text{tr}}$ variables and $3N_{\text{SM}}^2+N_{\text{SM}}N_{\text{tr}}+3N_{\text{SM}}+N_{\text{tr}}$ constraints, where especially the quadratic scaling of the latter with respect to the number of SMs is problematic. As the number of constraints and variables in the simplified optimization problem have notably been decreased and all the constraints are linear, it can efficiently be solved with CPLEX.

Figure 5.2 illustrates the steps involved in solving the DAP placement problem for PLC. We first import the geographical information for the SMs and transformer locations into the PLC-NS3 module [131] and emulate the PLC network accordingly. The PLC-NS3 module allows for simulating the PLC network topologies based on

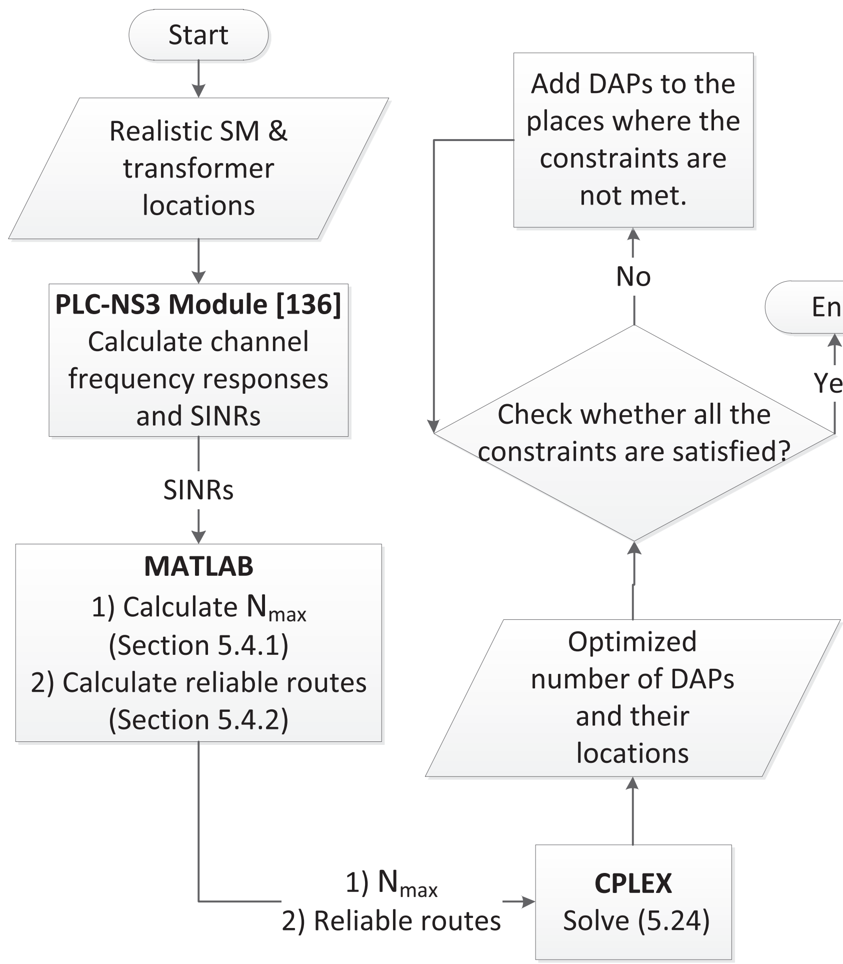

Figure 5.2: Steps of the heuristic algorithm for finding optimized DAP locations.

transmission line theory and calculating the channel frequency responses and accordingly SINRs from each transmitter to each receiver. We then import the SINRs into MATLAB and compute the relevant PERs according to the adaptive modulation. We give priority to the modulation and coding scheme that returns the higher data rate, provided that the obtained PER is less than $1 - \tau_r$. Then, we apply Algorithm 5.1 from Section 5.4.2 for calculating the reliable routes for each SM. We also compute the maximum number of nodes that can be connected to each relay, as per (5.23).

We use the set of reliable routes along with the simplified problem (5.24) as input to CPLEX and obtain the minimum required number of DAPs and their optimized locations. Finally, we check whether the resulting topology satisfies the delay constraint (5.22) considering the multi-hop traffic, and select additional DAPs where needed.

5.5 Simulation Settings and Results

In this section, we apply our network planning approach on a realistic smart metering infrastructure from the area of Kamloops, BC, Canada. In the following, we first discuss the set of parameters that we have used for running our simulations and then present the network planning solutions we have derived for different considered scenarios.

5.5.1 Simulation Settings

The set of parameters and traffic classes that we have used for running our simulations are summarized in Tables 5.1 and 5.2, respectively. Four traffic types, namely SCADA, meter reading (MR), alarm, and on-demand MR, with different arrival rates and required latencies are selected from [70]. The priorities shown in Table 5.2 are assigned to the traffic types according to their latency requirements. The load impedance of 10 Ω is considered at the smart meter and the DAP modems. In order to avoid the co-channel interference, we assign adjacent DAPs to operate over PRIME subchannels $1, 2, 7, 8$ and subchannels 3 to 6 [29]. The reason for selecting these two sets of subchannels is that they have the same total bandwidth and provide similar SINRs for most links. We assume that a transmission power of 20 mW is evenly distributed across the four subchannels and maintained regardless of the

Table 5.1: Simulation parameters

Parameter	**Value**
Req. reliability, τ	98%
Bandwidth	42-471 kHz
PLC technology	PRIME
Modulation and coding scheme (MCS)	Adaptive modulation
Maximum transmission power (P_{tx})	20 mW
Power line channel model	Bottom-up channel modelling [40, 131]
SM load impedance	10 Ω
Transformer	Pole-mounted 25 kVA Pad-mounted 50 kVA
Low voltage cable	NAYY150SE

access impedance at each transmitter. The additive noise is modeled as Gaussian with spectral density values adopted from the IEEE 1901.2 standard [132, Annex D] for both the low and the medium voltage sections of the power grid. The ABCD parameters associated with the transformer and medium voltage cables are also derived from [132, Annex D].

5.5.2 DAP Placement

Figure 5.3 shows a realistic example of a smart metering infrastructure selected from the Kamloops suburban area in BC, Canada. There are 3026 SMs and 318 overhead and pad-mounted transformers in this area.

As it can be observed, 47 transformers are selected for DAP placement, resulting in an average of 64 SM connections at one DAP. The number of SM connections per

Table 5.2: Traffic types and their properties

Traffic Priority	Traffic Type	Arrival Rate (packet per s)	Deadline (slots)
1	SCADA	$\frac{1}{5\times60}$	450
2	Alarm	$\frac{1}{60\times60}$	1350
3	Meter reading (MR)	$\frac{1}{15\times60}$	2250
4	On-demand MR	$\frac{1}{60\times60}$	13500

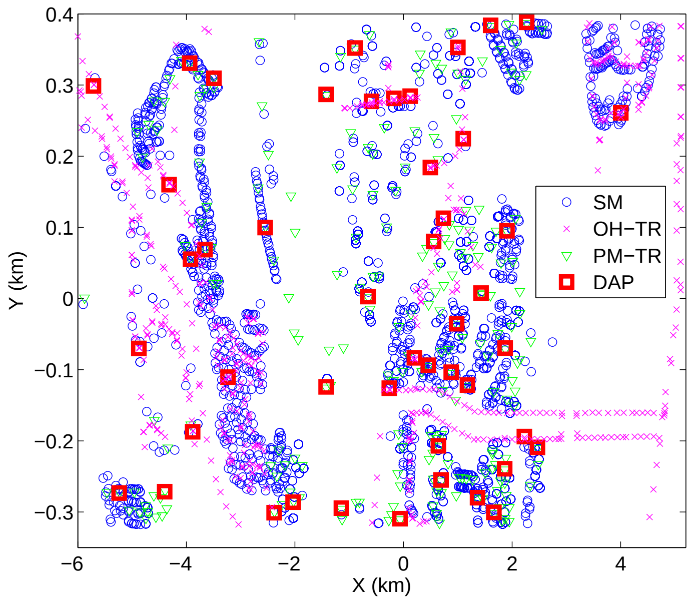

Figure 5.3: Result of the proposed DAP selection on a realistic set of SMs and transformers in Kamloops, BC, Canada. There are 3026 SMs, 96 overhead transformers (OH-TRs), and 222 pad-mounted transformers (PM-TRs). 47 transformers are selected for DAP installation.

DAP is larger in higher-density areas, e.g. around coordinates $(1.0, -0.1)$ and smaller in sparsely populated areas, e.g. around $(-4.5, 0.0)$. All SMs satisfy the reliability requirement, $\tau = 0.98$.

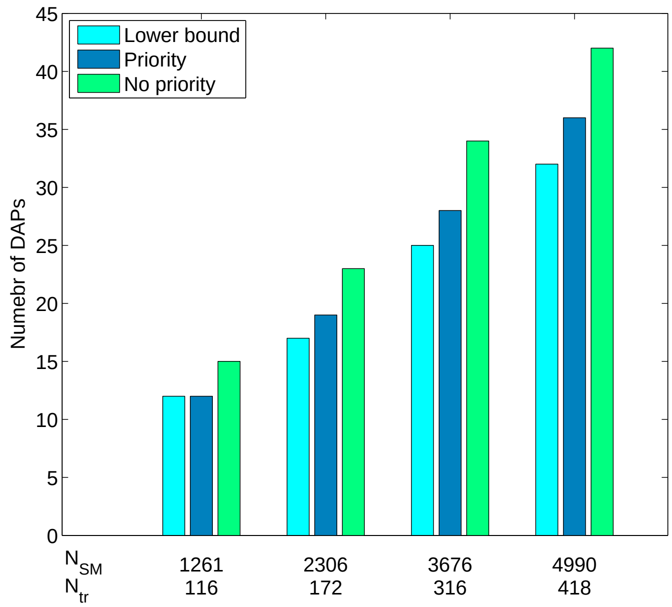

Figure 5.4: Number of selected DAPs for priority and non-priority based channel access considering an overhead infrastructure. For comparison, the lower bound to the optimal solution is also shown.

5.5.3 Priority and Non-Priority Channel Access

We next illustrate to what extent prioritized channel access compared to the non-prioritized channel access model, which is used in the IEEE 802.15.4g standard, can help to decrease the required number of DAPs. Figure 5.4 shows the number of selected DAPs for the traffic set presented in Table 5.2 in the priority-based and non-priority-based channel access models, considering a single-hop communication infrastructure. As can be observed from this figure, the priority-based channel access scheme decreases the required number of DAPs. This is because in the priority-based model, the traffic with the stricter latency requirement has a higher channel access rate compared to the lower priority traffic class. Therefore, a larger number of SMs can be served by a DAP while meeting the reliability requirement.

In order to investigate the optimality of our solution, we now consider the op-

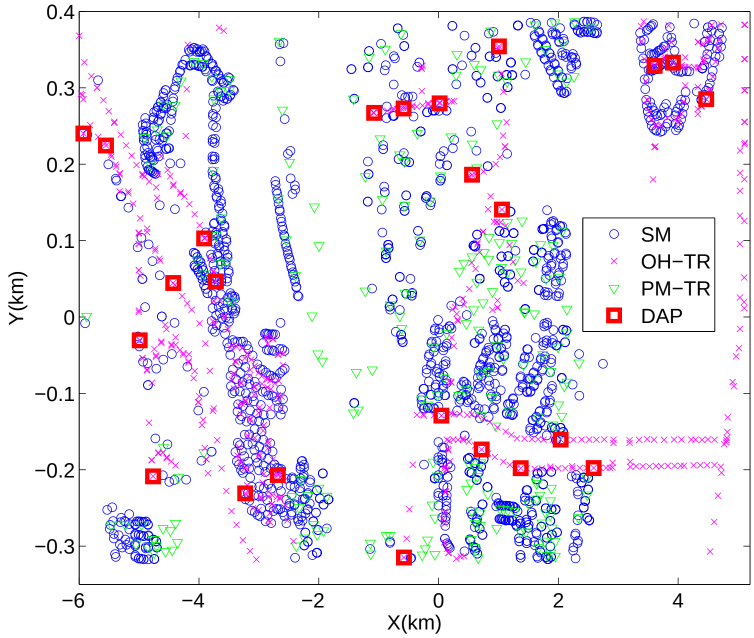

Figure 5.5: Results of the DAP selection for the AMI in Figure 5.3 when the 802.15.4g wireless communication is used instead of PLC.

timization problem with only the packet success ratio as the QoS constraint. In particular, we replace the reliability constraint (5.20) by (5.21) and ignore the effect of latency requirement (5.22). Hence, the solution of this problem returns a lower bound for the number of DAPs. The results from this simplified problem are also shown in Figure 5.4. We can observe that the solution of the actual optimization problem is very close to the lower bound. This suggests that the proposed DAP placement algorithm returns near-optimal solutions.

5.5.4 Comparison with Wireless AMI

Figure 5.5 shows the results for DAP placement on the same network as in Figure 5.3 when, instead of PLC, the IEEE 802.15.4g wireless standard for smart utility networks (SUN) [94] is used for providing multi-hop communication between nodes.

Here, we use the optimization formulation that we have derived in [124], for obtaining the minimum required number of DAPs and their optimized locations. From Figure 5.5, we observe that 24 transformers are selected for DAP installation for the SUN technology, which is about half of the DAP installations needed for PLC, i.e., 47 as reported above.

To provide a more complete picture for comparing PLC and SUN, Table 5.3 shows the required number of DAPs for the same scenario considering both single-hop and multi-hop infrastructures. As it can be seen, the required number of DAPs in the single-hop scenario is increased to 38 for SUN. There is little change in the number of DAPs for the case of PLC. This comparison thus shows that the SUN technology, due to its lower coverage range, benefits more from allowing multi-hop communication. We speculate that the only incremental benefit of multi-hop transmission in the case of PLC is due to the fact that only the nodes that are connected to the same transformer can forward the packets of each other, as otherwise the signal should pass through another transformer and the extra attenuation would make the multi-hop communication impossible.

To further highlight the effect of transformers, Table 5.3 also shows the results if we change the infrastructure such that all lines and transformers are overhead. In this case, the number of DAPs required for PLC is reduced from 47 to 28, which is due to the lower signal attenuation from overhead compared to pad-mounted transformers. Furthermore, there is no benefit from multihop transmission in terms of DAP placement. This corroborates our finding for multi-hop PLC transmission above, and also suggests that the data rate achievable over individual links, which would be improved through multi-hop transmission, is not the limiting factor for the PRIME based systems. We will elaborate on this in the following.

Table 5.3: Required number of DAPs with single and multi-hop communication. (OH and PM: original infrastructure with overhead and pad-mounted transformers. All OH: infrastructure changed to all-overhead lines and transformers.)

Network	**DAPs - Single-Hop**	**DAPs - Multi-Hop**
PLC OH and PM	50	47
SUN	38	24
PLC All OH	28	28

Table 5.4: Effect of the number of subchannels

Number of subchannels	**Data rate (kbps)**	**Required Number of DAPs**
2	79	infeasible
3	90	58
4	174	50
8	388	48

5.5.5 Effect of the Number of Available Subchannels

In particular, we investigate to what extent the available number of PRIME subchannels used for packet transmission, and thus the offered link rate, has an impact on the required number of DAPs. Assuming the same network as in Figure 5.3, Table 5.4 compares the offered link rate, that is computed based on the average SINR over all the SM-DAP links, and the required number of DAPs for different number of subchannels[15]. We observe that when the number of available subchannels is decreased from 8 to 4, only two additional DAPs are required. This highlights the fact that the aggregated traffic transmitted over SM-DAP links is well below the offered link rate over the entire PRIME bandwidth. We conclude that latency requirements and thus medium access ability constitute the bottleneck for the considered mix of SM traffic, and transmission over only 4 subchannels is sufficient in order to carry the traffic.

[15]We assume that there is negligible co-channel interference also for the case of 8 subchannels for all links for this comparison.

An interesting direction for further study would thus be the allocation of PRIME subchannels to SM-DAP links to improve medium access opportunities. Obviously, a further reduction in the number of subchannels eventually leads to a failure to meet the QoS requirements, as can be seen in Table 5.4.

5.6 Conclusion

In this chapter, we presented a powerful channel simulator for PLC. We then developed a PLC communication infrastructure for the AMI using PRIME technology. The network planning is conducted such that the smart grid QoS requirement, namely, reliability, can best be met and at the same time, the required number of DAPs are minimized. We formulated the reliability constraint based on the MAC characteristics of the PRIME technology, and then provided a heuristic method that enables us to solve large-scale scenarios with the IBM CPLEX software. The problem is solved for several realistic topologies of SM and transformer locations in the area of BC, Canada. The results showed that our optimization approach, by smart selection of transformers for DAP placement based on the priority-based CSMA/CA scheduling scheme, ensures the satisfaction of the reliability requirement for smart grid traffic, and at the same time, minimizes the DAP installation cost. We also observed that in a distribution grid with pad-mounted transformers, a large number of DAPs need to be installed if we use PLC for constructing the AMI. We note that the comparison will look different for other grid structures, such as for example in European countries, where the power grid has a larger SM-to-transformer ratio, and thus PLC is a more cost-efficient solution compared to the considered scenario for North America.

Chapter 6

Conclusion and Future Work

6.1 Conclusion

In this thesis, we have investigated the optimized configuration and system architecture for several communication technologies including WiMAX, IEEE 802.15.4g and PLC, when they used for smart grid implementation. In particular, in Chapter 2 we have devised a new profile configuration for WiMAX technology, when it is used for distribution automation. Characteristics such as frame duration, scheduling scheme, system architecture, and service type to traffic mapping were optimally configured such that smart grid QoS requirements namely latency and reliability can best be maintained. In particular, we observed that using 5 ms frame duration for the cases where the traffic load is low leads to a faster bandwidth allocation and lowers the experienced latency. On the other hand, for the medium to heavy load traffic, using 10 ms frame duration results in less packet fragmentation, wasting less bandwidth, and accordingly, experiencing a better packet delivery ratio. As smart grid traffic classes are different in their level of QoS requirements, we have proposed a priority-based scheduling scheme which can prioritize the transmission of traffic with stricter latency requirement. We have also devised an intra-class scheduling scheme, where within each traffic class we can prioritize the transmission of service flows with lower remaining latency and higher current data rate. We then compared the performance of two system architectures, namely direct access and aggregator architecture, in order to collect the traffic from SMs and transmit them to the utility control center. We have concluded that the aggregator architecture is more efficient as it decreases the possible collision that can occur between different traffic flows and leads to a higher throughput and fewer number of re-transmissions would be required. Accordingly, in Chapters 3-5 of the thesis, we have investigated how to implement the aggregator architecture such that smart grid QoS requirements namely, latency and reliability are best maintained. In order to achieve the latency requirement for smart grid traffic, we have derived analytical methods for modelling latency based on the characteristics of the MAC protocols of the IEEE 802.15.4g and PLC technologies. We have used the Markov chain model for tracking the state of the back-off procedure when CSMA/CA scheduling scheme is used for scheduling the non-critical traffic and we use the binomial distribution for ensuring whether all the mission-critical traffic can be scheduled within their required latency using TDMA scheduling scheme.

According to [6] and [120], existing utility poles and transformers are potential locations for DAP placement. The mathematical optimization formulation for DAP placement on top of the existing utility poles and transformers is an IP problem and is NP-hard. Accordingly, in order to avoid the exponential time complexity that is needed for solving the optimization problem, we have devised several heuristic algorithms for placing DAPs for different scenarios. In Chapter 3, we have investigated the DAP placement problem for a single-hop communication infrastructure that operates based on the characteristics of either WiMAX or IEEE 802.15.4g technology. We have devised a modified K-means algorithm for placing minimum number of DAPs on top of the existing utility poles while ensuring the network coverage. We have concluded that for a single-hop communication infrastructure, WiMAX is a more cost-efficient solution as it provides a larger coverage range and can access remote devices and accordingly, fewer number of DAPs would be required.

In Chapter 4, we have considered a multi-hop communication infrastructure and have devised a new heuristic algorithm for placing DAPs on top of the existing utility poles while ensuring the network coverage and latency satisfaction. We have assumed that SM to SM and SM to DAP connections operate based on the characteristics of the IEEE 802.15.4g technology. The heuristic algorithm uses a greedy approach for finding the potential pole locations for DAP placement and the Dijkstra's shortest path algorithm for constructing reliable routes between SMs and DAP locations. We have compared the performance of our algorithm with the solution of [20] for a similar large-scale scenario and have observed that our algorithm performs better both in terms of time-complexity and optimality. In particular, our algorithm has a computational complexity of $N_{\text{DAP}}O(N_{\text{SM}}^2)$ compared to $O(2^{(N_{\text{poles}}+N_{\text{SM}})})$ and it selects 37 poles for DAP placement while ensuring the QoS satisfaction whereas their algorithm selects 426 poles while only ensuring network coverage. We have also compared the solution of our algorithm with that of the IBM CPLEX software for small-scale scenarios. We have concluded that our algorithm is competitive in terms of performance while having much lower run-time complexity.

Finally, in Chapter 5, we have considered a multi-hop communication infrastructure based on PLC for collecting traffic from SMs and transmitting them to the utility control center. We have devised a new heuristic algorithm based on the characteristics of the transmission line theory for ensuring the network coverage in a PLC-based infrastructure. We have also used the priority-based CSMA/CA MAC scheme for scheduling traffic classes that require different levels of QoS. In order to decrease the run-time complexity of the heuristic algorithm that we have proposed for solving the DAP placement optimization problem in a PLC-based infrastructure, we have decomposed the reliability constraint into two constraints, one for ensuring the packet success ratio and the other for ensuring the latency requirement. Based on the suggestions in [20, 122], we have also calculated routes that have a packet error rate less than the tolerable ratio in advance and have imported those routes into the CPLEX. In order to decrease the run-time complexity further, we have also translated the latency constraint into an approximate linear constraint and have solved the equivalent optimization problem using the IBM CPLEX software. We have shown that our heuristic algorithm is capable of designing an AMI with few DAPs while ensuring the satisfaction of the latency and coverage constraints. We have also observed that due to the large attenuation experienced at the pad-mounted transformers, in a mixed infrastructure, which consists of both pad-mounted and pole-mounted transformers, larger number of DAPs would be required compared to the all pole-mounted and the wireless AMIs.

6.2 Future Work

We believe that the following areas can be considered as an extension to the works presented in this thesis.

6.2.1 Designing a Resilient AMI

For the successful operation of the power grid networks, it is crucial to ensure the satisfaction of the QoS requirements for smart grid traffic. Since wireless networks and PLC links experience varying link conditions, it would be very beneficial to design the networks based on multi-path routes. The works presented by [122] and [133] investigate the multi-path routes for SGCNs. In particular, the authors of [122] investigate the design of an $n-1$ multi-path routes for a medium voltage distribution network such that if at any time, one of the routes experiences low packet success ratio, the network can use the other $n-1$ routes. The application of the same concept would be beneficial when designing an AMI in the low voltage section of the power grid based on PLC or wireless technologies. For providing resiliency, [134], [135] and [136], investigate the application of hybrid networks such as IEEE 802.15.4g and narrow-band PLC for designing SGCNs. We believe the $n-1$ resiliency constraint can also be added to the mathematical formulation for the optimal DAP placement problem. Accordingly, we need to develop a new solution such that this constraint would also be addressed when placing DAPs for an AMI.

6.2.2 Designing a New Routing Protocol

In this thesis, we have proposed new scheduling schemes and derived analytical methods for modelling the behaviour of the existing MAC protocols. We believe the optimal design and application of the higher layer protocols such as routing and transmission protocols can also significantly improve the performance of SGCNs. For example, since PLC networks experience varying link conditions, the application of re-active routing protocols such as the 6LowPAN ad hoc distance-vector protocol (LOAD) [137], in which the route is found when it is necessary, would be beneficial. On the other hand, as smart grid applications are strict in their latency requirement, pro-active routing protocols such as the routing for low-power and lossy networks (RPL) [138], in which routes are determined in advance, seems to be more rewarding. We first suggest to do a qualitative and quantitative analysis of both routing protocols for SGCNs. The quantitative comparison can be done using the PLC module that we have developed based on NS-3 [139], cf. Appendix B. Secondly, a hybrid routing protocol that can benefit from the merits of both re-active and pro-active protocols should be devised for SGCNs.

Bibliography

[1] "Roadmap for Smart Grid Interoperability Standards, Release 1.0, Office of the National Coordinator for Smart Grid Interoperability, National Institute of Standards and Technology, US Department of Commerce," 2009. [Online]. Available: www.nist.gov/public_affairs/releases/smartgrid_interoperability.pdf

[2] "IEEE Guide for Smart Grid Interoperability of Energy Technology and Information Technology Operation with the Electric Power System (EPS), End-Use Applications, and Loads," *IEEE Std. 2030-2011*, pp. 1–126, Sept. 2011.

[3] E. Hossain, Z. Han, and H. Poor, Eds., *Smart Grid Communications and Networking*. Cambridge, 2012.

[4] L. Lampe, *Power Line Communications: Principles, Standards and Applications from Multimedia to Smart Grid*. John Wiley & Sons, 2016.

[5] "SG Network System Requirements Specification v5.1," Open Smart Grid (Open SG), Tech. Rep., 2010. [Online]. Available: http://osgug.ucaiug.org/default.aspx.

[6] "NIST PAP2 guidelines for assessing wireless standards for smart grid application," 2012. [Online]. Available: http://tinyurl.com/NIST-PAP2-Guidelines

[7] "WiMAX Forum system profile requirements for smart grid applications requirements for WiGRID," 2012.

[8] A. Mahdy, P.-Y. Kong, B. Zahawi, and G. K. Karagiannidis, "Data aggregate point placement for smart grid with joint consideration of communication and power networks," in *7th International Conference on Modeling, Simulation, and Applied Optimization (ICMSAO)*, 2017, pp. 1–5.

[9] F. Gomez-Cuba, R. Asorey-Cacheda, and F. Gonzalez-Castano, "WiMAX for smart grid last-mile communications: TOS traffic mapping and performance assessment," in *IEEE PES International Conference and Exhibition on Innovative Smart Grid Technologies (ISGT Europe)*, 2012, pp. 1–8.

[10] F. Aalamifar, L. Lampe, S. Bavarian, and E. Crozier, "WiMAX technology in smart distribution networks: Architecture, modeling, and applications," in *IEEE PES T&D Conference and Exposition*, April 2014, pp. 1–5.

[11] W. Alsalih, H. Hassanein, and S. Akl, "Placement of multiple mobile data collectors in wireless sensor networks," *Ad Hoc Networks*, vol. 8, no. 4, pp. 378–390, 2010.

[12] B. Lin, P.-H. Ho, L.-L. Xie, X. Shen, and J. Tapolcai, "Optimal relay station placement in broadband wireless access networks," *IEEE Trans. Mobile Comput.*, vol. 9, no. 2, pp. 259–269, 2010.

[13] S. Lee and M. F. Younis, "EQAR: Effective QoS-aware relay node placement algorithm for connecting disjoint wireless sensor subnetworks," *IEEE Trans. Comput.*, vol. 60, no. 12, pp. 1772–1787, 2011.

[14] S. Lee and M. Younis, "QoS-aware relay node placement in a segmented wireless sensor network," in *IEEE International Conference on Communications (ICC)*, 2009, pp. 1–5.

[15] B. Aoun, R. Boutaba, Y. Iraqi, and G. Kenward, "Gateway placement optimization in wireless mesh networks with QoS constraints," *IEEE J. Sel. Areas Commun.*, vol. 24, no. 11, pp. 2127–2136, 2006.

[16] "Communications requirements of smart grid technologies," US Department of Energy, Tech. Rep., 2010.

[17] "IBM CPLEX Optimization Studio," 2012. [Online]. Available: http://www-01.ibm.com/software/integration/optimization/cplex-optimization-studio

[18] A. Makhorin, "GLPK (GNU linear programming kit)," 2016. [Online]. Available: https://www.gnu.org/software/glpk/

[19] G. Souza, F. Vieira, C. Lima, G. Junior, M. Castro, and S. Araujo, "Optimal positioning of GPRS concentrators for minimizing node hops in smart grids considering routing in mesh networks," in *IEEE PES Conference On Innovative Smart Grid Technologies Latin America (ISGT LA)*, 2013, pp. 1–7.

[20] G. Rolim, D. Passos, I. Moraes, and C. Albuquerque, "Modelling the data aggregator positioning problem in smart grids," in *IEEE International Conference on Computer and Information Technology; Ubiquitous Computing and Communications; Dependable, Autonomic and Secure Computing; Pervasive Intelligence and Computing (CIT/IUCC/DASC/PICOM)*, 2015, pp. 632–639.

[21] "WiMAX forum system profile requirements for smart grid applications: Requirements for WiGRID," 2013. [Online]. Available: http://tinyurl.com/Smart-Grid-Utility-Requirement

[22] R. R. Mohassel, A. Fung, F. Mohammadi, and K. Raahemifar, "A survey on advanced metering infrastructure," *International Journal of Electrical Power & Energy Systems*, vol. 63, pp. 473–484, 2014.

[23] P. Y. Kong, "Wireless neighborhood area networks with QoS support for demand response in smart grid," *IEEE Trans. Smart Grid*, vol. 7, no. 4, pp. 1913–1923, July 2016.

[24] F. Gomez-Cuba, R. Asorey-Cacheda, and F. Gonzalez-Castano, "Smart grid last-mile communications model and its application to the study of leased broadband wired-access," *IEEE Trans. Smart Grid*, vol. 4, no. 1, pp. 5–12, March 2013.

[25] H. Ferreira, L. Lampe, J. Newbury, and T.G. Swart (Editors), *Power Line Communications: Theory and Applications for Narrowband and Broadband Communications over Power Lines.* John Wiley & Sons, Jun. 2010.

[26] S. Galli, A. Scaglione, and Z. Wang, "For the grid and through the grid: The role of power line communications in the smart grid," *Proc. IEEE*, vol. 99, no. 6, pp. 998–2017, 2011.

[27] L. Lampe, A. Tonello, and D. Shaver, "Power line communications for automation networks and smart grid," *IEEE Commun. Mag.*, vol. 49, no. 12, pp. 26–27, Dec. 2011.

[28] A. Sendin, I. Peña, and P. Angueira, "Strategies for power line communications smart metering network deployment," *Energies*, vol. 7, no. 4, pp. 2377–2420, 2014.

[29] "Specification for PoweRline Intelligent Metering Evolution," PRIME Alliance Technical Working Group, Specification, revision 1.4, 2014. [Online]. Available: https://tinyurl.com/kho639g

[30] "NIST Framework and Roadmap for Smart Grid Interoperability Standards, Release 2.0," 2012. [Online]. Available: www.nist.gov/smartgrid/upload/NIST_Framework_Release_2-0_corr.pdf

[31] A. Bettencourt and J. Malenfant, "Hydro One approach to smart grid," 2013. [Online]. Available: http://www.ontarioenergyboard.ca/oeb/_documents/eb-2013-0294/sgac_meeting4_hydroone_presentation.pdf

[32] UTC Canada, "Worldwide interoperability for microwave access (WiMAX) vs. long term evolution (LTE)," 2012. [Online]. Available: http://www.utccanada.org/sites/default/files/public/UTC_Public_files/UTCC-WiMAX%20vs%20LTE%202012.pdf

[33] K. McGuire, "RuggedCom & Kapsch to provide WiMAX to smart grid app for Austrian utility," 2010. [Online]. Available: http://www.mobilitytechzone.com/wimax/topics/wimax/articles/74015-ruggedcom-kapsch-provide-wimax-smart-grid-app-austrian.htm

[34] Participants of the Priority Action Plan 2 working group, "NIST smart grid interoperability panel PAP2 guidelines for assessing wireless

standards for smart grid application," 2014. [Online]. Available: http://nvlpubs.nist.gov/nistpubs/ir/2014/NIST.IR.7761r1.pdf

[35] M. Zimmermann and K. Dostert, "A multipath model for the powerline channel," *IEEE Trans. Commun.*, vol. 50, no. 4, pp. 553–559, Apr. 2002.

[36] F. Canete, J. Cortes, L. Diez, and J. Entrambasaguas, "A channel model proposal for indoor power line communications," *IEEE Commun. Mag.*, vol. 49, no. 12, pp. 166–174, Dec. 2011, http://www.plc.uma.es/channels.htm.

[37] T. Sartenaer and P. Delogne, "Powerline cables modelling for broadband communications," in *Intl. Symp. Power Line Commun. (ISPLC)*, Apr. 2001.

[38] T. Esmailian, F. Kschischang, and P. Gulak, "In-building power lines as high-speed communication channels: Channel characterization and a test channel ensemble," *International Journal of Communication Systems*, vol. 16, pp. 381–400, 2003.

[39] L. Lampe, R. Schober, and S. Yiu, "Distributed space-time block coding for multihop transmission in power line communication networks," *IEEE J. Sel. Areas Commun.*, vol. 24, pp. 1389–1400, Jul. 2006.

[40] A. Tonello and F. Versolatto, "Bottom-up statistical PLC channel modeling Part I: Random topology model and efficient transfer function computation," *IEEE Trans. Power Del.*, vol. 26, no. 2, pp. 891–898, Apr. 2011.

[41] L. Lampe and A. Vinck, "On cooperative coding for narrowband PLC networks," *Int. J. Electron. Commun. (AEÜ)*, no. 8, pp. 681–687, Aug. 2011.

[42] A. Dabak, I. Kim, and T. Pande, "Channel modeling of medium to low voltage links for AMI applications of PLC," Texas Instruments, Tech. Rep., Jun. 2012, http://www.ti.com/lit/wp/spry202/spry202.pdf.

[43] "Network simulator-3 (ns-3)," 2015. [Online]. Available: http://www.nsnam.org/

[44] R. Ma, H.-H. Chen, Y.-R. Huang, and W. Meng, "Smart grid communication: Its challenges and opportunities," *IEEE Trans. Smart Grid*, vol. 4, no. 1, pp. 36–46, March 2013.

[45] V. C. Gungor, D. Sahin, T. Kocak, S. Ergüt, C. Buccella, C. Cecati, and G. P. Hancke, "Smart grid and smart homes: Key players and pilot projects," *IEEE Ind. Electron. Mag.*, vol. 6, no. 4, pp. 18–34, 2012.

[46] M. Kuzlu, M. Pipattanasomporn, and S. Rahman, "Communication network requirements for major smart grid applications in HAN, NAN and WAN," *Computer Networks*, vol. 67, pp. 74–88, 2014.

[47] E. Bou-Harb, C. Fachkha, M. Pourzandi, M. Debbabi, and C. Assi, "Communication security for smart grid distribution networks," *IEEE Commun. Mag.*, vol. 51, no. 1, pp. 42–49, Jan. 2013.

[48] R. Khan and J. Khan, "A heterogeneous WiMAX-WLAN network for AMI communications in the smart grid," in *IEEE Third International Conference on Smart Grid Communications (SmartGridComm)*, Nov. 2012, pp. 710–715.

[49] B. Sivaneasan, P. So, H. Gooi, and L. Siow, "Performance measurement and analysis of WiMAX-LAN communication operating at 5.8 GHz," *IEEE Trans. Ind. Informat.*, vol. 9, no. 3, pp. 1497–1506, Aug. 2013.

[50] J. Aguirre and F. Magnago, "Viability of WiMAX for smart grid distribution network," *European International Journal of Science and Technology*, vol. 2, no. 3, pp. 181–196, 2013.

[51] P. Rengaraju, C.-H. Lung, and A. Srinivasan, "Communication requirements and analysis of distribution networks using WiMAX technology for smart grids," in *IEEE Wireless Communications and Mobile Computing Conference (IWCMC)*, Aug. 2012, pp. 666–670.

[52] D. Bian, M. Kuzlu, M. Pipattanasomporn, and S. Rahman, "Analysis of communication schemes for advanced metering infrastructure (AMI)," in *IEEE PES General Meeting, Conference & Exposition*, 2014, pp. 1–5.

[53] P. Priya and V. Saminadan, "Performance analysis of WiMAX based smart grid communication traffic priority model," in *IEEE International Conference on Communications and Signal Processing (ICCSP)*, 2014, pp. 778–782.

[54] V. C. Güngör, D. Sahin, T. Kocak, S. Ergüt, C. Buccella, C. Cecati, and G. P. Hancke, "Smart grid technologies: communication technologies and standards," *IEEE Trans. Ind. Informat.*, vol. 7, no. 4, pp. 529–539, 2011.

[55] "Wimax forum," 2015. [Online]. Available: http://www.wimaxforum.org

[56] M.-T. Zhou, M. Oodo, V. D. Hoang, L. Lu, X. Zhang, and H. Harada, "Greater reliability in disrupted metropolitan area networks: Use cases, standards, and practices," *IEEE Commun. Mag.*, vol. 53, no. 8, pp. 198–207, August 2015.

[57] F. Aalamifar. (2015) An extension to the WiMAX-NS3 Module. [Online]. Available: https://bitbucket.org/Saba_Al/wimax/

[58] *Distribution automation implementation plan*, BC Hydro, B.C., Canada, 2012, internal report.

[59] D. Byrne, "Smart grid standards activity," 2011. [Online]. Available: https://www.metering.com/wp-content/uploads/Declan_Byrne.pdf

[60] A. Mahmood, N. Javaid, and S. Razzaq, "A review of wireless communications for smart grid," *Renewable and sustainable energy reviews*, vol. 41, pp. 248–260, 2015.

[61] I. Aldmour, "LTE and WiMAX: comparison and future perspective," *Communications and Network*, vol. 5, no. 04, p. 360, 2013.

[62] L. Nuaymi, *WiMAX: Technology for Broadband Wireless Access.* John Wiley & Sons, 2007.

[63] "IEEE Standard for Air Interface for Broadband Wireless Access Systems," *IEEE Std 802.16-2012 (Revision of IEEE Std 802.16-2009)*, pp. 1–2542, Aug 2012.

[64] C. Eklund, R. B. Marks, and S. Ponnuswamy, *WirelessMAN: Inside the IEEE 802.16 Standard for Wireless Metropolitan Area Networks.* Standards Information Network, 2006.

[65] C. So-In, R. Jain, and A.-K. Tamimi, "Scheduling in IEEE 802.16e mobile WiMAX networks: Key issues and a survey," *IEEE J. Sel. Areas Commun.*, vol. 27, no. 2, pp. 156–171, 2009.

[66] C. So-In, R. Jain, and A.-K. Al Tamimi, "SWIM: A scheduler for Unsolicited Grant Service (UGS) in IEEE 802.16e Mobile WiMAX networks," in *Access Networks.* Springer, 2010, pp. 40–51.

[67] T. Khalifa, A. Abdrabou, K. Naik, M. Alsabaan, A. Nayak, and N. Goel, "Split-and aggregated-transmission control protocol (SA-TCP) for smart power grid," *IEEE Trans. Smart Grid*, vol. 5, no. 1, pp. 381–391, 2014.

[68] J. Farooq and T. Turletti, "An IEEE 802.16 WiMAX module for the NS-3 Simulator," in *Proceedings of the 2nd International Conference on Simulation Tools and Techniques (SIMUTools)*, 2009.

[69] M. A. Ismail, G. Piro, L. A. Grieco, and T. Turletti, "An improved IEEE 802.16 WiMAX module for the NS-3 simulator," in *Proceedings of the 3rd International Conference on Simulation Tools and Techniques (SIMUTools)*, 2010.

[70] "Open Smart Grid (open SG)." [Online]. Available: http://osgug.ucaiug.org/default.aspx.

[71] M. Daoud and X. Fernando, "On the communication requirements for the smart grid," *Energy and Power Engineering*, vol. 3, no. 1, pp. 53–60, 2011.

[72] R. Jain, D. Chiu, and W. Hawe, "A Quantitative Measure Of Fairness And Discrimination For Resource Allocation In Shared Computer Systems," DEC Research, Tech. Rep. TR-301, Sep. 1984. [Online]. Available: http://www.cse.wustl.edu/~jain/papers/fairness.htm

[73] "BC Hydro‘s Smart Metering Program," BC Hydro, Tech. Rep., 2013. [Online]. Available: http://www.bchydro.com/content/dam/hydro/medialib/internet/documents/smi/smart_meter_kam_customer.pdf

[74] Z. Lu and Y. Wen, "Distributed algorithm for tree-structured data aggregation service placement in smart grid," *IEEE Syst. J.*, vol. 8, no. 2, pp. 553–561, 2014.

[75] R. Peng, X. Rui-Hua, and Q. Jin, “Bi-level simulated annealing algorithm for facility location problem,” *International Conference on Information Management, Innovation Management and Industrial Engineering*, vol. 3, pp. 17–22, 2008.

[76] D. B. Shmoys, E. Tardos, and K. Aardal, “Approximation algorithms for facility location problems,” in *29th Annual ACM Symposium on Theory of Computing*, 1997, pp. 265–274.

[77] V. Kekatos, G. B. Giannakis, and B. Wollenberg, “Optimal placement of phasor measurement units via convex relaxation,” *IEEE Trans. Power Syst.*, vol. 27, no. 3, pp. 1521–1530, 2012.

[78] B. Abolhassani, J. Salt, and D. Dodds, “A two-phase genetic K-means algorithm for placement of radioports in cellular networks,” *IEEE Trans. Syst., Man, Cybern. B*, vol. 34, no. 1, pp. 533–538, 2004.

[79] “IEEE Standard for Local and metropolitan area networks–Part 15.4: Low-Rate Wireless Personal Area Networks (LR-WPANs) Amendment 3: Physical Layer (PHY) Specifications for Low-Data-Rate, Wireless, Smart Metering Utility Networks,” *IEEE Std 802.15.4g-2012 (Amendment to IEEE Std 802.15.4-2011)*, pp. 1–252, April 2012.

[80] M. Ringwelski, C. Renner, A. Reinhardt, A. Weigel, and V. Turau, “The hitchhiker’s guide to choosing the compression algorithm for your smart meter data,” in *IEEE International Energy Conference and Exhibition (ENERGYCON)*. IEEE, 2012, pp. 935–940.

[81] J. Zhou, R. Q. Hu, and Y. Qian, "Scalable distributed communication architectures to support advanced metering infrastructure in smart grid." *IEEE Trans. Parallel Distrib. Syst.*, vol. 23, no. 9, pp. 1632–1642, 2012.

[82] V. Gungor, D. Sahin, T. Kocak, S. Ergut, C. Buccella, C. Cecati, and G. Hancke, "Smart grid technologies: Communication technologies and standards," *Industrial Informatics, IEEE Transactions on*, vol. 7, no. 4, pp. 529–539, Nov 2011.

[83] Y. Yang, H. Hu, J. Xu, and G. Mao, "Relay technologies for WiMAX and LTE-advanced mobile systems," *IEEE Commun. Mag.*, vol. 47, no. 10, pp. 100–105, 2009.

[84] "Ontario energy board: Electricity prices." [Online]. Available: http://www.ontarioenergyboard.ca/OEB/Consumers/Electricity/Electricity+Prices

[85] "Cisco 1000 series connected grid routers." [Online]. Available: http://www.cisco.com/c/en/us/products/routers/1000-series-connected-grid-routers/index.html

[86] K. Ali, W. Alsalih, and H. Hassanein, "Set-cover approximation algorithms for load-aware readers placement in RFID networks," in *IEEE International Conference on Communications (ICC)*, 2011, pp. 1–6.

[87] D. Niyato, L. Xiao, and P. Wang, "Machine-to-machine communications for home energy management system in smart grid," *IEEE Commun. Mag.*, vol. 49, no. 4, pp. 53–59, 2011.

[88] B. E. Bilgin and V. C. Gungor, "Adaptive error control in wireless sensor networks under harsh smart grid environments," *Sensor Review*, vol. 32, no. 3, pp. 203–211, 2012.

[89] S. Gormus, Z. Fan, Z. Bocus, and P. Kulkarni, "Opportunistic communications to improve reliability of AMI mesh networks," in *IEEE PES International Conference and Exhibition on Innovative Smart Grid Technologies*, Dec. 2011, pp. 1–8.

[90] H. Mohammadi Nejad, N. Movahhedinia, and M. R. Khayyambashi, "Improving the reliability of wireless data communication in smart grid NAN," *Peer-to-Peer Networking and Applications*, pp. 1–13, 2016.

[91] D. Sahin, V. C. Gungor, T. Kocak, and G. Tuna, "Quality-of-service differentiation in single-path and multi-path routing for wireless sensor network-based smart grid applications," *Ad Hoc Networks*, vol. 22, pp. 43–60, 2014.

[92] Z. Xie, G. Manimaran, V. Vittal, A. G. Phadke, and V. Centeno, "An information architecture for future power systems and its reliability analysis," *IEEE Trans. Power Syst.*, vol. 17, no. 3, pp. 857–863, Aug. 2002.

[93] D. Niyato, P. Wang, and E. Hossain, "Reliability analysis and redundancy design of smart grid wireless communications system for demand side management," *IEEE Wireless Commun.*, vol. 19, no. 3, pp. 38–46, June 2012.

[94] "IEEE Standard for Local and metropolitan area networks–Part 15.4: Low-Rate Wireless Personal Area Networks (LR-WPANs) Amendment 3: Physical Layer (PHY) Specifications for Low-Data-Rate, Wireless, Smart Metering Util-

ity Networks," *IEEE Std 802.15.4g-2012 (Amendment to IEEE Std 802.15.4-2011)*, pp. 1–252, April 2012.

[95] Z. Shi, C. Beard, and K. Mitchell, "Analytical models for understanding space, backoff, and flow correlation in CSMA wireless networks," *Wireless Networks*, vol. 19, no. 3, pp. 393–409, 2013.

[96] P. Di Marco, P. Park, C. Fischione, and K. H. Johansson, "Analytical modeling of multi-hop IEEE 802.15.4 networks," *IEEE Trans. Veh. Technol.*, vol. 61, no. 7, pp. 3191–3208, 2012.

[97] S. Ray, D. Starobinski, and J. B. Carruthers, "Performance of wireless networks with hidden nodes: A queuing-theoretic analysis," *Computer Communications*, vol. 28, no. 10, pp. 1179–1192, 2005.

[98] J. Shi, T. Salonidis, and E. W. Knightly, "Starvation mitigation through multi-channel coordination in CSMA multi-hop wireless networks," in *ACM International Symposium on Mobile Ad Hoc Networking and Computing*, 2006, pp. 214–225.

[99] S. K. Bose, *An Introduction to Queueing Systems*. Springer Science & Business Media, 2013.

[100] J. Gao, J. Hu, and G. Min, "A new analytical model for slotted IEEE 802.15. 4 medium access control protocol in sensor networks," in *Communications and Mobile Computing, 2009. CMC'09. WRI International Conference on*, vol. 2. IEEE, 2009, pp. 427–431.

[101] M. Baz, P. D. Mitchell, and D. A. Pearce, "Analysis of queuing delay and medium access distribution over wireless multihop PANs," *IEEE Trans. Veh. Technol.*, vol. 64, no. 7, pp. 2972–2990, 2015.

[102] M. Fernandez and S. Williams, "Closed-form expression for the Poisson-Binomial probability density function," *IEEE Trans. Aerosp. Electron. Syst.*, vol. 46, no. 2, pp. 803–817, April 2010.

[103] D. Bertsekas and R. Gallager, *Data Networks (2nd Ed.)*. Upper Saddle River, NJ, USA: Prentice-Hall, Inc., 1992.

[104] F. Aalamifar, G. N. Shirazi, M. Noori, and L. Lampe, "Cost-efficient data aggregation point placement for advanced metering infrastructure," in *Smart Grid Communications (SmartGridComm), 2014 IEEE International Conference on*. IEEE, 2014, pp. 344–349.

[105] W. Meng, R. Ma, and H.-H. Chen, "Smart grid neighborhood area networks: A survey," *IEEE Netw.*, vol. 28, no. 1, pp. 24–32, 2014.

[106] W. Alsalih, S. Akl, and H. Hassanein, "Placement of multiple mobile data collectors in underwater acoustic sensor networks," in *IEEE International Conference on Communications (ICC)*, 2008, pp. 2113–2118.

[107] H. Samet, *The Design and Analysis of Spatial Data Structures*. Addison-Wesley Reading, MA, 1990, vol. 199.

[108] R. Chandra, L. Qiu, K. Jain, and M. Mahdian, "Optimizing the placement of internet taps in wireless neighborhood networks," in *IEEE International Conference on Network Protocols*, 2004, pp. 271–282.

[109] U. Feige, "A threshold of Ln N for approximating set cover," *Journal of the ACM*, vol. 45, no. 4, pp. 634–652, Jul. 1998.

[110] W. I. Zangwill, *Nonlinear Programming: A Unified Approach.* Prentice-Hall, 1969.

[111] D. G. Luenberger, *Introduction to Linear and Nonlinear Programming.* Addison-Wesley Reading, MA, 1973, vol. 28.

[112] F. Hutter, H. H. Hoos, K. Leyton-Brown, and T. Stützle, "ParamILS: an automatic algorithm configuration framework," *Journal of Artificial Intelligence Research*, vol. 36, pp. 267–306, 2009.

[113] "Complexity of the integer linear programming," 2014. [Online]. Available: https://www.ibm.com/developerworks/community/forums/html/topic?id=77777777-0000-0000-0000-000014393637

[114] "How to measure the difficulty of a mixed-linear integer programming (MILP) problem," 2015. [Online]. Available: https://www.researchgate.net/post/How_to_measure_the_difficulty_of_a_Mixed-Linear_Integer_Programming_MILP_problem

[115] "Guidelines for estimating CPLEX memory requirements based on problem size," 2012. [Online]. Available: http://www-01.ibm.com/support/docview.wss?uid=swg21399933

[116] M. Carlesso, A. Antonopoulos, F. Granelli, and C. Verikoukis, "Uplink scheduling for smart metering and real-time traffic coexistence in LTE networks," in *IEEE International Conference on Communications (ICC)*, June 2015, pp. 820–825.

[117] H. Y. Tung, K. F. Tsang, H. C. Tung, V. Rakocevic, K. T. Chui, and Y. W. Leung, "A WiFi-ZigBee building area network design of high traffics AMI for smart grid," *Smart Grid and Renewable Energy*, vol. 3, no. 4, p. 324, 2012.

[118] S. Galli, A. Scaglione, and Z. Wang, "For the grid and through the grid: The role of power line communications in the smart grid," *Proceedings of the IEEE*, vol. 99, no. 6, pp. 998–1027, 2011.

[119] H. Farhangi, "The path of the smart grid," *IEEE Power Energy Mag.*, vol. 8, no. 1, pp. 18–28, 2010.

[120] A. Dabak, H. Kim, and T. Pande, "Channel modeling of medium to low voltage links for AMI applications of PLC," *Texas Instruments White Paper*, 2012.

[121] A. Dabak, I. H. Kim, B. Varadarajan, and T. Pande, "Channel modeling for MV/LV AMI applications in the frequency range < 500kHz," in *Workshop on Power Line Communications*, 2011.

[122] S. Canale, A. Di Giorgio, A. Lanna, A. Mercurio, M. Panfili, and A. Pietrabissa, "Optimal planning and routing in medium voltage powerline communications networks," *IEEE Transactions on Smart Grid*, vol. 4, no. 2, pp. 711–719, 2013.

[123] A. Sendin, J. Simon, I. Urrutia, and I. Berganza, "PLC deployment and architecture for smart grid applications in Iberdrola," in *18th IEEE International Symposium on Power Line Communications and Its Applications (ISPLC)*, March 2014, pp. 173–178.

[124] F. Aalamifar and L. Lampe, "Cost-efficient QoS-Aware Data Acquisition Point Placement for Advanced Metering Infrastructure," *Submitted*. [Online]. Available: https://arxiv.org/abs/1802.06656

[125] E. Alonso, J. Matanza, C. Rodriguez-Morcillo, and S. Alexandres, “Performance evaluation of AMR simultaneous polling strategies in a PRIME PLC network,” in *19th IEEE International Symposium on Power Line Communications and Its Applications (ISPLC)*. IEEE, 2015, pp. 101–106.

[126] P.-Y. Kong, C.-W. Liu, and J.-A. Jiang, “Cost-efficient placement of communication connections for transmission line monitoring,” *IEEE Transactions on Industrial Electronics*, vol. 64, no. 5, pp. 4058–4067, 2017.

[127] J. Virtamo, “Queueing theory / priority queues.” [Online]. Available: https://www.netlab.tkk.fi/opetus/s383143/kalvot/E_priority.pdf

[128] M. Baz, P. D. Mitchell, and D. A. Pearce, “Versatile analytical model for delay and energy evaluation in WPANs: A case study for IEEE 802.15.4 CSMA-CA,” *Wireless personal communications*, vol. 75, no. 1, pp. 415–445, 2014.

[129] P. Park, P. Di Marco, P. Soldati, C. Fischione, and K. H. Johansson, “A generalized Markov chain model for effective analysis of slotted IEEE 802.15.4,” in *Mobile Adhoc and Sensor Systems (MASS)*. IEEE, 2009, pp. 130–139.

[130] D. G. Luenberger and Y. Ye, *Linear and Nonlinear Programming*. Springer, 2015, vol. 228.

[131] F. Aalamifar, A. Schlögl, D. Harris, and L. Lampe, “Modelling power line communication using network simulator-3,” in *Global Communications Conference (GLOBECOM), 2013 IEEE*, Dec 2013, pp. 2969–2974.

[132] “IEEE Standard for Low-Frequency (less than 500 kHz) Narrowband Power Line Communications for Smart Grid Applications,” vol. 31, p. 269, 2013.

[133] Y. Hong, D. Kim, D. Li, L. Guo, J. Son, and A. O. Tokuta, "Two new multi-path routing algorithms for fault-tolerant communications in smart grid," *Ad Hoc Networks*, vol. 22, pp. 3–12, 2014.

[134] A. M. Sarafi, G. I. Tsiropoulos, and P. G. Cottis, "Hybrid wireless-broadband over power lines: A promising broadband solution in rural areas," *IEEE Communications Magazine*, vol. 47, no. 11, 2009.

[135] M. Sayed, T. A. Tsiftsis, and N. Al-Dhahir, "On the diversity of hybrid narrowband-plc/wireless communications for smart grids," *IEEE Transactions on Wireless Communications*, vol. 16, no. 7, pp. 4344–4360, July 2017.

[136] J. Mafra, M. Hosami, L. Freitas, M. Martinelli, and A. Almeida, "Hybrid communication module - motivations, requirements, challenges and implementations," in *2015 IEEE PES Innovative Smart Grid Technologies Latin America (ISGT LATAM)*, Oct 2015, pp. 25–29.

[137] "ITU G.9903 Recommendation: Narrowband orthogonal frequency division multiplexing power line communication transceivers for G3-PLC networks," Feb. 2014. [Online]. Available: http://www.itu.int/ITU-T/recommendations/rec.aspx?rec=12088

[138] "RFC 6550, RPL: IPv6 routing protocol for low power and lossy networks," Mar. 2012.

[139] F. Aalamifar, A. Schlögl, D. Harris, and L. Lampe, "NS-3-based PLC Software," 2013. [Online]. Available: http://www.ece.ubc.ca/~lampe/PLC

[140] A. Tonello, "Wideband impulse modulation and receiver algorithms for multiuser power line communications," *EURASIP Journal on Advances in Signal Processing*, vol. 2007, pp. 1–14.

[141] G. Marrocco, D. Statovci, and S. Trautmann, "A PLC broadband channel simulator for indoor communications," in *IEEE Intl. Symp. Power Line Commun. (ISPLC)*, Johannesburg, South Africa, Mar. 2013.

[142] G. Srinivasa Prasanna, A. Lakshmi, S. Sumanth, V. Simha, J. Bapat, and G. Koomullil, "Data communication over the smart grid," in *IEEE Intl. Symp. Power Line Commun. (ISPLC)*, 2009, pp. 273–279.

Appendix A

Deriving $\Phi_x(k, m, p)$

In this section, we calculate $\Phi_x(k, m, p)$, which denotes the probability that the node senses the channel at an arbitrary slot k in sensing stage m for its traffic priority p. These values are used in (5.7), and can recursively be computed as a cumulative probability of sensing the channel at slot j in the previous sensing stage and finding the channel as busy in one of the $C(p)$ sensing iterations for finding the channel as idle and then, backing off for $\frac{1}{W(m,p)}$ in the current sensing stage m.

$$\Phi_x(k, m, p) = \begin{cases} \frac{1}{W(0,p)}, & m = 0, \quad 1 \leq k \leq W(0, p) \\ \sum_{d=1}^{C(p)} \alpha_x(d) \prod_{i=1}^{d-1} \Big(1 - \alpha_x(i)\Big) \cdot \\ \sum_{j=1}^{k-(I+d)} \Big(\Phi_x\big(j, m-1, p\big)\delta\big(k - (j + I + d - 1), m, p\big)\Big), \\ m > 0, \text{ and } m(I+1) + 1 \leq k \leq W^{\text{tot}}(m, p) + m(I + 1 + p) \\ 0, & \text{otherwise,} \end{cases} \tag{A.1}$$

where $\delta(j, m, p) = \frac{1}{W(m,p)}, 1 \leq j \leq W(m, p)$ is the probability that the node backs off for j slots in stage m for its traffic priority p, and $W^{\text{tot}}(m, p) = \sum_{m'=0}^{m} W(m', p)$. Assuming $P = 2$ traffic priorities and $M + 1 = 6$ backoff stages, the corresponding values for $\Phi_x(k, m, p)$ are shown in Figure A.1.

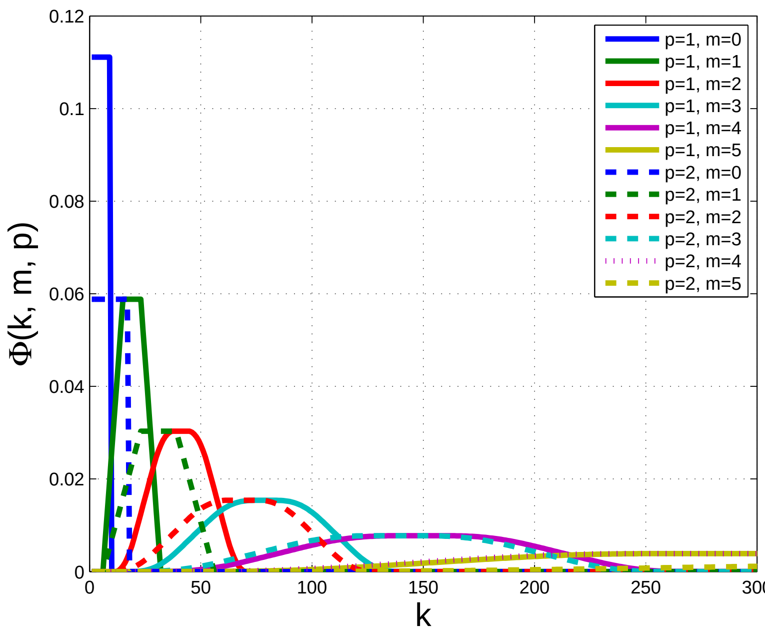

Figure A.1: The values of $\Phi_x(k, m, p)$ for 6 different backoff stages for $p = 1, 2$, assuming $1 - \beta_x(p) = \sum_{d=1}^{p} \alpha_x(d) \prod_{i=1}^{d-1} \Big(1 - \alpha_x(i)\Big) = 1$.

Appendix B

Modelling PLC using Network Simulator-3 (NS-3)

In order to evaluate the performance of DAP placement in a PLC AMI, a channel simulator which is capable of emulating the behaviour of PLC transmission links is required.

Cañete *et al.* [36] and Tonello *et al.* [140] have been pioneers by developing and making freely available software programs based on MATLAB which generate channel realizations for individual links. However, these cannot be used for simulations in PLC networks with multiple node-to-node links. Marrocco *et al.* [141] presented a MATLAB tool that generates multiple channel transfer functions (CTFs) for indoor PLC networks. This tool is based directly on the methodology presented in [40] and thus assumes an indoor-specific network topology with a service panel, which connects to distribution boxes, from which outlets are reached in a star or line topology. Furthermore, the network impedances (i.e., loads) are assumed time invariant, which is only an approximation for PLC networks operating over AC grids [36].

We have developed a suite of new software modules for the simulation of PLC networks [131, 139]. This simulator when integrated with upper layer protocols can be used to design and provide guidance on setting up a suitable PLC architecture for distribution networks. The provided simulator accepts user-specified grid topologies and is flexible enough to capture the time- and frequency-selective behaviour of PLC channels. Our software uses the NS-3 library, which we chose for its popularity and already available modules for numerous networking functionalities. It is open-source and shared and enhanced easily. Thus, together with our new simulator for emulating the PLC channel, researchers can directly simulate PLC networks supporting, for example, smart grid applications. We have made our code available at [139]. In this appendix, we present the core elements of our software package, which are the modules for the generation of CTFs and noise in a PLC network based on TLT principles. We first provide the details about our PLC channel simulator, how it has been implemented and how it works. Then, some results for different sample topologies are provided.

B.1 Grid and Network Elements

We now introduce the features of the new PLC simulator [139] and explain how a user can create a PLC topology and include and adjust grid elements.

The user can build a grid topology as a graph, which consists of two logical elements: nodes and edges. In general, these elements have frequency-dependent attributes, i.e., nodes may have shunt impedances and edges are characterized by frequency-dependent parameters (explained below). Hence the simulation environment allows to specify a global frequency range and resolution for which simulations are performed.

Nodes Nodes represent vertices of the network graph. They may have been assigned a special role as PLC transmitter and/or receiver, or a source of noise, or act as a simple junction point.

- Impedance: Our PLC channel simulator supports four impedance types, which are fixed, frequency-selective, time-selective, and frequency- and time-selective impedance. For these four types, different flexible methods have been implemented for passing the parameters to build the required objects, e.g., via constructors or assignment operator overrides, as described in the following.

– Fixed impedance: The simplest type of impedance is the static impedance which only requires a complex number as the parameter.

– Frequency-selective impedance: The user can provide a vector of complex numbers, whose elements correspond to the impedance at each sample frequency. Alternatively, the frequency-selective impedance can be constructed according to the parallel RLC resonant circuit model defined in [36, Eq. (1)] as

$$Z(\omega) = \frac{R}{1 + \mathrm{j}Q\left(\frac{\omega}{\omega_0} - \frac{\omega}{\omega_0}\right)}\,, \tag{B.1}$$

for which a resonance angular frequency ω_0, resistance R, and quality factor Q need to be input.

– Time-selective impedance: The user can provide a vector of complex numbers, whose elements correspond to the impedance during one mains cycle. This models periodically changing impedances, as experienced in PLC, e.g. [25, Ch. 2], [36]. To capture non-periodic or asynchronous variations, impedances can be altered at predefined points in simulation time by use of the NS-3 scheduler, which will trigger a re-computation of the network's transfer functions.

– Frequency- and time-selective impedance: This class combines the properties of the frequency-selective and time-variant data types. The parameters for this impedance type are input as a matrix of complex numbers, where each element of the matrix corresponds to a specific time-frequency pair, yielding a periodically (with the mains cycle) time-varying frequency-selective impedance. Alternatively, this matrix can also be computed according to the parametric model from [36, Eq. (2)],

$$Z(\omega, t) = Z_A(\omega) + Z_B(\omega) \sin\left(\frac{2\pi}{T_0} t + \phi\right) , \tag{B.2}$$

where $Z_A(\omega)$ and $Z_B(\omega)$ can be provided as vector or through model (B.1), and T_0 is the mains period.

- PLC node: Nodes with assigned PLC transmitter and/or receiver role can be given the attribute of an NS-3 network device. Thus, an interface to the NS-3 framework is provided, which allows the integration of higher level protocols, like TCP/IP, for network simulations.

- Noise source: A node can also have the role of a noise source. To represent the aggregate effect of many noise sources, two functions for background noise have been implemented. The first is a white background noise at a certain level. The second function represents colored noise according to the three-parameter power spectral density (cf. [38]),

$$N(f) = a + b|f|^c \quad [\text{dBm/Hz}] , \tag{B.3}$$

where f is the frequency in MHz.

To capture impulse-like noise sources, we have implemented two additional noise functions. In the first function, a noise source with a user-specified power spectral density is enabled for a certain duration of the time. The second function generates a random variable to determine the length of an impulse noise event and the gap to the next event.

- Junction: Every node can serve as a junction, at which multiple edges fork.

Edges An edge connects two nodes. An edge is described as a two-port network, which means that it can include network elements such as transformers. The two-port network is described by its ABCD matrix, whose elements can be fixed, or frequency-, time-, or frequency- and time-selective. Since in most cases an edge corresponds to a line piece, we have included a dedicated instance of the class edge for line pieces. As specific examples, the current implementation includes three commonly used power cable types, namely the four-sector cables NAYY 150SE and NAYY 50SE and the three-core concentrated cable AL3X95XLPE.

Creating a Topology The nodes and lines mentioned in the previous section form a topology. The topology creation is handled through the PLC_Graph module. This module is very flexible in that it can support an arbitrary number of nodes and edges, and thus network elements.Noise sources can be added to the topology for computing the noise power spectral density and SNR at the receiver side. It is also possible for the user to draw the topology and set the node and line properties in the graphical user interface (GUI), as will be explained later in Section B.2.1.

B.2 Core Modules

After creating the topology, the next step is to calculate the transfer functions using the core modules which is based on the voltage-ratio approach. The core modules consist of PLC_Channel and PLC_ChannelTransferImpl classes. The PLC_Channel class provides an interface for attaching PLC network device instances to a PLC channel, and the PLC_ChannelTransferImpl implements the TLT computations as outlined in Section 1.7.

Figure B.1(a) illustrates the computation of the CTF $H(f)$ for one transmitter-receiver (Tx-Rx) network which is the product of all subunits' CTF. First, the shortest path between the transmitter and the receiver needs to be determined. Travelling backwards on this so-called backbone path, i.e., from Rx to Tx, the topology is then divided into smaller subunits (two-port networks). For each subunit, the local transfer function $H_i(f)$ is computed as the ratio between output and input voltage for this two-port network, which has been illustrated in Figure B.1(b).

To calculate the CTF for each subunit, the input impedance of each subunit needs to be calculated. According to carry-back impedance method, we need to start travelling on the backbone path from the very end node (subunit n). Each subunit is usually a line piece connected to a load and for generality, we consider that the line piece of each subunit ends to a shunt impedance parallel at its input on the backbone path. Hence, the input impedance to each subunit is defined as (B.4):

$$Z_{\mathrm{in},i} = \left(Z_{\mathrm{c},i} \frac{1 + \rho_{i+1} \mathrm{e}^{-2\gamma_i l_i}}{1 - \rho_{i+1} \mathrm{e}^{-2\gamma_i l_i}} \right) \; || \; Z_{\mathrm{sh},i} \; , \tag{B.4}$$

where $Z_{\mathrm{c},i}$ and γ_i are the characteristic impedance and propagation constant of the ith line piece, $Z_{\mathrm{sh},i}$ is the shunt impedance at the ith subunit, ρ_{i+1} is the reflection coefficient of the $(i+1)$th subunit which has already been computed as we are travelling backwards, and "||" denotes the parallel connection of two impedances. The reflection coefficient is obtained as (cf. [40])

$$\rho_{i+1} = \frac{(Z_{\mathrm{in},i+1} - Z_{\mathrm{c},i})}{(Z_{\mathrm{in},i+1} + Z_{\mathrm{c},i})} \; . \tag{B.5}$$

Finally, the CTF for the subunit follows as (cf. [40])

$$H_i(f) = \frac{V_{o_i}}{V_{i_i}} = \frac{(1 + \rho_{i+1})}{(\mathrm{e}^{\gamma_i l_i} + \rho_{i+1}\mathrm{e}^{-\gamma_i l_i})} \, . \tag{B.6}$$

Since NS-3 is an event-driven simulation environment, an efficient implementation of the CTF computation is the key aspect to have a quick simulation performance. For example, the calculation of the equivalent impedances for outgoing edges from a node is performed simultaneously using multi-threaded programming. Furthermore, partial results, e.g., the CTFs of backbone units, are stored in the memory for future reuse.

B.2.1 Graphical User Interface (GUI)

In addition to the underlying simulator software, a flexible GUI has been devised which provides tools to visually represent the topologies under consideration. The GUI presents an intuitive interface for designing topologies, adjusting model and simulation parameters, and generating CTFs. By providing this high level interface to the underlying simulator, users are able to dramatically reduce the amount of time necessary to generate and analyze new topologies. This also allows users who have no experience with the NS-3 code base to still take advantage of the simulators basic functionality. More advanced users can integrate GUI generated topologies directly with NS-3 in order to leverage the software to their specific purposes.

Through the GUI, the user can add arbitrary number of nodes and edges. The user is able to define the properties of the nodes as defined in Section B.1 and measure the channel transfer functions between any two PLC devices and noise power spectral densities at any PLC receiver.

B.2.2 PLC Channel Simulator Results for Sample PLC Networks

Firstly, we apply our PLC module to the relatively complex topology with 21 PLC network nodes presented in [142]. The load impedances are as specified in [142], and the power lines are four-conductor cables of type NAYY 150SE, cf. [25, Ch. 2]. Figure B.2(a) shows a snapshot of the topology created in the GUI described in the previous section. Figure B.2(b) shows the CTFs for the links from Zs to Z2, Z3, and Z7 (see Figure B.2(a)). We observe the frequency-selective behaviour of the channel due to unmatched junctions and terminations and the increasing attenuation for larger distances and frequencies.

As a second example, we test our module on a topology which includes time-selective, frequency-selective and fixed impedances, as shown in Figure B.3(a). As can be seen, there are five nodes, Z0 to Z4, where Z0 is the transmitter. While the impedance of Z3 and Z4 is fixed to 100 Ω, Z1 and Z2 have a time-varying and a frequency-selective impedance, respectively. The simulation is run over a 500 kHz frequency band and the temporal sampling rate is 200 samples per cycle. Figure B.3(b) show the CTF from Z0 to Z1 as a function of frequency and time. The periodically time-varying behaviour of the link due to the periodically time-varying load Z1 can nicely be observed.

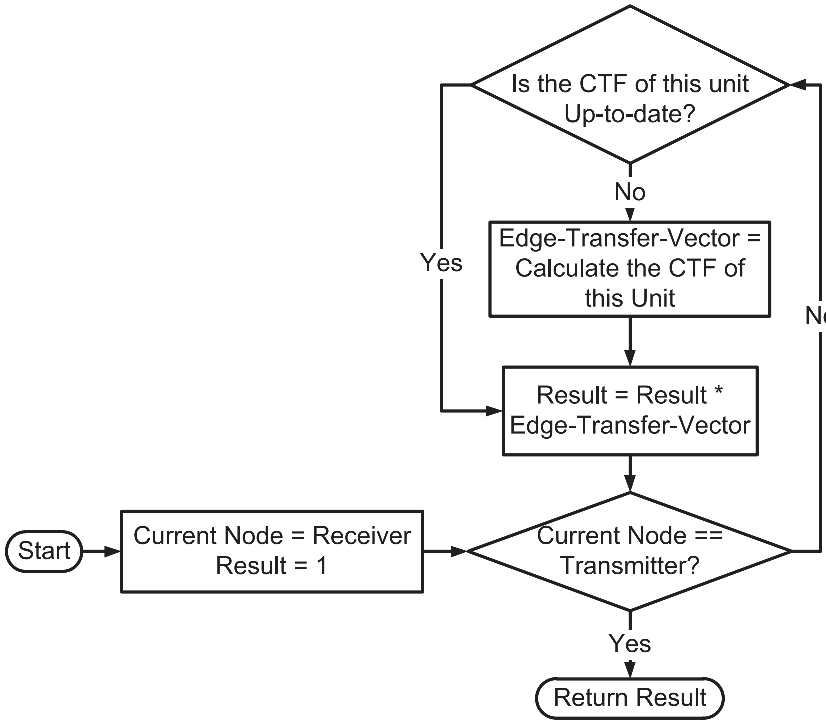

(a)

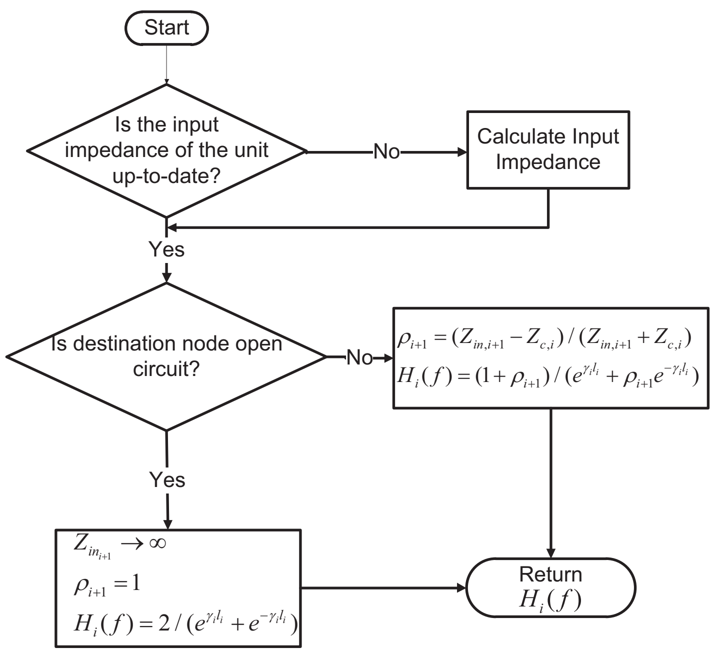

(b)

Figure B.1: (a) Calculation of CTF for one transmitter-receiver link considering the whole underlying power line grid. (b) Calculation of the CTF of a subunit.

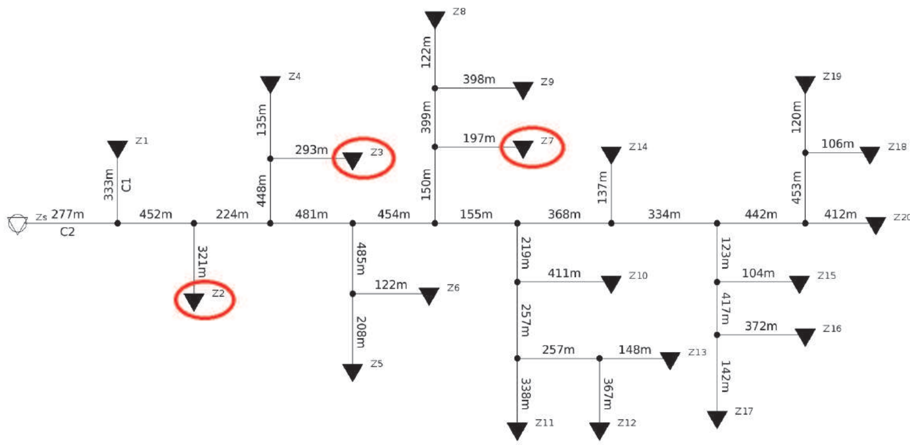

(a)

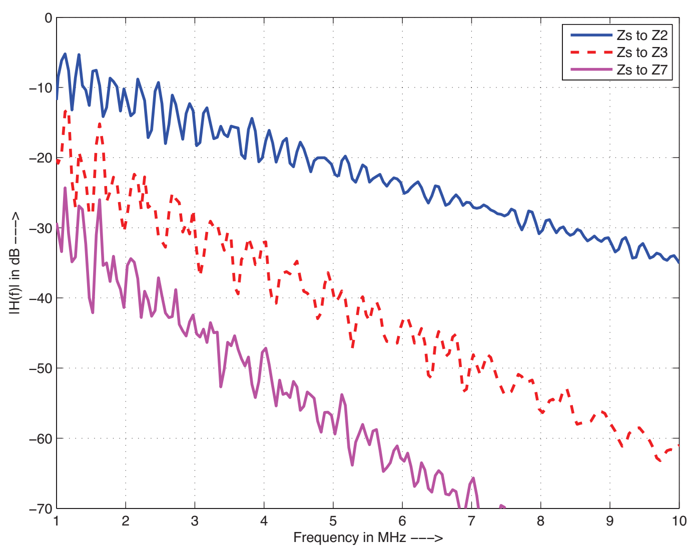

(b)

Figure B.2: (a) PLC network topology with 21 fixed impedances and 39 edges created with our GUI. (b) CTFs for links from Zs to Z2, Z3, and Z7.

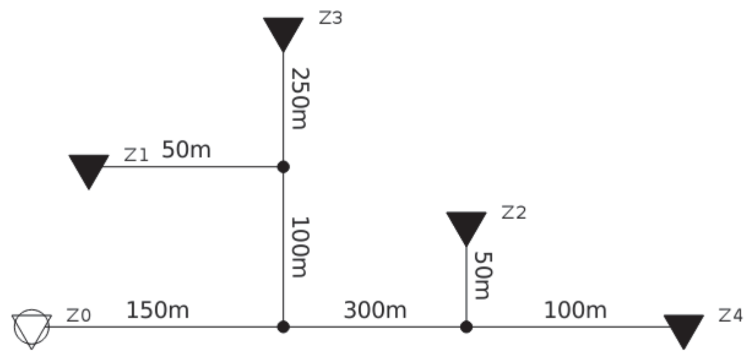

(a)

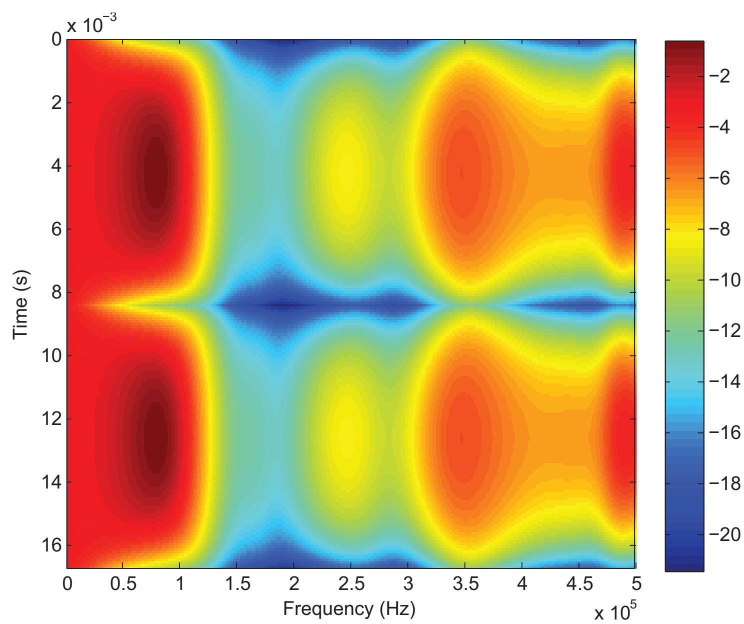

(b)

Figure B.3: (a) Topology with time-varying (Z1) and frequency-selective (Z4) impedances. (b) Time- and frequency-selective CTF between Z0 and Z1.